ABSTRACT

WIMPEY, JAMES FRANK. Electromagnetic Decay of Fragmented Analogue States in ^{45}Sc and ^{63}Cu. (Under the direction of GARY E. MITCHELL.)

Capture excitation functions were measured for $^{44}Ca(p,\gamma)^{45}Sc$ from 1.56 to 2.28 MeV and for $^{62}Ni(p,\gamma)^{63}Cu$ from 2.30 to 2.70 MeV. Detailed study of the electromagnetic decay of 57 resonances in ^{45}Sc and 35 resonances in ^{63}Cu was performed using an 80 cm^3 Ge(Li) detector. The experiments were performed with the TUNL 3 MV Van de Graaf accelerator and associated electrostatic analyzer-homogenizer system. The overall energy resolution of the proton beam was about 350 eV.

For the 92 resonances studied in detail, absolute partiaand total gamma-ray widths and inelastic widths were determined. Three fragmented analogues were studied in ^{45}Sc. These states had spin and parity 3/2-, 1/2-, and $1/2^+$, and were the analogues of the sixth, eighth, and tenth excited states of ^{45}Ca, respectively. One analogue state was studied in ^{63}Cu, the analogue of the 3/2- second excited state of ^{63}Ni. The decay of a number of non-analogue (or background) resonances were also studied in both ^{45}Sc and ^{63}Cu.

Emphasis was placed on correlations between partial widths in different channels. Statistically significant correlations were measured between the elastic and inelastic widths on the 1/2- analogue in ^{45}Sc and the 3/2- analogue in ^{63}Cu. The correlations between elastic and total capture widths are statistically significant on each of the analogue states. There are also statistically significant

correlations between the elastic widths and the gamma-ray widths to particular final states. The correlations between the elastic widths and gamma-ray widths of the background $1/2^+$ resonances in ^{63}Cu and the background 1/2- resonances in ^{45}Sc are consistent with purely statistical behavior.

The strengths of the M1 decay of the 3/2- analogues are as expected for this mass region. Surprisingly the M1 strength for the 1/2- analogue in ^{45}Sc is about the same as for the 3/2- analogue in the same nucleus.

In addition to information concerning analogue states, decay of the background states yielded a number of statistical results such as the effective number of degrees of freedom. The combined results for both analogue and background states yielded several hundred transitions strengths of known multipolarity.

Inelastic spectroscopic factors were calculated for the 1/2- and the $1/2^+$ analogue states in ^{45}Sc and the 3/2- analogue state in ^{63}Cu. These results indicate that the inelastic spectroscopic factors are often comparable to the elastic spectroscopic factors.

ELECTROMAGNETIC DECAY OF FRAGMENTED ANALOGUE STATES IN ^{45}Sc AND ^{63}Cu

by

JAMES FRANK WIMPEY

A thesis submitted to the Graduate Faculty of
North Carolina State University at Raleigh
in partial fulfillment of the
requirements for the Degree of
Doctor of Philosophy

DEPARTMENT OF PHYSICS

RALEIGH

1 9 7 4

APPROVED BY:

_____ _____
Chairman of Advisory Committee

_____ _____

BIOGRAPHY

Name: James Frank Wimpey

Personal: Born October 13, 1946, Blairsville, Georgia.

Education: B.S. in Physics, North Georgia College, 1968.

Positions: Teaching Assistant, N.C.S.U., 1968 to 1969;
NSF Traineeship, N.C.S.U., 1969 to 1973;
Research Assistant, N.C.S.U., 1973 to present.

Membership: Sigma Pi Sigma.

Publication: Electromagnetic Decay of Fragmented Analog States, (with G.E. Mitchell, E.G. Bilpuch, and W.C. Peters); Proceeding of the International Conference on Photonuclear Reactions and Applications. B. L. Berman, Editor. U.S. Atomic Energy Commission, Oak Ridge, Tenn., 1973), p. 297.

Abstract: Gamma Decay of the Fine Structure of Analog States in ^{45}Sc. (With G.E. Mitchell and E.G. Bilpuch). To be published in Bull. Am. Phys. Soc.

ACKNOWLEDGEMENTS

I would like to thank my research advisor, Prof. G. E. Mitchell, for his guidance and encouragement during all phases of this research project, especially during the preparation of this dissertation. I am grateful to Prof. E.G. Bilpuch for his advice and consultations during the course of these experiments.

I would like to acknowledge Dr. W.C. Peters for his assistance in the early stages of these experiments. To Dr. W.M. Wilson, I am indebted for hours of discussions about his results on ^{45}Sc. I wish to thank Dr. J.D. Moses for his assistance in analysis using the maximum likelihood technique. Grateful thanks go to Dr. R.O. Nelson for his advice concerning the practical problems with electronics and data taking procedures.

Efforts of W.K. Wells, T.R. Dittrich and D.A. Outlaw are gratefully appreciated, particularly for assistance during the marathon data taking runs. Mr. W.K. Wells deserves additional thanks for his assistance in the analysis of the ^{45}Sc data.

The assistance of Mr. Sidney Edwards, Mr. Robert Rummel, Mr. Malcolm Smith, Mr. A.W. Lovette and Mr. Gene Harris in constructing and maintaining the equipment used in these experiments is gratefully appreciated. The figures in this dissertation were expertly drawn by Mrs. Joseph Bailey and superbly photographed by Mr. Al Rade.

I would like to thank my wife, Linda for her encouragement and understanding during these five years.

I am thankful for the NSF Traineeship for the academic years 1969-1973. This work was supported in part by the United States Atomic Energy Commission. Data analysis was performed at the Triangle Universities Computation Center, which is supported in part by the National Science Foundation.

TABLE OF CONTENTS

INTRODUCTION

Soon after the discovery of the neutron, the concept of isospin was introduced by Heisenberg (1932). The neutron and proton have the same intrinsic angular momentum (spin) and almost the same mass, but differ in both charge and magnetic moment. The neutron and proton may be considered different states of one entity -- the nucleon. Then an isospin quantum number T may be introduced, which is analogous with intrinsic angular momentum 1/2. In nuclear physics, the component with $Tz = 1/2$ is defined as the neutron and the component with $tz = -1/2$ is defined as the proton. Thus, for a system of nucleons, the z-component of the total isospin Tz is just the number of excess neutrons divided by two. Wigner (1937) suggested that the total isospin of a system of nucleons would be a good quantum number if the energy associated with the Coulomb forces was small compared with the energy associated with the nuclear forces. Since this is true for light nuclei ($A < 25$), much of the early experimental and theoretical work was concentrated on these nuclei.

Trainer (1952) incorporated isospin into the Coulomb interaction. This resulted in isospin selection rules for electromagnetic transitions, particularly E1 transitions. These selection rules were successful in explaining the behavior of E1 transitions in self conjugate nuclei. Later, Morpurgo (1958) showed that the isospin selection rules were also valid for M1 transitions.

In spite of the success of the isospin formalism in light nuclei, it was commonly believed that in heavier nuclei the Coulomb forces would be so strong that isospin would not even be approximately conserved. This

view was shown to be incorrect by Anderson et al. (1961), who studied the (p,n) reaction on many medium mass nuclei. The resulting neutron time-of-flight spectra in every case showed a strong neutron group at a neutron energy equal to the difference between the incident proton energy and the Coulomb energy of a proton in the residual nucleus. The state of the residual nucleus is highly excited and has the same quantum numbers (except for Tz which differs by one unit) as the ground state of the target nucleus. This state in the residual nucleus is identified as the analogue of the ground state of the target nucleus. These results were explained by Lane (1962), who postulated an isospin dependent term in the optical model Hamiltonian. With this model, the results of Anderson et al. were interpreted as a "charge exchange" reaction.

Although the (p,n) reaction was an excellent way to observe the analogue of the ground state of a nucleus, proton elastic scattering has since proved a more comprehensive method for investigation of analgoue states. Addition of a proton to a target with isospin T = To results in the compound system (p + C) which contains "ordinary" states with $T = Tz = T_< = To - 1/2$ and also states with $T = T_> = To + 1/2$. These $T_>$ states are the analogues of the To + 1/2 states of the neutron plus target system (n + C) . These $T_>$ states differ from the neutron plus target system by the Coulomb energy of the additional proton and the proton-neutron mass difference. Therefore, with proton elastic scattering it is possible to form the analogue of an excited state in the (n + C) system as well as the ground state analogue. These analogue resonances in the compound system were first observed by Fox et al. (1964). A very large number of analogue experiments have now been performed, with most of

the effort directed towards spectroscopic application. A partial list of quantities obtained by analogue experiments includes: spectroscopic factors, the spin and parity of the parent state, the Coulomb displacement energy between an isobaric pair, etc.

Independent of application to nuclear spectroscopy, analogue states are intrinsically important and interesting. Soon after the discovery of analogue resonances by Fox et al. an experiment by Richard et al. (1964) suggested that analogue resonances were not single resonances but were actually composed of many resonances. These results were first explained by Robson (1965). Robson showed that an analogue state occurring in the compound nucleus is mixed with ordinary compound nuclear states through the Coulomb field outside the nucleus, producing an enhancement of the widths of these states for the elastic channel. Robson demonstrated that the enhancement of these background states should follow an asymmetric distribution. The fine structure of an analogue state was first fully resolved when Keyworth et al. (1966) performed an elastic scattering experiment on ^{40}A . This work, with a cryogenically-pumped gas target and a very high resolution beam, proved the analogue state does not consist of a single resonance but instead has "fine structure". Two highly fragmented analogue states were observed. The distribution of widths of the two analogue states displayed the expected asymmetric distributions.

Meanwhile, another facet of analogue states was being examined -- the study of the electromagnetic decay of analogue states. Some of the earliest studies were performed by Endt (1966). He observed that in the s - d shell the electromagnetic decay of analogue states proceeded

primarily to one final state with the same spin and parity as the analogue state. These special states were later called anti-analogue states. The anti-analogue state is described as having the same particle-core components as the analogue state but with different (isospin dependent) weights so that the two states are orthogonal. In this case the isovector contribution of the M1 operator has a large contribution to the analogue to anti-analogue state transition.

The fragmentation of an analogue state complicated the study of the decay of analogue states. Some of the first studies of fragmented analogue states were performed by Erne et al. (1966) and Chasman et al. (1967). They studied an analogue state in ^{38}A which consisted of two fragments. The decay from each fragment was similar and dominated by a strong transition which could be explained by the analogue to anti-analogue transition.

From 1966 to 1969 there were a number of important developments in the field of analogue states. One of these was the innovation of solid targets for high resolution measurements (Browne et al., 1968; Wilhjelm et al., 1969). Their results demonstrated that it was possible to resolve the fine structure of analogue states using solid targets, even though the resolution was about three times the resolution attainable with gas targets. Another development concerned the electromagnetic decay of analogue states. Experiments in the f - p shell (Vingiani et al., 1968a and 1968b; Chilosi et al., 1968; and Walinga et al., 1969) showed that the decay of analogue states in this shell was not as simple as the decay of analogue states in the s - d shell. Maripuu (1970c) and Hirata (1970) attempted to explain this inhibition in terms of core polarization effects.

Analogue to anti-analogue transitions were inhibited by factors of 10 to 1000. The (^{3}He,d) reactions also indicated that the anti-analogue was often fragmented.

The study of the electromagnetic decay of analogue states provides other spectroscopic information. For example, the electromagnetic decay of the ground state analogue of a parent state which also beta-decays to the ground state of the daughter nucleus provides an opportunity to compare the electromagnetic decay to the beta-decay (Hanna, 1969). Analogue state decay provides a means of comparing the strength of $\Delta T = 1$ electromagnetic transitions with the usual $\Delta T = 0$ transitions. Therefore, the study of the decay of an analogue state is of great interest in nuclear spectroscopy.

Independent of applications the study of fine structure and of the electromagnetic decay of analogue states is very important. In a comprehensive review article, Lane (1969) presents a thorough treatment of fine structure and predicts correlations between the widths of different channels. Analogue states are doorway states for elastic scattering of protons. If an analogue state is also a doorway for other channels (e.g., inelastic, capture, neutron, etc.), then correlations should exist between the partial widths of the different channels. Early experiments (Vingiani et al., 1968b and 1971b) indicated correlations between the total capture widths and the corresponding elastic widths for the fragmented analogue state (although the authors made no reference to the existence of correlations in their data). More recent experiments using the proton induced reactions on ^{54}Cr and ^{58}Fe (Peters et al., 1971 and 1973; Mitchell et al., 1972; and Peters, 1972) have shown large

correlations between the elastic and inelastic widths and between the elastic and parital gamma-ray widths on highly fragmented analogue states.

This dissertation describes experiments undertaken to study the electromagnetic decay of three highly fragmented analogue states of ^{45}Ca in ^{45}Sc and a highly fragmented analogue state of ^{63}Ni in ^{63}Cu. The primary objective of these experiments was to determine if correlations existed between the widths in different exit channels. In the earlier work correlations were measured on analogue states. Since essentially no data existed on the correlation of non-analogue resonances, a secondary objective of these experiments was to search for correlations off analogue states. In ^{63}Cu twenty $1/2^+$ resonances were selected for study and in ^{45}Sc fourteen 1/2- resonances not associated closely with an analogue state were selected for study. The study of these analogue states also provides an opportunity to measure certain spectroscopic quantities. For example, the inelastic spectroscopic factors can be calculated from results of these data. Also the study of two $\ell = 1$ analogue states with different J-values in the same nucleus permits the examination of another aspect of inhibition of the M1 strength between analogue and anti-analogue states in the f-p shell.

In these experiments, excitation functions were measured (with NaI(Tl) crystals) for the ^{44}Ca(p,γ)^{45}Sc reaction (Ep = 1.58 to 2.28 MeV) and for the ^{62}Ni(p,γ)^{63}Cu reaction (Ep = 2.30 to 2.70 MeV). Absolute gamma-ray widths were then measured for transitions from fragments of the analogue states. In Chapter 2, general background is given for analogue and anti-analogue states, the relevant theory of

electromagnetic transition rates (particularly for M1 transitions), correlations and inelastic spectroscopic factors. The experimental equipment and data taking procedures are described in Chapter 3. In Chapter 4, the method of data reduction is described and preliminary analysis of the data presented. Detailed analysis and discussion of the data are given in Chapter 5. Results and conclusions are summarized in Chapter 6. The gamma-ray widths are tabulated in the Appendix. The new scattering chamber used in these experiments is described in the Appendix. Also in the Appendix is a description of the Monte Carlo calculations (used to determine the statistical significance of the measured correlations).

GENERAL BACKGROUND

At a symposium on nuclear properties in the s - d shell, Endt (1966) presented some of the first results on the electromagnetic decay of analogue states. He observed decay patterns which were relatively simple; the decay proceeded primarily to one final state whose spin and parity was the same as the analogue state. This state was called the anti-analogue state. Since 1966 a number of related experiments have been performed on both s - d shell and f - p shell nuclei. The analogue states were populated with the proton capture reaction. In the s - d shell the primary mode of electromagnetic decay of analogue states is by M1 transition to the anti-analogue state. In this shell the M1 strengths are on the order of a Weisskopf unit (W.u.). In the f - p shell, the M1 transitions to the anti-analogue state are retarded by factors of 10 - 1000 for 3/2- to 3/2- transitions; however, for the $9/2^+$ to $9/2^+$ transitions in ^{59}Cu, ^{61}Cu and ^{63}Cu the M1 strength is reported to be on the order of a Weisskopf unit (Fodor et al., 1970; Szentpetery and Szucs, 1972; Maripuu et al., 1972). In the remainder of this chapter the following topics are discussed:

1) properties of analogue and anti-analogue states,
2) properties of M1 transitions from analogue to anti-analogue states,
3) correlations between widths in different channels, and
4) inelastic spectroscopic factors.

Analogue and Anti-Analogue States

The existence of isobaric analogue states may be understood by an examination of the symmetry properties of neighboring nuclei. Consider a low-lying level in a nucleus with mass number A, charge number Z, and neutron number $(N + 1)$. If a neutron is changed into a proton, the resulting nucleus has mass number A, charge number $(Z + 1)$ and neutron number N. If the nuclear force is charge independent, then the resulting state differs energetically from the initial state only by the Coulomb energy of the last proton and the neutron-proton mass difference. The similarity of the nuclear properties of these states was verified by elastic scattering experiments. In most of these experiments, the parent state had a large single particle component (neutron + inert core) and a known spin and parity. The unbound daughter states were excited by protons at a suitable energy on the nucleus with charge number Z and neutron number N. Large resonances were observed with spin and parity the same as the parent; these resonances have a large single particle component. The relationship between parent state and daughter state is illustrated in Figure 1.

Theories have been proposed by several authors to explain analogue state phenomena. Robson (1965) was first to describe analogue states in terms of isospin algebra and R-matrix theory. His treatment is a special case of external mixing in one channel. Mello (1967) extended Robson's work to include the many channel case. Treatment of the fine structure of analogue states was examined by Lane (1969). Other treatments of analogue state phenomena are presented in terms of various formalisms; a more complete list of references can be found in a compilation by Wilkinson (1969).

Figure 1 Energy level diagram showing the relationship between the analogue state and the parent state

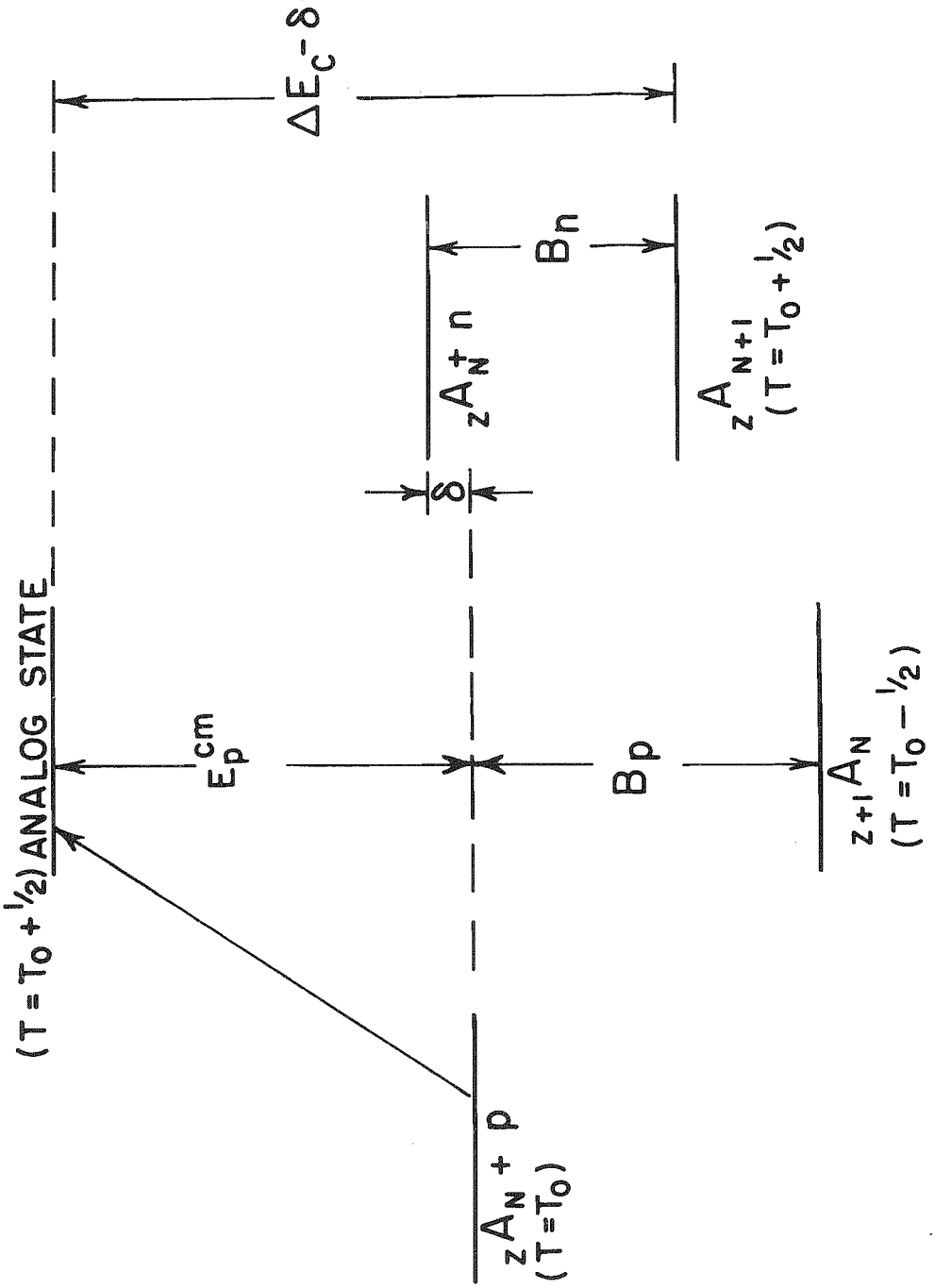

δ = neutron – proton mass difference

In the following, a brief description of analogue states is given in the isospin formalism. A nucleon is defined to have total intrinsic isospin $T = 1/2$. The state with z component of isospin $T_z = 1/2$ is defined as the neutron and the state with $T_z = -1/2$ the proton. The total isospin of a system of A nucleons (Z protons and N neutrons) is given by

$$\bar{T} = \sum_{i=1}^{A} \bar{t}_i \tag{1}$$

with z component

$$T_z = \sum_{i=1}^{A} t_{zi} = \frac{N-Z}{2} . \tag{2}$$

Raising and lowering operators for individual nucleons can be defined following the analogy with angular momentum. Thus, for a system of A nucleons, one obtains raising and lowering operators given by

$$\hat{T}^{\pm}_z = \sum_{i=1}^{A} \hat{t}^{\pm}_i . \tag{3}$$

By analogy with the ordinary angular momentum results, operating on a state $|T,T_z>$ with the operator $\hat{T}^2$ yields

$$\hat{T}^2 |T,T_z> = T(T+1)|T,T>$$

where

$$\hat{T}^2 = \hat{T}^2_x + \hat{T}^2_y + \hat{T}^2_z .$$

Similarily one obtains

$$\hat{T}_z = |T,T_z> = T_z|T,T_z> = \frac{N-Z}{2}|T,T_z>$$

and

$$\hat{T}^{\pm}|T,T_z\rangle = \sqrt{(T\pm T_z)\cdot(T\mp T_z+1)}\ |T,T_z\pm 1\rangle \ . \tag{5}$$

By physical arguments (conservation of charge) T_z must be a constant of the motion. The total isospin T is a constant of the motion (within a few percent) with respect to nuclear forces (e.g., see the review article by Henley (1969)), i.e.,

$$[\hat{T},H_n] \approx 0 \tag{6}$$

where the nuclear Hamiltonian H_n does not include the Coulomb interaction. If the Coulomb potential is included, then the total isospin is not a constant of the motion since the Coulomb potential is a function of T_z . Thus it follows that

$$[\hat{T},V_c] \neq 0 \tag{7}$$

where V_c is the Coulomb interaction. This simply says that the Coulomb forces can distinguish between charged and uncharged nucleons.

Following Robson's procedure, a single particle state in the parent nucleus is formed by coupling a neutron to the core with charge number Z and neutron number N . This state can be written in isospin space as

$$|nC\rangle = |\tfrac{1}{2},\tfrac{1}{2}\rangle|T_o,T_o\rangle \tag{8}$$

where $|\frac{1}{2},\frac{1}{2}\rangle$ and $|T_o,T_o\rangle$ are the uncoupled neutron and core vectors, respectively. The parent state is assumed to have pure isospin $T = T_z = T_o + 1/2$. This assumption, according to Lane and Soper (1962), is good to order $(2T_o + 1)^{-1}$.

To form the analogue state, one exchanges a neutron for a proton without changing any quantum numbers other than T_z. Formally, this can be accomplished by the isospin lowering operator $\hat{T}^-$:

$$(9) \qquad \hat{T}^- |T_o + \tfrac{1}{2}, T_o + \tfrac{1}{2}\rangle = (2T_o + 1)^{1/2} |T_o + \tfrac{1}{2}, T_o - \tfrac{1}{2}\rangle$$

$$= (2T_o + 1)^{1/2} |T_>\rangle$$

where the state $|T_>\rangle = |T_o + 1/2,\ T_o - 1/2\rangle$ is the analogue state configuration. Applying $\hat{T}^-$ to $|nC\rangle$ directly, $|T_>\rangle$ can be written in terms of the uncoupled state vectors;

$$(10) \quad |T_>\rangle = (2T_o+1)^{-1/2}\{|\tfrac{1}{2},-\tfrac{1}{2}\rangle|T_o,T_o\rangle + (2T_o)^{1/2}|\tfrac{1}{2},\tfrac{1}{2}\rangle|T_o,T_o-1\rangle\}$$

noting that $|1/2,-1/2\rangle$ is the isospin representation of a proton and that $|T_o,T_o-1\rangle$ is the analogue of the core, $|T_>\rangle$ can be written as

$$(11) \qquad |T_>\rangle = (2T_o+1)^{-1/2}\{|pC\rangle + (2T_o)^{1/2}|nA\rangle\} .$$

In isospin space, the anti-analogue state is a state with the same components as the analogue state but with different weights such that the analogue and anti-analogue state are orthogonal. Since $|T_>\rangle$ is normalized, the representation of the anti-analogue state is

$$(12) \qquad |T_<\rangle = (2T_o+1)^{-1/2}\{(2T_o)^{1/2}|pC\rangle - |nA\rangle\}$$

and $|T_<\rangle$ has isospin $T = T_o - 1/2$ and $T_z = T_o - 1/2$ with the other quantum numbers the same as for the state $|T_>\rangle$. Figure 2 shows schematically the relationship between parent, analogue and anti-analogue states.

Figure 2 Diagram of the relationship between the parent, analogue, and anti-analogue states

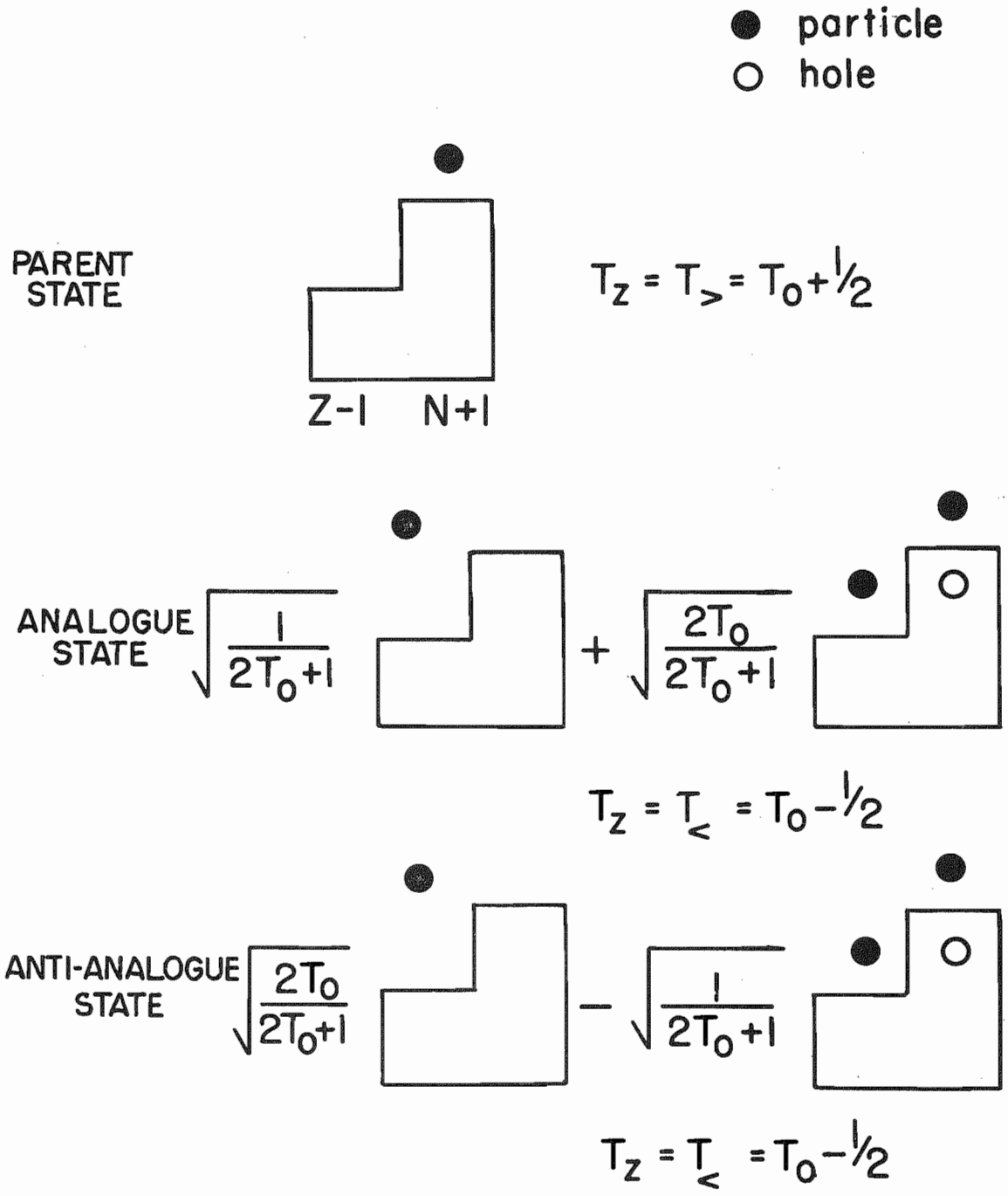
particle
hole
PARENT STATE
Z-1
N+1
$T_z = T_> = T_0 + 1/2$
ANALOGUE STATE
$\sqrt{\frac{1}{2T_0+1}}$
+
$\sqrt{\frac{2T_0}{2T_0+1}}$
$T_z = T_< = T_0 - 1/2$
ANTI-ANALOGUE STATE
$\sqrt{\frac{2T_0}{2T_0+1}}$
−
$\sqrt{\frac{1}{2T_0+1}}$
$T_z = T_< = T_0 - 1/2$

It can be shown that the energy difference between states $|T_>\rangle$ and $|T_<\rangle$ is given by (Maripuu, 1969)

$$E_{T_>} - E_{T_<} = (2T_o+1)\frac{V_1}{A} \tag{13}$$

where V_1 is independent of mass number A. This splitting is due to the $\vec{T}_o \cdot \vec{t}$ interaction. Since this energy separation between an analogue and anti-analogue is typically several MeV, the $T_<$ states are usually bound states in the daughter nucleus. Since the $T_<$ states are bound, it is not possible to populate them directly using compound nuclear reactions. The proton capture reaction may be used to populate these states indirectly or proton stripping reactions such as $(^3He,d)$ and (d,n) may be used to populate these states directly.

It should be noted that the definition of an anti-analogue state as discussed above is not unique -- particularily in heavy nuclei. Robson (1969) showed that if there are more than two orbits involved for the excess neutrons, then the anti-analogue state is not well defined. For example, in the parent nucleus ^{89}Sr the excess neutrons are in the $g_{9/2}$ and $p_{1/2}$ shells, with another neutron coupled to this core in the (nlj) orbital. The analogue state is found in the usual way by operating on the parent with the $\bar{T}-$ operator yielding

$$|T_>\rangle = \frac{1}{\sqrt{13}}\{|1\rangle + \sqrt{10}\,|2\rangle + \sqrt{2}\,|3\rangle\}$$

where

$$|1\rangle = |(n\ell j)_p\, G^{10}_{9/2}\, P^2_{1/2}\rangle$$

$$|2\rangle = |(n\ell j)_n (G_{9/2})_p G^9_{9/2}\, P^2_{1/2}\rangle$$

$$|3> = |(n\ell j)_n G^{10}_{9/2}(P_{1/2})_p \; P_{1/2}> \; .$$

The usual procedure for defining the anti-analogue state then yields

$$|T_<> = \frac{1}{\sqrt{13}} \{\sqrt{12} \; |1> - (\sqrt{10/12} \; |2> + \sqrt{2/12} \; |3>)\} \; .$$

Another linear combination of $|1>$, $|2>$ and $|3>$ that is also orthogonal to the analogue state is

$$|a> = \frac{1}{\sqrt{12}} \{\sqrt{2} \; |2> - \sqrt{10} \; |3>\} \; .$$

Thus there are different linear combinations of the components of the analogue state that are orthogonal to the analogue state.

Electromagnetic Transitions

As shown in the previous section, the analogue and anti-analogue states have the same spin and parity and differ by one unit of isospin. Therefore, electromagnetic transitions between these states are $\Delta J = 0$, with no parity change (M1) . Thus, if one considers analogue to anti-analogue transitions, the theory of M1 transitions is of paramount importance. The theory of electromagnetic interactions is well known; detailed description of the process involving various multipole operators can be found in numerous references, see Blatt and Weisskopf (1952), Jackson (1962) for classical treatment of multipole moments and Preston (1962) for a summary of electromagnetic theory.

The following is a sketch of the high points of the applicable theory of electromagnetic radiation. Basically one has an initial state I and final state F and an interaction which takes the system from state I to state F . Writing the Hamiltonian as

(14) $$H = H_o + H_{int}$$

where H_o is the nuclear Hamiltonian and H_{int} is the interaction of charged particle in an electromagnetic field, the transition probability for a transition from state I to F is

(15) $$T = \frac{2\pi}{\hbar} |\langle F|H_{int}|I\rangle|^2 \rho_E$$

where ρ_E is the density of final states. Writing out H_{int} explicitly for a system of A nucleons

(16) $$H_{int} = - \sum_{i=1}^{A} \{\frac{e_i}{m_i c} \tilde{P}_i \cdot \tilde{A}(r_i) + \mu_i \tilde{S}_i \cdot \tilde{H}(r_i)\}$$

where e_i and m_i are the charge and mass on the $i^{\underline{th}}$ nucleon. $\tilde{P}_i$ is the momentum operator for the $i^{\underline{th}}$ particle and $\tilde{A}(r_i)$ and $\tilde{H}(r_i)$ are the vector potential and magnetic field, respectively, at the position r_i. $\tilde{A}(r_i)$ and $\tilde{H}(r_i)$ are given by

(17) $$\tilde{A}(r) = q^{\sigma}_{\lambda\mu} \tilde{A}_k(r)$$

and

(18) $$\tilde{H}(r) = \text{Curl } \tilde{A}(r)$$

where $k = \omega/c$ and $\tilde{A}_k$ satisfies the following equation

(19) $$\text{Curl}(\text{Curl } \tilde{A}_k) - k^2 \tilde{A}_k = 0 .$$

The operators $q^{\sigma}_{\lambda\mu}$ create or destroy a proton of type λ, μ, σ. Solutions of the above equations are given by many authors (Morse and Feshbach, 1953; Jackson, 1962; Blatt and Weisskopf, 1952). Their solutions differ only in normalization. The solutions are of the form

(20) $$A^{\sigma=E}_{\lambda\mu} = -\frac{i}{k} C_{url}\ \bar{r} \times G_{rad}[j_\lambda(kr)Y^\mu_\lambda(\Omega)]$$

and

(21) $$A^{\sigma=M}_{\lambda\mu} = \bar{r} \times G_{rad}[j_\lambda(kr)Y^\mu_\lambda(\Omega)]$$

where $j_\lambda(kr)$ is the spherical Bessel function and Y^μ_λ the spherical harmonics with λ μ integers. Note that the matrix element $\langle F|H_{int}|I\rangle$ is dependent on the q's and on a part H' of the total Hamiltonian

(22) $$H' = -\sum_{i=1}^{A} \{\frac{e_i}{m_i C} \tilde{P}_i \cdot \tilde{A}^{\sigma}_{\lambda\mu}(r_i) + \mu_i \tilde{S}_i \cdot \tilde{H}^{\sigma}_{\lambda\mu}(r_i)\} .$$

Many important relationships may be obtained by considering the properties of $\langle F|H'|I\rangle$. These relationships are used to show various properties of electromagnetic transitions. Of particular importance here are isospin selection rules. Rewriting H_{int} and taking into account proton and neutron charges and magnetic moments, one obtains

(23) $$H_{int} = -\sum_{i=1}^{A} \{\frac{e}{mC} \tilde{P}_i \cdot \tilde{A}(\bar{r}_i)[\frac{1}{2} - t_{zi}] + [\mu_p(\frac{1}{2} - t_{zi})$$

$$+ \mu_n(\frac{1}{2} + t_{zi})]\tilde{S}_i \cdot \tilde{H}(r_i)\} .$$

H_{int} can be written as the sum of two parts,

$$H_{int} = H_o + H_1 t_z .$$

H_o has no isospin dependence and H_1 is the z component of a vector in isospin space. Reduction of H_{int} in isospin space by the Wigner-Eckart theorem gives

$$(24)\qquad \langle FTT_z|H_{int}|IT_oT_{oz}\rangle = \langle T_oT_{oz}00|TT_{oz}\rangle\langle F\|H_o\|I\rangle + \langle T_oT_{oz}10|TT_{oz}\rangle\langle F\|H_1\|I\rangle .$$

From the properties of the coefficients in the above equation, one obtains isospin selection rules of $\Delta T = 0,1$. This rule was first presented by Trainer (1952) for E1 transitions and Morpurgo (1958) for M1 transitions. For transitions between analogue and anti-analogue states, the only part contributing is H_1 or the isovector component of the multipole operator.

Another important rule can be derived from the matrix element $\langle F|H'|I\rangle$. One can show that M1 transitions from resonances with $J = \ell + 1/2$ are enhanced over M1 transitions from resonances with $J = \ell - 1/2$. Using the expressions for $\hat{A}(r)$ and $\hat{H}(r)$, one can show that $\langle F|H'|I\rangle$ is proportional to $\langle F|Q_{\lambda\mu}|I\rangle$ or $\langle F|M_{\lambda\mu}|I\rangle$ where $Q_{\lambda\mu}$ and $M_{\lambda\mu}$ are given by

$$(25)\quad Q_{\lambda\mu} = \sum_{i=1}^{A} \{e_i r_i^{\lambda} Y_{\lambda}^{\mu}(\Omega_i) - g_{si}\mu_o k(\lambda+1)^{-1}\tilde{\sigma}_i \bar{Xr}_i \cdot \mathrm{Grad}(r^{\lambda}Y_{\lambda}^{\mu *})_i\}$$

and

$$(26)\qquad M_{\lambda\mu} = \mu_o \sum_{i=1}^{A} \{(g_s\tilde{s}_i + \frac{2}{\lambda+1} g_{\ell i}\bar{\ell}_i)\cdot \mathrm{Grad}(r^{\lambda}Y_{\lambda}^{\mu *})_i\} .$$

For M1 transitions, the M1 operator is the sum of single particle M1 operators given by

$$(27)\qquad M_1 = \mu_o \sum_{i=1}^{A} \{(g_s\tilde{s}_i + g_{\ell i}\bar{\ell}_i)\cdot \mathrm{Grad}(rY_1^{*})_i\} .$$

The M1 transition probability can be written as

$$T^{M1}_{I\to F} = \frac{16\pi}{9}\frac{k^3}{\hbar}\left| \langle F|\tilde{M1}|I\rangle\right|^2 . \tag{28}$$

Talmi and Unna (1960) have shown that the M1 operator in the case of pure jj coupling can be written as the sum of an isoscalar and a isovector,

$$\Omega(M1) = \Omega_o(M1) + \Omega_1(M1) \tag{29}$$

where

$$\Omega_o(M1) = \sqrt{\frac{3}{4\pi}}\mu_o \sum_{k=1} \frac{g_j^p + g_j^n}{2}\tilde{j}_k \tag{30}$$

and

$$\Omega_1(M1) = \sqrt{\frac{3}{4\pi}}\mu_o \sum_k \frac{g_j^p - g_j^n}{2}\tilde{j}_k\cdot\tilde{t}_k . \tag{31}$$

μ_o is a nuclear magneton and the g-factors are given below

$$g_k = (g_\ell \ell + \frac{1}{2}g_s)/j \qquad j = \ell + \frac{1}{2} \tag{32}$$

$$g_k = \{g_\ell^{(\ell+1)} - \frac{1}{2}g_s\}/(j+1) \qquad j = \ell - \frac{1}{2}$$

where $g_\ell = 1$ for proton, and 0 for a neutron while $g_s = 5.586$ for proton and -3.828 for neutron.

Since the transition from the state $|T_>\rangle$ to the state $|T_<\rangle$ involves only the isovector part Ω_o does not contribute to the transition probability. The transition probability and, thus, the width,

is therefore proportional to $(g_j^p - g_j^n)^2$. From this proportionality, one obtains (assuming the other contributions are equal) a retardation for transitions from $j = \ell - 1/2$ analogue states as compared to $j = \ell + 1/2$ analogue states. For example, for $\ell = 1, 2, 3$

$$\frac{\Gamma_{j>}}{\Gamma_{j<}} \simeq 5, 16, 117 \quad . \tag{33}$$

Maripuu (1969) quotes the retardation as being from 20 to 200, attributable mostly to the $(g_j^p - g_j^n)^2$ term.

Correlations

The study of partial widths in different channels provides an opportunity to study non-statistical effects in nuclei. Lane (1972) has shown the study of correlations between partial widths of different channels is an interesting part of a more general subject of non-statistical effects in nuclei, which he interprets as a growth point of present-day nuclear physics. This is because the existence of correlations contradicts the "compound nucleus model" of Bohr (1936). In this model, reactions proceed in two distinct stages, the formation and the subsequent decay into a number of channels. The independence of the formation and subsequent decay is the major assumption of the compound nuclear model. Thus, if large correlations exist between different decay channels, the decay into these channels is clearly not independent.

Before proceeding further, a quantitative definition of correlation will be discussed. Consider measurements where the data are measured in pairs (x,y). To determine if there is a linear relationship between x and y a least square fit to the data is made treating y as the dependent

variable and a relationship of the form $y = a + bx$ where

$$b = \frac{N \sum_{i}^{N} x_i y_i - \sum_{i}^{N} x_i \sum_{i}^{N} y_i}{N \sum_{i}^{N} x_i^2 - \left(\sum_{i}^{N} x_i\right)^2} \quad (34)$$

If x and y are independent, the the slope of the least square fit will be zero. However, the value of the slope alone is not sufficient to show a correlation b since there may be a linear relationship with a very small slope. In this event when x is treated as the dependent variable, the slope would be very large and would indicate a strong relationship. Thus, the data are also fit with x as the dependent variable obtaining a least square fit of the form $x = a' + b'y$ where

$$b' = \frac{N \sum_{i=1}^{N} x_i y_i - \sum_{i=1}^{N} x_i \sum_{i=1}^{N} y_i}{N \sum_{i=1}^{N} y_i^2 - \left(\sum_{i=1}^{N} y_i\right)^2} \quad (35)$$

Again if there is no relationship then $b' = 0$. Consider the case where there is a linear relationship between x and y, then

$$Y = -\frac{a'}{b'} + \frac{1}{b'} x = a + bx \quad (36)$$

Equating coefficients the following relationships are obtained

$$a = -\frac{a'}{b'}$$

$$b = \frac{1}{b'}, \qquad bb' = 1 \quad (37)$$

Thus, if there is a correlation the value of bb' is between zero and one. This leads to the definition of the linear correlation coefficient (Bevington, 1969)

$$(38)\quad r = \sqrt{bb'} = \frac{N\sum_{i=1}^{N} x_i y_i - \sum_{i=1}^{N} x_i \sum_{i=1}^{N} y_i}{\left[N\sum_{i=1}^{N} x_i^2 - \left(\sum_{i=1}^{N} x_i\right)^2\right]^{1/2}\left[N\sum_{i=1}^{N} y_i^2 - \left(\sum_{i=1}^{N} y_i\right)^2\right]^{1/2}}$$

where b and b' are determined from the least square fitting procedure of $x = a' + b'y$ and $y = a + bx$. The sign of r is the sign of b (and hence b'). The range of r is -1 to $+1$.

Specifying only the correlation coefficient r is not sufficient to determine the significance of the correlation. To determine the significance of a given correlation, it is necessary to consider the distribution from which the variables would originate if they were random. Porter and Thomas (1956) have shown that in a particular channel the distribution of partial reaction widths in nuclei obey a chi-squared distribution of one degree of freedom (the Porter-Thomas distribution). The expected statistical distribution of r can therefore be obtained and the significance of the measured correlation determined. The methods used to determine the statistical significance are discussed in the Appendix.

In similar experiments there have been two types of correlation phenomena observed. One is the correlation between the relative strengths of the population of particular final states by different reactions on the same target. Correlations have been observed between (d,p) and (n,γ) strengths to particular final states. In the mass 40-60 region about ten cases are reported where the correlation is greater than 0.8 (Lane, 1972). These (d,p) - (n,γ) correlations are observed on both thermal neutron capture and on neutron resonances. An analogous correlation in the present (p,γ) experiment would be between

the (d,n) and (p,γ) reactions or between (^{3}He,d) and (p,γ) reactions.

The second type of correlation (and probably the more interesting one for the present work) is the correlation between partial widths in different channels. This involves correlations between the elastic widths and inelastic widths and also between the elastic widths and the gamma-ray widths. The theoretical background for correlations of this type is discussed in detail by Lane (1969). A brief summary of this topic is given in a later paper by Lane (1972). The conclusion drawn from this theory is that correlations between two channels will not be large merely because the two channels separately have non-statistical behavior. In order to have large correlations, the two channels must share a common doorway state.

Inelastic Spectroscopic Factors

Inelastic decay of protons from analogue states provides a method of obtaining certain spectroscopic information not available by any other means. Suppose the parent state is a neutron coupled to an excited core. For example, in ^{90}Zr(p,p) and ^{90}Zr(p,p′) (Moore et al., 1967) analogue states are observed that are identified as the $5/2^+$, $1/2^+$, and $3/2^+$ resonances in the elastic data. At approximately 1.75 MeV higher in energy than the corresponding elastic resonances, large anomalies are observed in the inelastic channel, these latter resonances are identified as analogue states of neutron coupled to the 1.75 MeV 0^+ level in ^{90}Zr. Thus, one may think of inelastic decay from an analogue state as similar to performing a (d,p) reaction on a target in an excited state.

Results such as the ^{90}Zr results are related to processes involving excited core phenomena. Usually the parent states are not pure. Instead

of a pure ground state core coupled to a neutron, the parent state is more likely to have the following configuration:

$$\alpha|n_j C> + \sum_{ik} \beta_{ik}|n_k C_i^*> \tag{39}$$

where C_i^* indicates the core in the $i^{\underline{th}}$ excited state, and n_k is the neutron coupled to this core to give the same J-value as the configuration $|n_j C>$. In this picture, the analogue state wave function would have more components than those wave functions indicated in an earlier section. Applying the operator $\hat{T}^-$ to the parent state the following representation of the analogue state is obtained.

$$\hat{T}^-\{\alpha|n_j C> + \sum_{ik} \beta_{ik}|n_k C_i^*>\} \tag{40}$$

$$= \alpha(2T_o+1)^{-1/2}\{|p_j C> + (2T_o)^{1/2}|n_j A>\}$$

$$+ \sum_{ik} \beta_{ik}(2T_o+1)^{-1/2}\{|p_k C_i^*> + (2T_o)^{1/2}|n_k A_i^*>\} .$$

Consider the first component, $1/\sqrt{(2T_o + 1)}|p_j C>$. This component has as one mode of decay $p_j + |C>$ with an associated width proportional to $\alpha^2/(2T_o + 1)$. This matrix element is analogous to the (d,p) matrix element relating the parent configuration $|n_j C>$ to the core $|C>$. The spectroscopic information in this matrix element can be compared to the (d,p) spectroscopic factor. The spectroscopic factor can be shown to be

$$S_{pp} = \frac{(2T_o+1)\Gamma_p^A}{\Gamma_p^{sp}} \tag{41}$$

where Γ_p^{sp} is the single particle width of the state and Γ_p^A is the proton width of the analogue state. Consider the analogue state configuration of

$1/\sqrt{(2T_o + 1)}\,|p_k C_i^*>$. This configuration can decay to $p_k + |C_i^*>$ with an associated width proportional to $\beta_{ik}^2/(2T_o+1)$. From this one learns about the neutron plus excited core structure of states in the parent nucleus. Analogous to the proton spectroscopic factor one can define an inelastic spectroscopic factor (as a typical recent example see Kern et al., 1973)

$$S_{pp'} = \frac{(2T_o+1)\Gamma^A_{p'}}{\Gamma^{sp}_{p'}} \quad . \tag{42}$$

To summarize, the inelastic spectroscopic factors are of particular interest since this spectroscopic information is not directly observable through any other process.

The other configurations of the analogue state involve $|n_j A>$ and $|n_k A_i^*>$. These configurations can decay by proton emission to neutron particle-hole plus core, or excited core final state configurations. Discussion of these modes of decay are beyond the scope of this dissertation.

EQUIPMENT AND PROCEDURE

These experiments were performed on the TUNL 3 MV Van de Graaff accelerator, using the high resolution system. This system has been developed over many years; a description of the basic approach is given by Parks et al. (1958). Since that time many modifications and improvements have been added. Figure 3 shows a schematic of the 3 MV accelerator and the high resolution system. The removal of the beam energy fluctuations is accomplished in two steps: first the low frequency fluctuations of the dome potential are removed and then the higher frequency fluctuations are removed.

To control the dome potential, the difference between currents on the exit slits of the analyzing magnet is used to generate a signal which modulates the current flowing to the dome of the accelerator. This difference signal modulates the grid to cathode voltage of a power triode; connected to the plate of this triode is a set of sharp needles pointing directly at the dome. The voltage on this set of needles controls the corona discharge rate. Thus the potential of the dome can be modulated to keep the beam centered on the exit slits of the analyzing magnet. The frequency response of the system is very poor because of the large capacitance of the dome. Thus this corona control can only be used to remove slow fluctuations (less than about 10 Hz).

The primary fast fluctuations in the beam energy have frequencies of 60 and 400 Hz. The method used to correct for these fast fluctuations (Parks et al., 1964) operates as follows: the beam from the accelerator has two components, an atomic and a molecular hydrogen beam. These two components are separated by the analyzing magnet. The proton (atomic)

Figure 3 Floor plan of the 3 MV Van de Graaff laboratory showing the electrostatic analyzer-homogenizer system

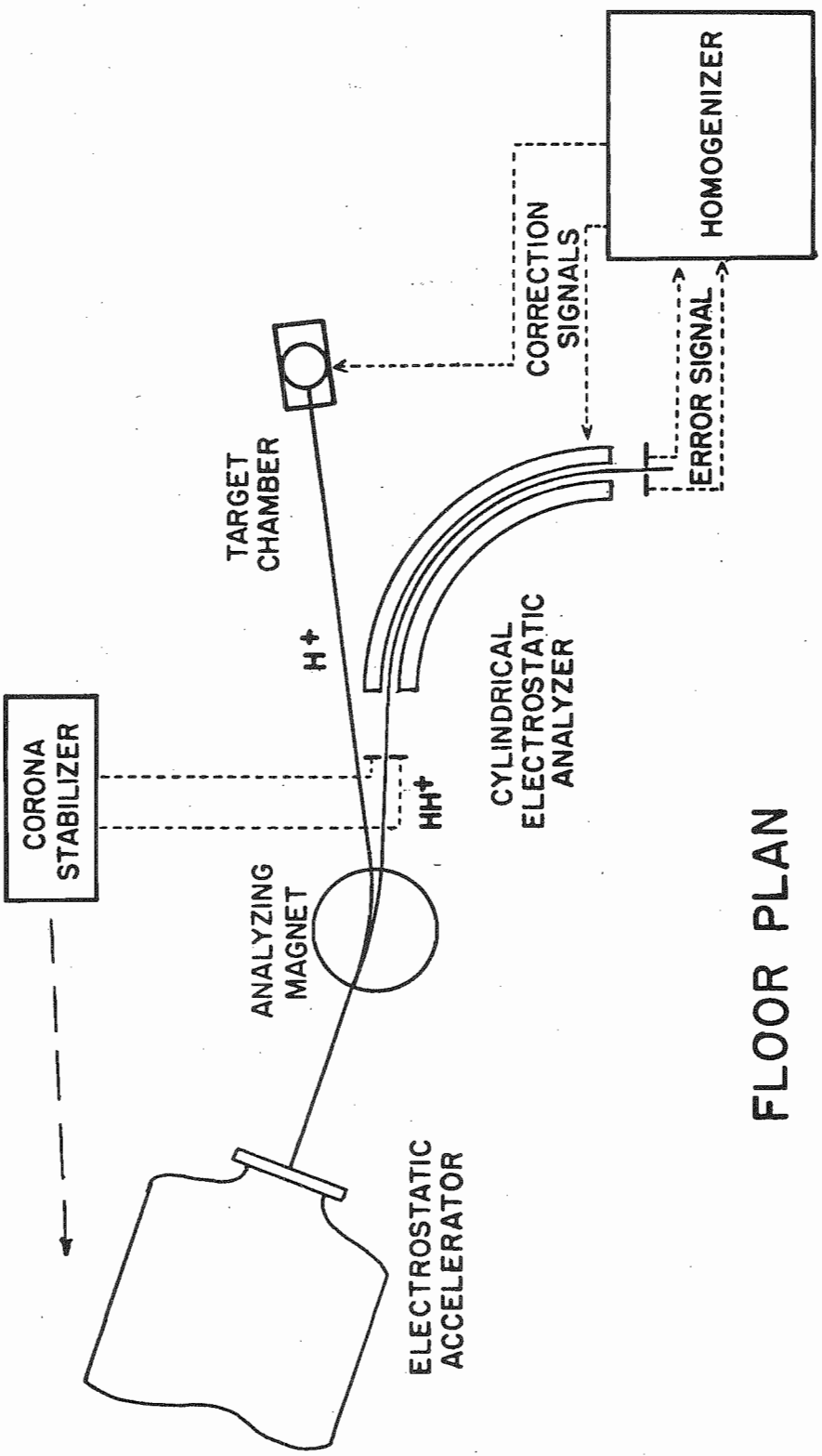
HOMOGENIZER
CORRECTION SIGNALS
ERROR SIGNAL
TARGET CHAMBER
H+
CYLINDRICAL ELECTROSTATIC ANALYZER
CORONA STABILIZER
HH+
ANALYZING MAGNET
ELECTROSTATIC ACCELERATOR

FLOOR PLAN

beam strikes the target while the HH^+ (molecular) beam enters the cyclindrical electrostatic analyzer. The deflecting potential for the electrostatic analyzer is provided by a very stable, high voltage power supply connected to the inner plate of the analyzer. The difference of currents on the two exit slits of the electrostatic analyzer is measured by a high gain difference amplifier. The output of this amplifier controls a voltage which is applied to the outer plate of the cylindrical analyzer. As the HH^+ beam changes energy, the image of the entrance slits move across the exit slits. The resulting signal to the outer plate changes the applied potential to force the beam back towards the center of the exit slits. If the gain of the amplifier is sufficiently high, the beam will be centered on the exit slits essentially all of the time.

Since the energy of a beam of charged particles which passes through the center of the entrance and exit slits is proportional to the voltage across the plates (Bondelid and Kennedy, 1958), the voltage fluctuations on the outer plate are a direct measure of the energy fluctuations of the HH^+ beam. The constant of proportionality is determined by the geometry of the particular analyzer. The constant for the analyzer used on the TUNL 3 MV accelerator is 111 (Toller, 1954). Thus, if the outer plate voltage is multiplied by 111 and applied to the target, the fast energy fluctuations in the beam are removed. This assumes neglible phase lag between the target and outer plate voltages, in practice this phase lag is not significant for frequencies of a few hundred Hz . Figure 4 shows the voltages applied to the outer plate and target tracking.

Seibel (1968) added a circuit to correct for slow, long term drifts in the high voltage power supply. The circuit measures a voltage at the

Figure 4 Energy fluctuations and correction signals

(a) shows the voltage applied to the outer plate (solid line) of the analyzer tracking the voltage fluctuations of the dome (broken line)

(b) shows the target voltage (dashed line) tracking the outer plate voltage (solid line)

(In this figure the target voltage is divided by 111.

a)

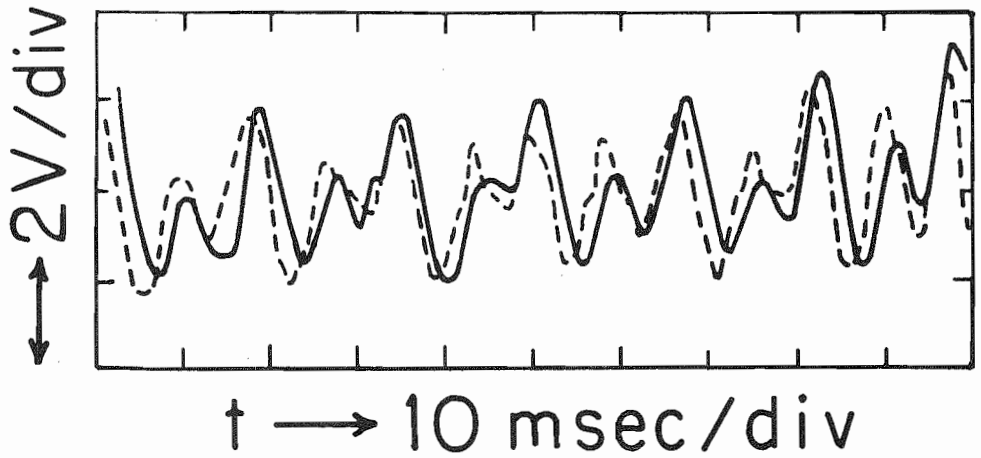

b)

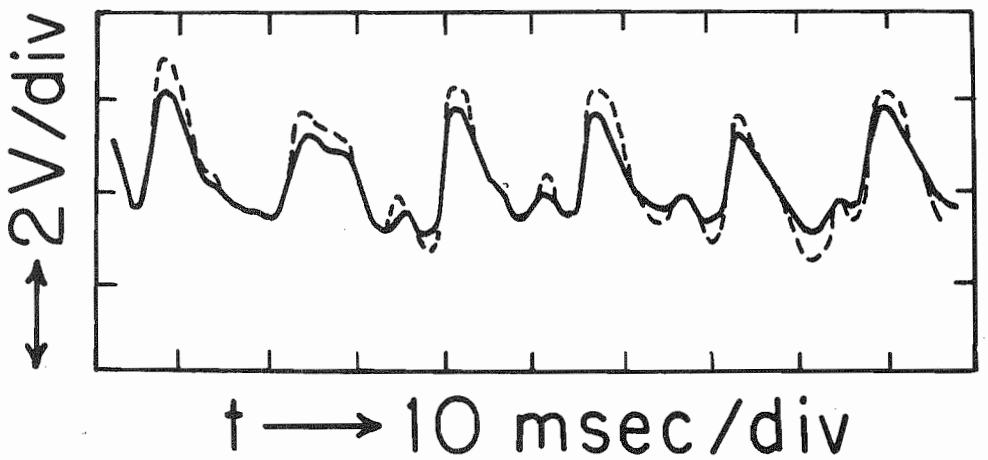

bottom of the shielded stack (to which the high voltage power supply is connected) with a precision digital voltmeter. Fluctuations in this voltage are proportional to the instabilities in the power supply. The recorder output of the voltmeter is amplified and added to the outer plate to correct for the slow, long term drifts in the power supply. Figure 5 shows the current electronics associated with the homogenizer and analyzer systems.

Energy Calibration

The energy calibration of the accelerator is determined by measuring the $^{7}Li(p,n)^{7}Be$ threshold; this threshold is taken to be 1880.6 $\pm$ 0.07 KeV (Marion and Young, 1968). Figure 6 shows the $^{44}Ca(p,p)$, $^{44}Ca(p,\gamma)^{45}Sc$, and the $^{7}Li(p,n)^{7}Be$ excitation functions in the region of the $^{7}Li(p,n)$ threshold. The procedure adopted in these measurements was as follows: the molecular beam was not removed from the analyzer throughout the measurements. After approximately eight hours, the analyzer reached an equilibrium temperature and energy shifts were no longer observed. Elastic and capture data were measured under these conditions. Following these measurements the $^{7}Li(p,n)^{7}Be$ counters were used to measure the neutron threshold at 0°. Following this threshold measurement, the $1/2^{+}$ level at 1.884 MeV in $^{44}Ca(p,p)$ was again measured; no measureable shift in energy was found. Therefore the energy of this level is known to the accuracy of the $^{7}Li(p,n)^{7}Be$ threshold plus or minus 200 eV.

Figure 5 Current electronic circuit of the electrostatic analyzer-homogenizer system

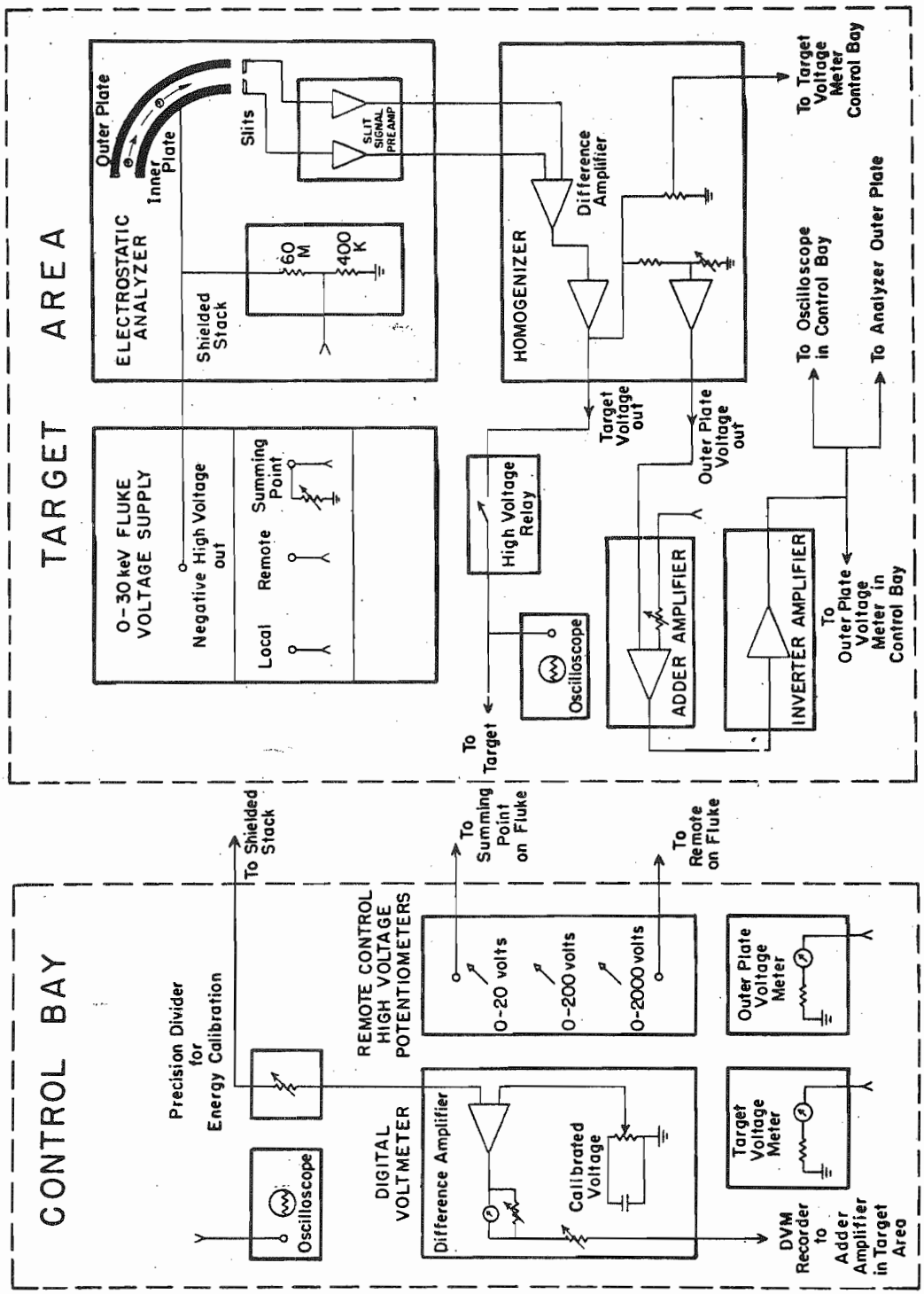
TARGET AREA
ELECTROSTATIC ANALYZER
Outer Plate
Inner Plate
Slits
SLIT SIGNAL PREAMP
Shielded Stack
60 M
400 K
0-30 keV FLUKE VOLTAGE SUPPLY
Negative High Voltage out
Local
Remote
Summing Point
HOMOGENIZER
Difference Amplifier
To Target Voltage Meter Control Bay
To Oscilloscope in Control Bay
To Analyzer Outer Plate
Target Voltage out
Outer Plate Voltage out
High Voltage Relay
Oscilloscope
To Target
ADDER AMPLIFIER
INVERTER AMPLIFIER
To Outer Plate Voltage Meter in Control Bay
CONTROL BAY
To Shielded Stack
Precision Divider for Energy Calibration
Oscilloscope
REMOTE CONTROL HIGH VOLTAGE POTENTIOMETERS
To Summing Point on Fluke
To Remote on Fluke
0-20 volts
0-200 volts
0-2000 volts
DIGITAL VOLTMETER
Difference Amplifier
Calibrated Voltage
Outer Plate Voltage Meter
Target Voltage Meter
DVM Recorder to Adder Amplifier in Target Area

Figure 6 $^{44}Ca(p,\gamma)^{45}Sc$ and $^{44}Ca(p,p)^{44}Ca$ excitation functions in the region of the $^{7}Li(p,n)^{7}Be$ threshold; the lines through the data are intended as visual aids and not as a fit to the data

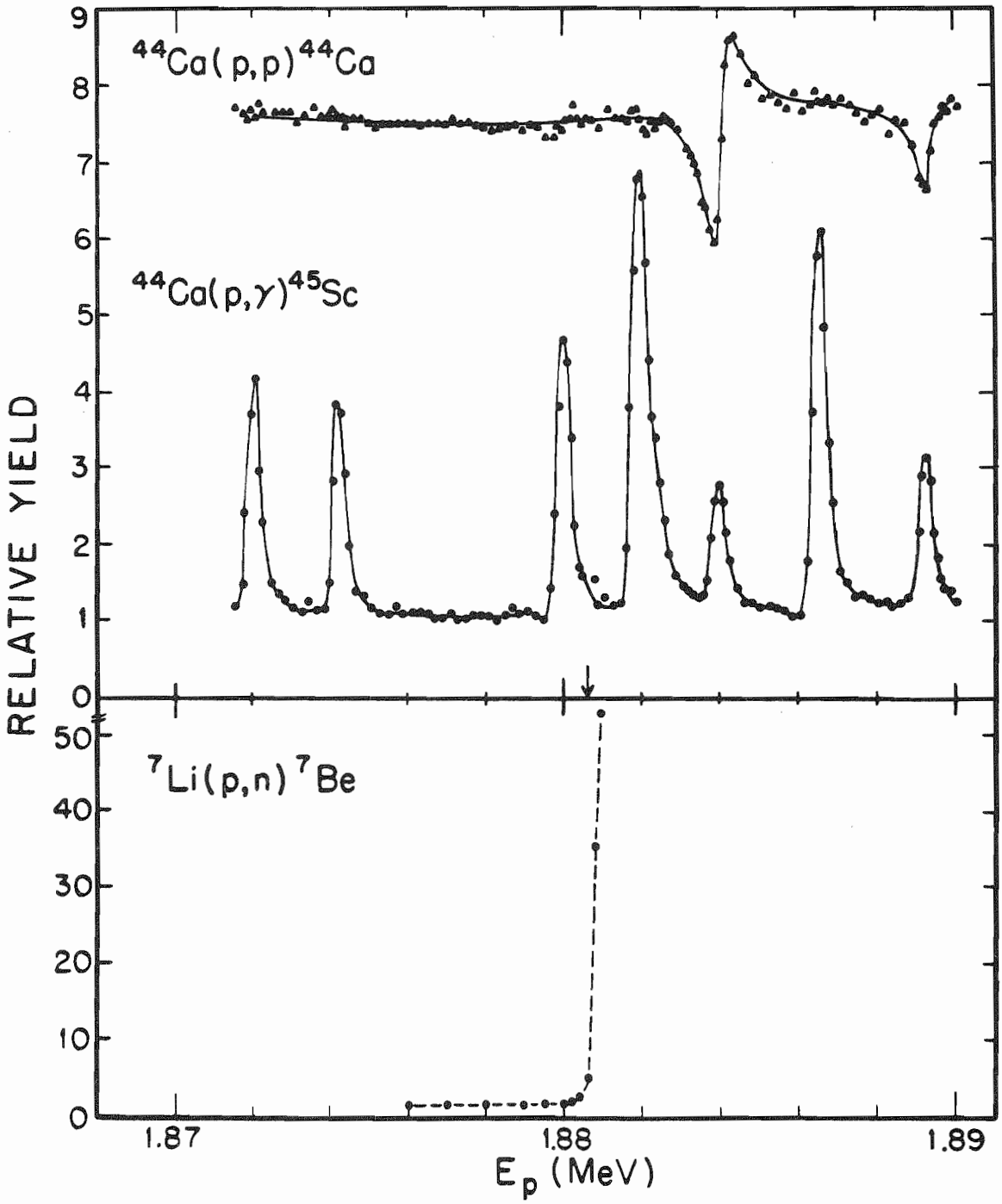
$^{44}Ca(p,p)^{44}Ca$
$^{44}Ca(p,\gamma)^{45}Sc$
$^{7}Li(p,n)^{7}Be$
RELATIVE YIELD
0
1
2
3
4
5
6
7
8
9
10
20
30
40
50
1.87
1.88
1.89
E_p (MeV)

Energy Shifts

To avoid repeating this measurement daily, sequential data runs were overlapped by repeating a known resonance near the end of the previous day's data. Since measurements by Wilson (1973) and experience from early capture experiments have shown the energy shifts to be nearly a linear function of time the following procedure was adopted to correct for energy shifts in the capture excitation functions: data were taken only after the molecular beam had been in the analyzer for about three hours, then data were taken continuously for 16-20 hours. While taking the data with the Ge(Li) detector, data were taken continuously. Observed energy shifts between runs were corrected using the following equation

$$E_{r'} = E_r + \delta\left(1 - \frac{E_\ell - E_\ell}{75}\right) \quad |E_\ell - E_r| \leq 75 \text{ KeV} \tag{43}$$

$$E_{r'} = E_r \quad |E_\ell - E_r| > 75 \text{ KeV}$$

where

E_r is the energy of the resonance as measured in the present run,

E_ℓ is the energy of the last resonance in the previous run, and

δ is the difference between the resonance energy in the last run and the same resonance in the present run. Delta was typically less than 300 eV.

Scattering Chambers

Two scattering chambers were used in the present experiments. The scattering chamber used for the elastic scattering measurements was designed to permit the use of solid targets (Browne, 1969). A typical vacuum during the elastic scattering experiments was on the order of 5×10^{-7} torr.

A new, smaller chamber was designed for the capture experiments. This chamber is now permanently installed about 4 meters behind the existing elastic scattering chamber. Since previous work by Peters (1972) and early work on ^{62}Ni indicated problems with target deterioration and with target voltage breakdown, the new chamber was designed with a separate pumping station in order to maintain a high vacuum. A cold surface, at liquid nitrogen temperature, surrounds the target. This arrangement reduces the problem with carbon build-up on the target surface and improves the ultimate vacuum attainable in the chamber. A new collimating system was designed for use with the new chamber. To reduce the amount of fluorine in the system, molybdenum was used for the limiting slits instead of tantalum (tantalum is usually processed with hydrofluoric acid and the resulting fluorine contaminant is very troublesome). A typical vacuum in the new chamber (used for the $^{44}Ca(p,\gamma)^{45}Sc$ experiment) was less than 5×10^{-7} torr. With this vacuum target life increased by a factor of three over the target life in the $^{62}Ni(p,\gamma)^{63}Cu$ experiment. The new pumping station, collimator, and chamber are described in detail in the Appendix.

Detectors

Both charged particle and gamma-ray detectors were used in this experiment. The charged particle detector was an Ortec silicon surface barrier detector with an active area of 50 $(mm)^2$, a depletion depth of 300 microns, and a resolution of 14 keV. The gamma-ray detectors were a NaI(Tl) crystal and a lithium drifted germanium (Ge(Li)) detector. The NaI(Tl) detector was a 10.2 cm by 10.2 cm cylindrical crystal mounted on a RCA 8555 phototube. This unit, obtained from the Harshaw Chemical Company, had a resolution of 9% at the 662 keV line of ^{137}Cs. The bias voltage for best resolution was found empirically to be + 1100 V. The Ge(Li) detector had an active volume of 80 cm^3 (as specified by Princeton Gamma-Tech). For the $^{62}Ni(p,\gamma)^{63}Cu$ experiment the bias was set to -2000 volts and the observed resolution was 4 keV at the 1332 keV line of ^{60}Co. Following the ^{62}Ni experiment a new preamplifier was installed on the detector by Princetor Gamma Tech. With this modification, the bias was changed to -2300 volts and the resolution quoted by the manufacturer was 2.84 keV at 1332 keV . Also, the manufacturer quotes a peak to Compton ratio of 22.7 and an efficiency of 11.4% relative to a NaI crystal. In the $^{44}Ca(p,\gamma)^{45}Sc$ experiment a resolution of 2.87 keV was measured for the 1332 keV line of ^{60}Co.

Peters (1972) measured an absolute efficiency curve for this detector. In the present experiments the efficiency was remeasured in the new chamber after the modifications to the detector. Agreement with previous calibration work was excellent. In the process of measuring the efficiency both calibrated sources and the $^{27}Al(p,\gamma)^{28}Si$ resonances at

992, 1381, and 1388 keV were used. In the ^{44}Ca experiment, the Ge(Li) detector was 2.54 cm closer to the target chamber than in the ^{62}Ni experiment. The efficiency was remeasured in this geometry. Relative efficiencies were unaffected but the absolute efficiency increased by a factor of 1.79. Detector geometries as used in the $^{62}Ni(p,\gamma)^{63}Cu$ are illustrated in Figure 7 and Figure 8 shows the absolute efficiency as measured in this geometry.

Electronics and Computer

In the present experiments data were recorded with the digital read-out system developed by Lindstrom (1970) and/or with the TUNL on-line computer. The electronics for the elastic scattering measurements are shown schematically on Figure 9. The system was developed for the high resolution elastic scattering program at TUNL and its operation is described elsewhere (Browne, 1969 and Lindstrom, 1970). Figure 10 shows a block schematic of the electronics associated with the NaI(Tl) and Ge(Li) detectors. The electronics for both detectors are quite similar. Signals from the Ge(Li) detector were amplified by a Princeton Gamma Tech preamp model RG-11 which was mounted on the crystal (the field effect transistor (FET) was not cooled) and by a Canberra model 1417 or 1413 Spectroscopy amplifier. These signals were then processed by a Northern Scientific analog-to-digital converter (ADC). The gain of the amplifiers and the zero levels of the ADC were adjusted to give an approximate gain of 2 keV/channel and a zero level of 400 keV . The TUNL on-line computer was used to store a 4096 channel spectrum and to

Figure 7 Schematic of the target chamber showing detector geometries used in the $^{62}Ni(p,\gamma)^{63}Cu$ experiment

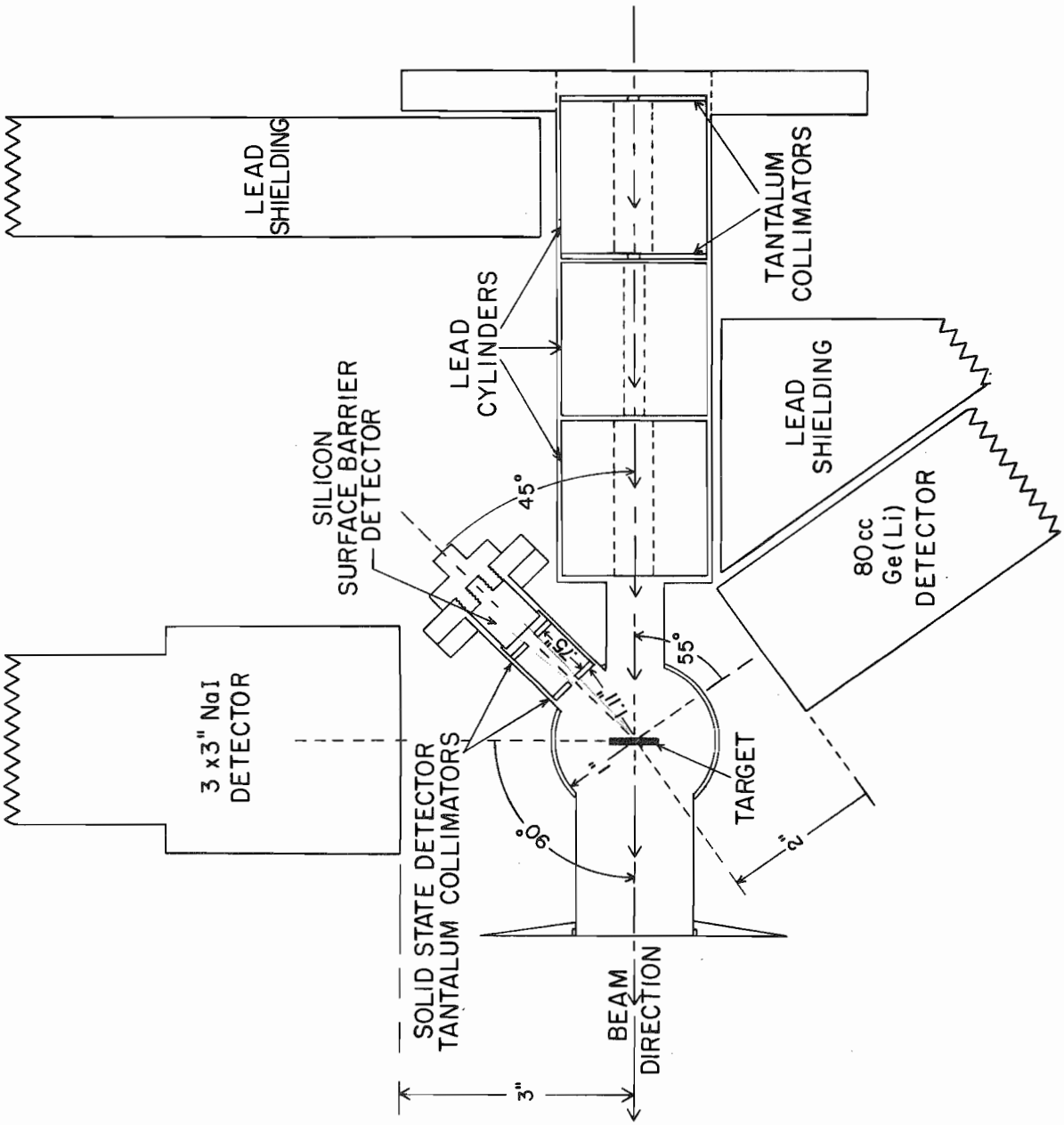
LEAD SHIELDING
TANTALUM COLLIMATORS
LEAD CYLINDERS
SILICON SURFACE BARRIER DETECTOR
45°
LEAD SHIELDING
80 cc Ge(Li) DETECTOR
55°
3 x 3" NaI DETECTOR
TARGET
90°
SOLID STATE DETECTOR TANTALUM COLLIMATORS
BEAM DIRECTION
3"

Figure 8 Absolute efficiency curve for the 80 cm^3 Ge(Li) detector in the geometry shown in Figure 7

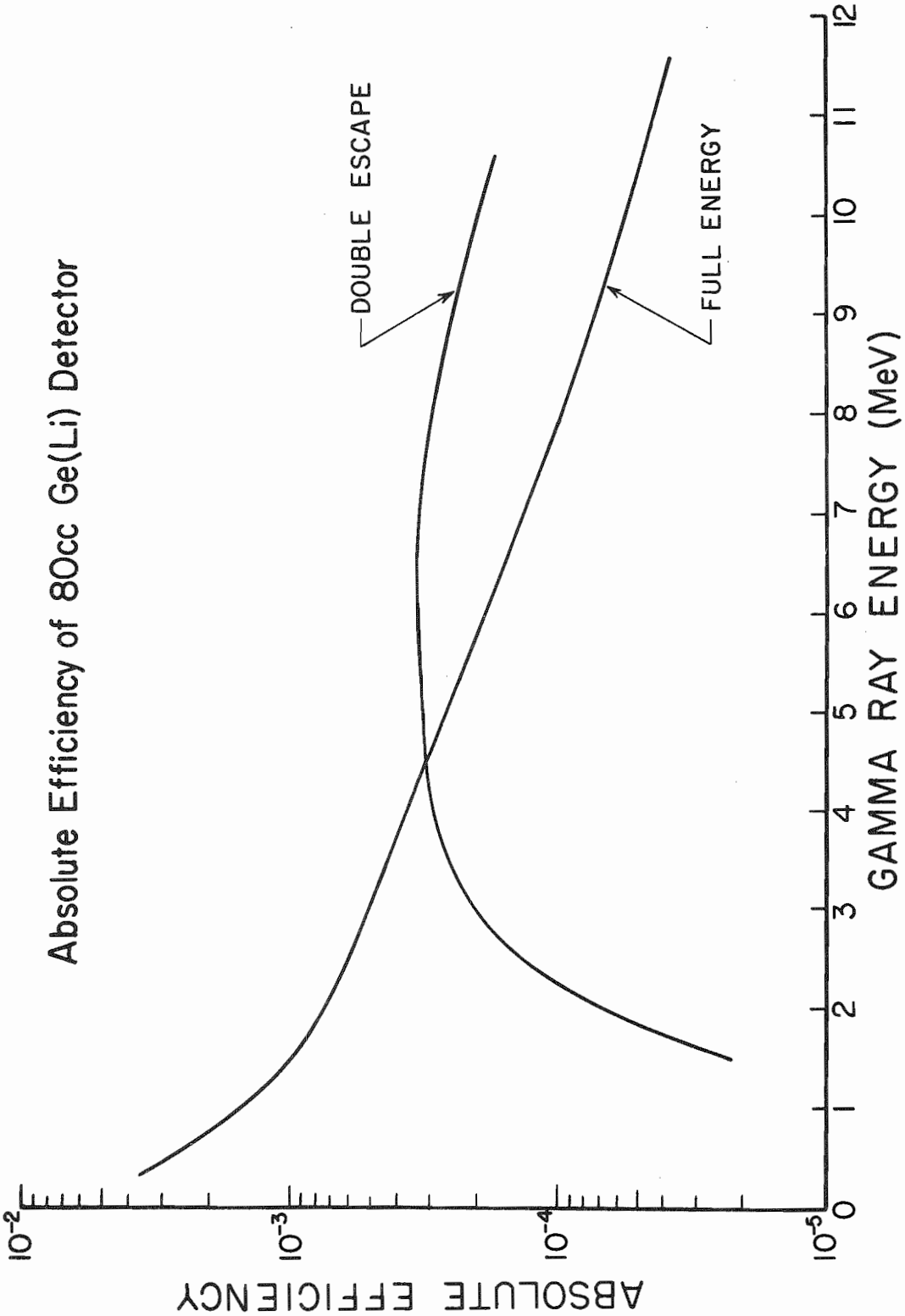
Absolute Efficiency of 80cc Ge(Li) Detector
DOUBLE ESCAPE
FULL ENERGY
ABSOLUTE EFFICIENCY
GAMMA RAY ENERGY (MeV)
10^-2
10^-3
10^-4
10^-5
0
1
2
3
4
5
6
7
8
9
10
11
12

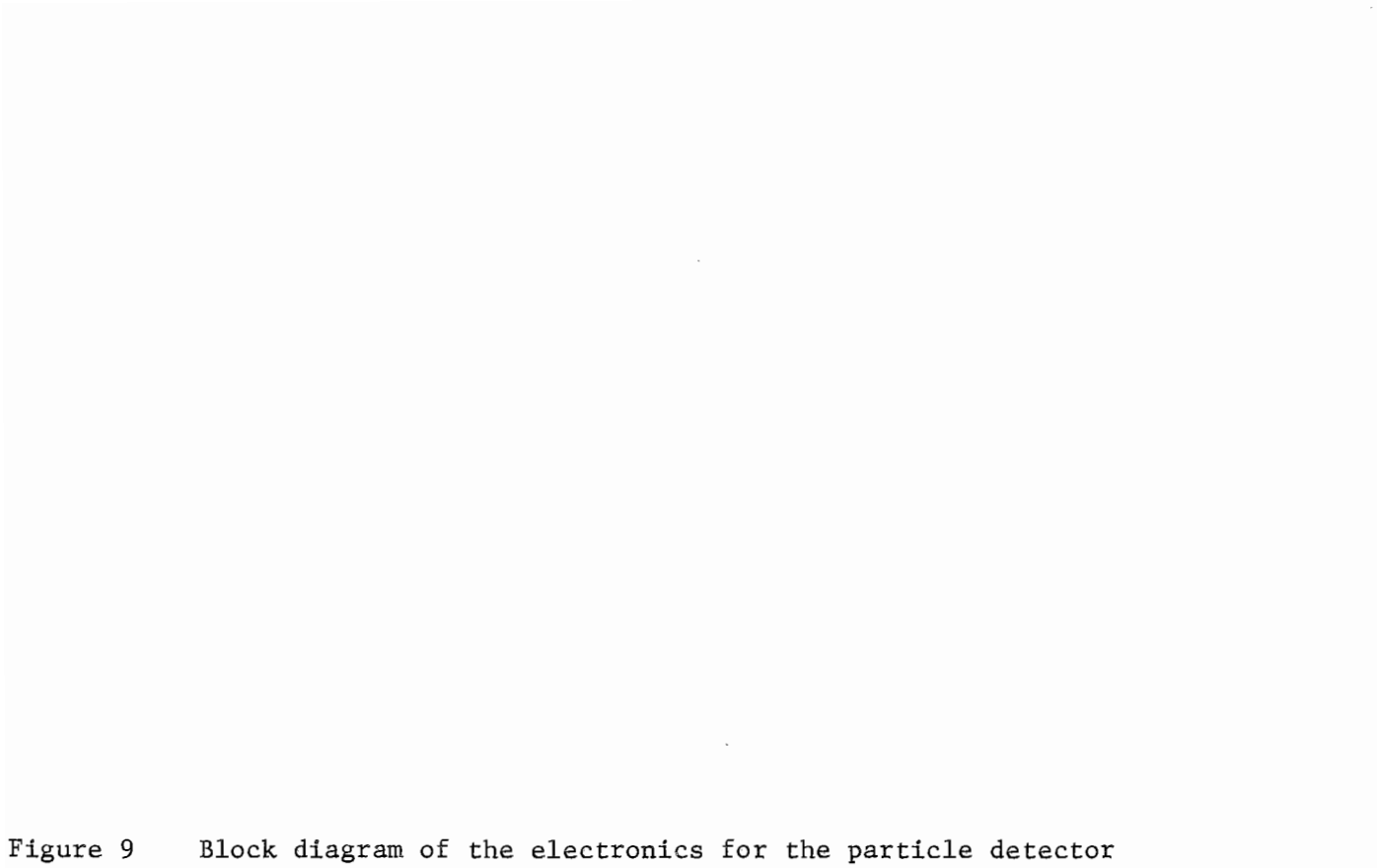

Figure 9 Block diagram of the electronics for the particle detector

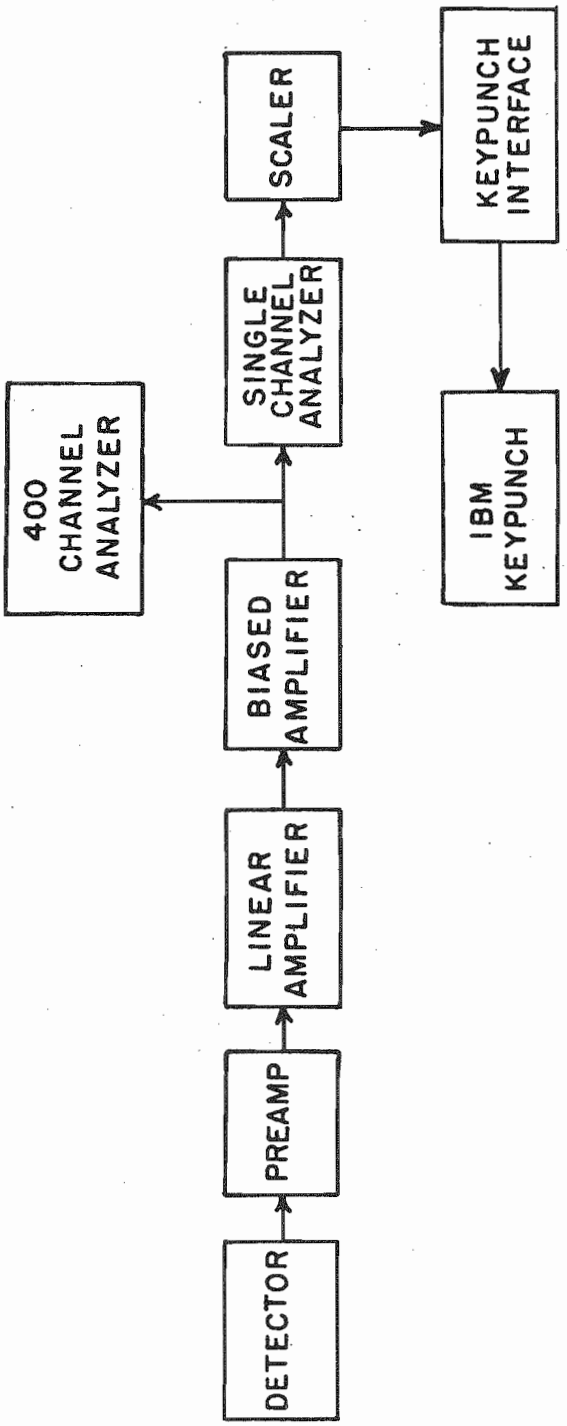
DETECTOR
PREAMP
LINEAR AMPLIFIER
BIASED AMPLIFIER
400 CHANNEL ANALYZER
SINGLE CHANNEL ANALYZER
SCALER
KEYPUNCH INTERFACE
IBM KEYPUNCH

Figure 10 Block diagram showing the electronics associated with the Ge(Li) and NaI(Tl) detectors

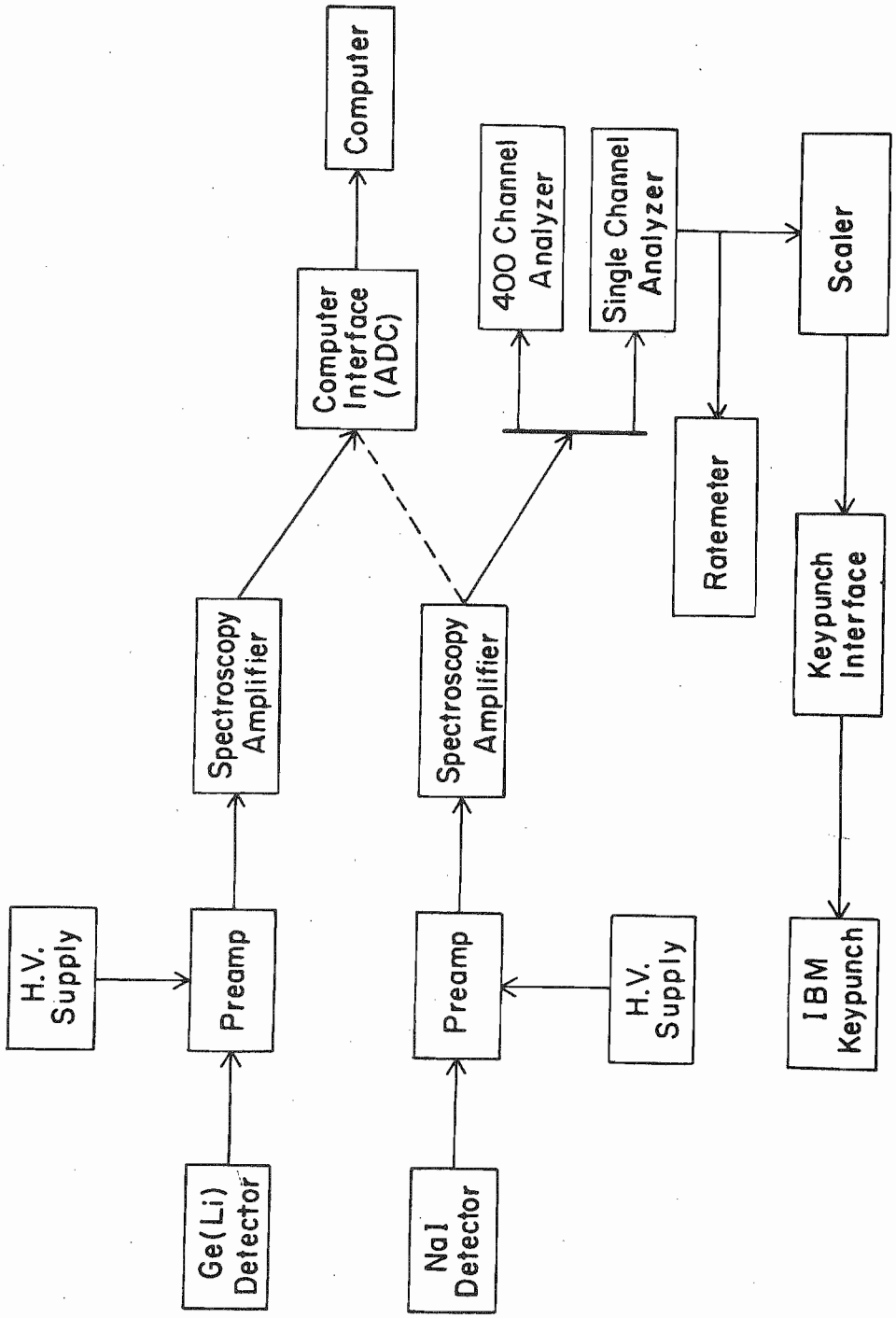
Computer
Computer Interface (ADC)
400 Channel Analyzer
Single Channel Analyzer
Scaler
Ratemeter
Keypunch Interface
IBM Keypunch
Spectroscopy Amplifier
Spectroscopy Amplifier
H.V. Supply
Preamp
Preamp
H.V. Supply
Ge(Li) Detector
NaI Detector

provide an on-line display. For the NaI(Tl) system an Ortec model 113 preamp was used and the computer stored a 512 channel spectrum.

While the Ge(Li) spectra were being accumulated, it was necessary to monitor the fraction of the time that the ADC was busy and could not analyze incoming signals. This fraction is commonly called "ADC dead time" or just "dead time". Figure 11 shows a schematic of the system designed to measure this so-called "dead time". The basic elements are two scalers and a 60 cycle pulser. One scaler counts continuously whenever the ADC is turned on; the other scaler counts only while the ADC is not busy. Typical values for ADC dead time in this experiment were about 2-3%.

Target Preparation

Targets were prepared by evaporation of enriched $CaCo_3$ powder and Ni metal onto 5-10 $\mu g/cm^2$ carbon foils. The specific enrichments are listed in Table 1. Since Ni forms a low melt eutectic with various metals, a 10 mil molybdenum boat with a coating of Al_2O_3 was used for the evaporation of Ni. For $CaCO_3$ best results were obtained by using equal parts of $CaCO_3$ and tantalum powder in a closed tantalum boat (the tantalum powder was an effective reducing agent). Figures 12 and 13 show typical charged particle spectra for $^{62}Ni + p$ and $^{44}Ca + p$, respectively. Target thicknesses for these experiments were from 0.5 to 3 $\mu g/cm^2$.

Data Taking Procedure

The data taking procedure adopted was as follows: first a general excitation function was measured using the 10.2 cm by 10.2 cm NaI(Tl)

Figure 11 Block diagram of the circuit to monitor "dead time"

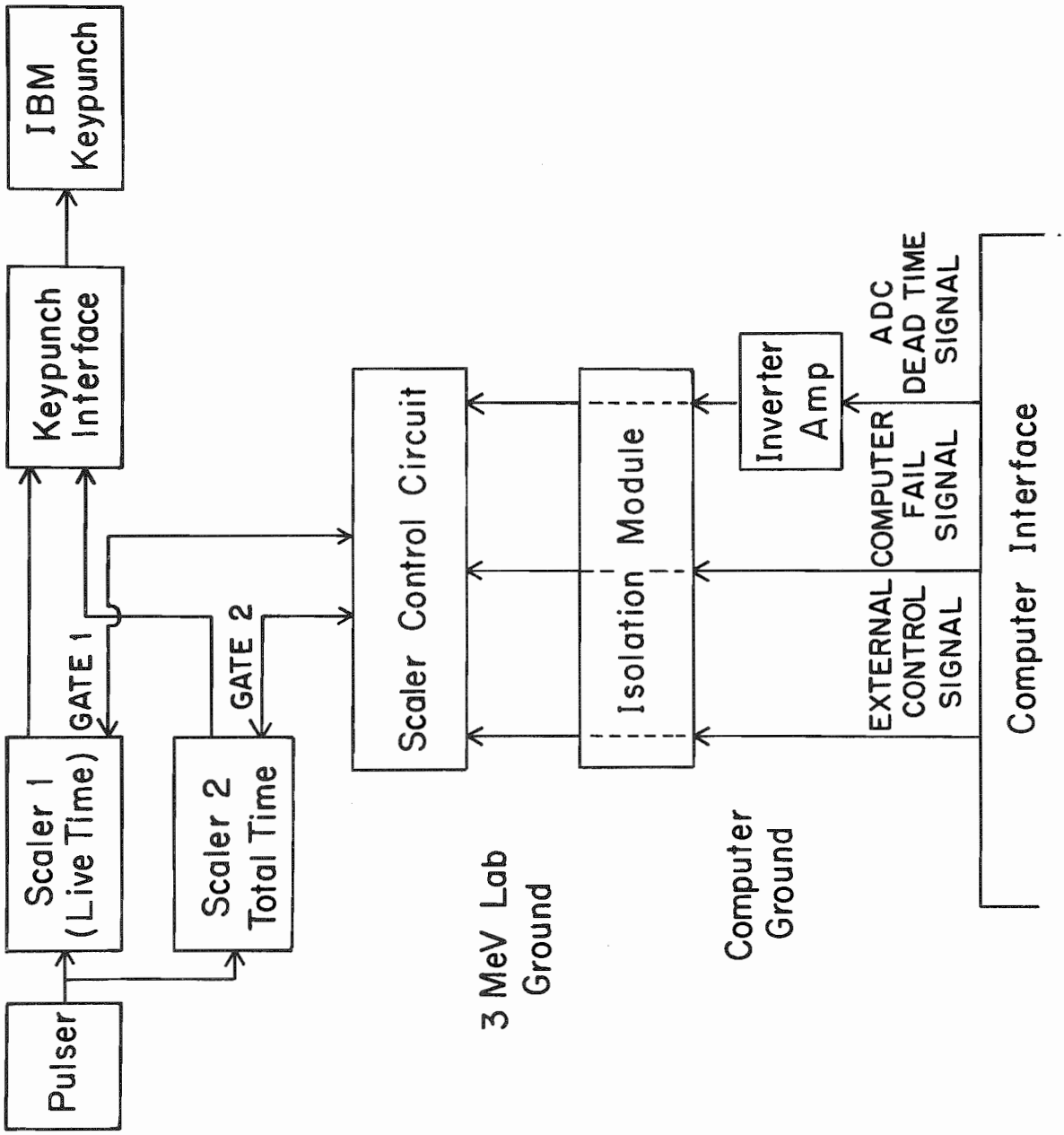
IBM Keypunch
Keypunch Interface
Scaler 1 (Live Time)
Scaler 2 Total Time
GATE 1
GATE 2
Pulser
Scaler Control Circuit
Isolation Module
Inverter Amp
ADC DEAD TIME SIGNAL
COMPUTER FAIL SIGNAL
EXTERNAL CONTROL SIGNAL
Computer Interface
3 MeV Lab Ground
Computer Ground

Table 1 Isotopic composition of samples

Isotope	% Enrichment	Contaminant	%
^{44}Ca	98.55	^{40}Ca	1.36
($CaCo_3$ Powder)		^{42}Ca	0.06
		^{43}Ca	0.04
		^{46}Ca	<0.01
		^{48}Ca	<0.01
^{62}Ni	98.83	^{58}Ni	0.32
(Metal)		^{60}Ni	0.63
		^{61}Ni	0.13
		^{64}Ni	0.09

Figure 12 A typical charged particle spectrum for protons scattered from a ^{44}Ca target on a carbon foil

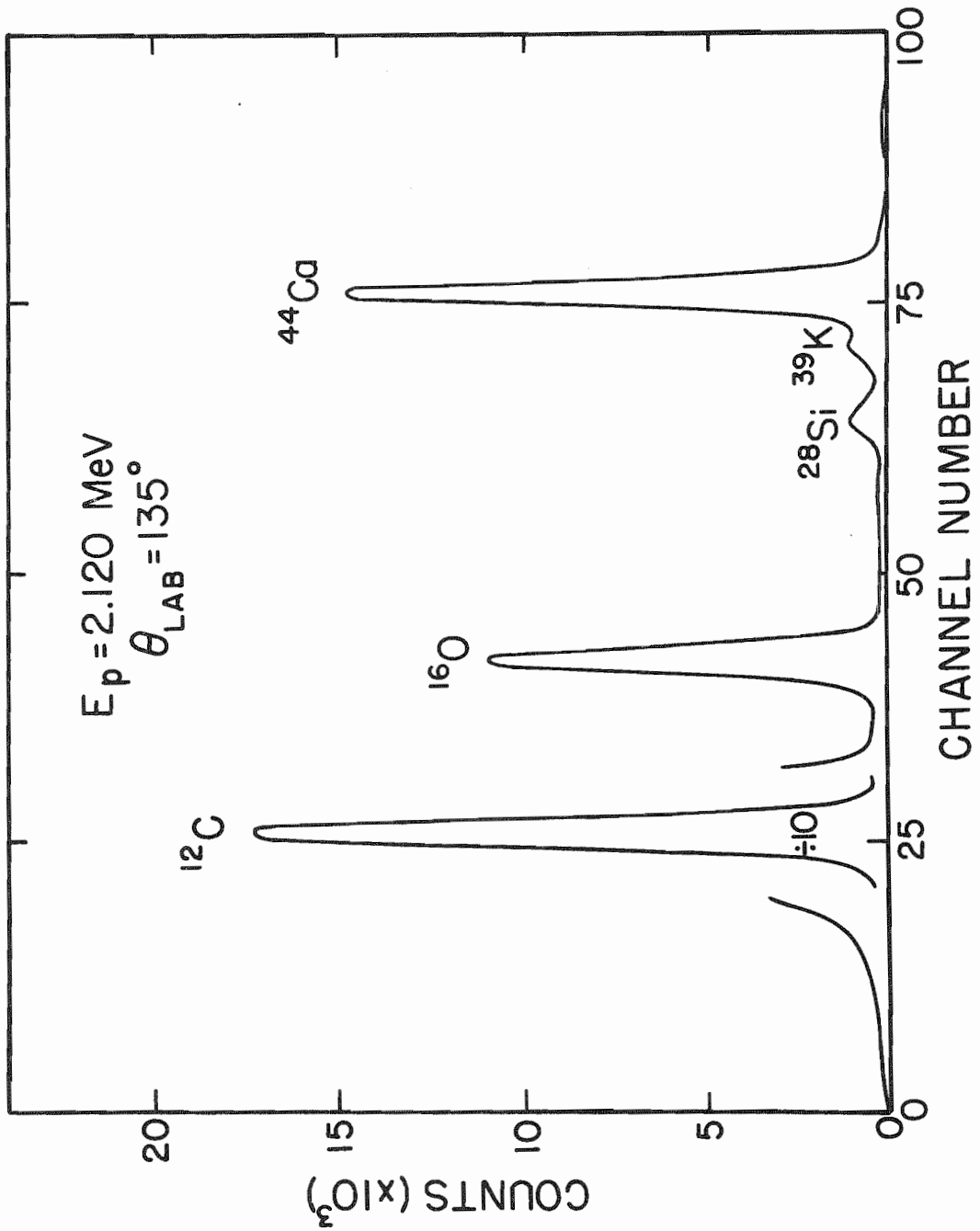
COUNTS (x10³)
CHANNEL NUMBER
E_p = 2.120 MeV
θ_LAB = 135°
÷10
12C
16O
28Si
39K
44Ca
0
5
10
15
20
25
50
75
100

Figure 13 A typical charged particle spectrum for protons scattered from a ^{62}Ni target on a carbon foil

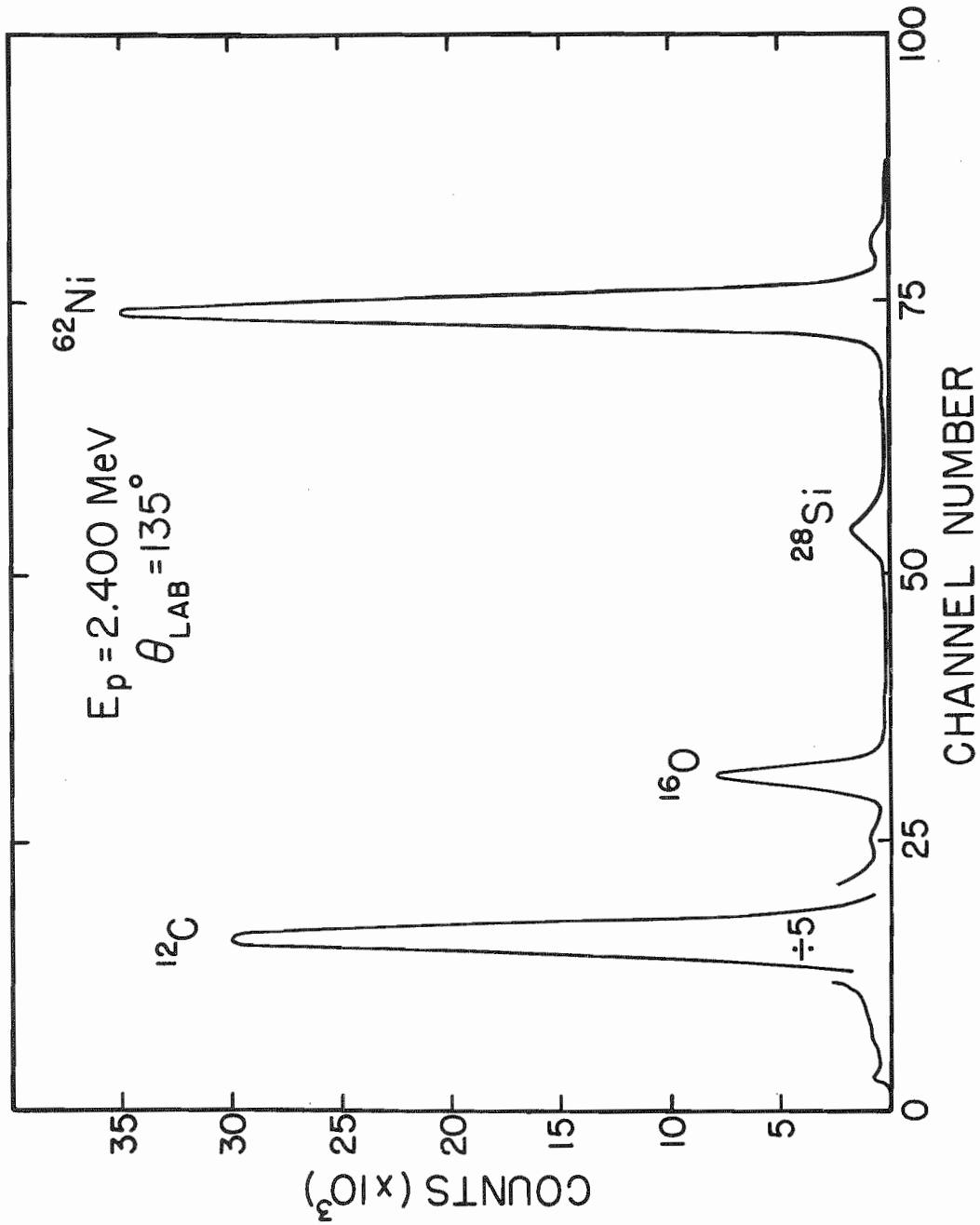
$E_p = 2.400$ MeV
$\theta_{LAB} = 135°$
^{62}Ni
^{28}Si
^{16}O
^{12}C
÷5
COUNTS (x10³)
CHANNEL NUMBER
0
25
50
75
100
5
10
15
20
25
30
35

detector with the spectra at each energy written on to magnetic tape. Simultaneously, the elastic cross section was measured with the particle detector to aid in identifying the particular capture resonance. Then, immediately before obtaining a detailed Ge(Li) spectrum for a particular resonance, an excitation function in the region of interest was measured with the NaI crystal. The yield was recorded on cards. At the end of each run the Ge(Li) spectrum was written on to magnetic tape, and dead time and other parameters needed for further analysis were recorded. The capture excitation functions taken prior to each run were used to find the area to peak height ratio, which was used in the computation of the absolute gamma-ray widths (see Chapter 4), as well as monitoring target deterioration.

DATA REDUCTION AND PRELIMINARY ANALYSIS

Analysis of these capture data involves two distinct stages: first obtaining the partial gamma-ray widths and second, treating these widths collectively. In this chapter, reduction of the data is discussed and preliminary analyses presented. Examination of the results for both statistical properties and for spectroscopic information will be discussed in Chapter 5.

The partial gamma-ray widths are calculated with an equation valid for thin targets (Gove, 1959).

$$\frac{(2J+1)}{(2J_1+1)(2J_o+1)} \frac{\Gamma_p \Gamma_\gamma}{\Gamma} = \frac{2\varepsilon}{\lambda^2} \left(\frac{Y}{T}\right) \tag{44}$$

where

J_o = spin of target

J_1 = spin of projectile

J = spin of resonance

Γ_p = proton partial width in eV

Γ_γ = gamma-ray partial width in eV

Γ = total width in eV

T = target thickness in eV ($T = t\, dE/dx$, t in $\mu g/cm^2$)

Y = yield (Area of resonance in units of reactions per incident particle times energy)

ε = stopping power of target in units of eV cm^2 (ε = 1/B dE/dx)

λ = center of mass wavelength in cm .

Specializing for protons ($J_1 = 1/2$) on a spin zero target ($J_o = 0$) , one obtains

$$(45) \qquad (2J+1)\frac{\Gamma_p \Gamma_\gamma}{\Gamma} = \frac{4\varepsilon}{\lambda^2}\left(\frac{Y}{T}\right) .$$

The parameters Γ_p and J are determined from elastic scattering experiments. Usually these were taken from previous work, Wilson (1973) for the ^{45}Sc parameters and Browne (1969) for the ^{63}Cu parameters. The constant B relates the energy loss per unit target thickness and the stopping power of the target; this parameter is taken from a compilation by Marion (1960). The target thickness was determined by measuring the Rutherford scattering cross section in a known geometry. The yield Y is obtained from the following equation

$$(46) \qquad Y = \frac{N\ R\ (\text{Area})}{\text{Eff}(E_\gamma)\cdot(\#\ \text{of Incident Particles})}$$

where N is a correction factor to account for the deadtime, R is the area to peak height ratio. The number of incident particles is determined from the integrated beam current and the efficiency of the detector was taken from the calibration previously discussed.

$^{44}Ca(p,\gamma)^{45}Sc$

Excitation functions for $^{44}Ca(p,p)^{44}Ca$ and $^{44}Ca(p,\gamma)^{45}Sc$ were were measured from 1.56 to 2.28 MeV with an overall proton energy resolution of 300-350 eV . The elastic scattering data were monitored at

an angle of 135° in order to identify the capture resonances corresponding to particular elastic resonances. All of the proton resonances analyzed by Wilson (1973) in this energy range were resolved in the present experiment. Nearest neighbor spacings measured in the excitation function were in excellent agreement with Wilson's results; however, there was a difference in the absolute energy of 6.3 keV . Since the present calibration was carefully measured twice using the $^{7}Li(p,n)^{7}Be$ threshold, (see discussion in Chapter 3), the present calibration is thought to be correct. Wilson (1974) confirms this measurement.

The resonance parameters of all levels studied in this energy region are listed in Table 2. The inelastic and total gamma-ray widths were obtained in the present experiment, while the elastic widths are taken from Wilson's work.

The low-lying levels in ^{45}Sc are well known up to about 2 MeV . Recent work (Rust and Naudé, 1972) has made probable J-value assignments to a number of levels. These levels are listed below: 1234 keV, 11/2-; 1303 keV, $3/2^{+}$; 1409 keV, 7/2-; 1434, $(7/2, 9/2)^{+}$; 1556 keV, 1/2-; 1662 keV, (1/2, 9/2)-; and 1801 (1799) keV, $5/2^{+}$. Shown on Figure 14 is the adopted level scheme for ^{45}Sc (Nuclear Data Sheets, 1970) with some additional J-values indicated. These additional J-values are based on the above reference.

Three analogue states had been identified in this energy region of ^{45}Sc . A group of states with spin and parity 3/2- is centered at 1.65 MeV . This cluster of states is identified as the analogue of the sixth excited state of ^{45}Ca (Gaarde et al., 1966; Browne et al., 1968 ; Wilson, 1973). The group of states with spin and parity 1/2- whose centroid is

Table 2 Resonance parameters for ^{45}Sc

Ep (MeV)	J^{π}	Γ_p (eV)	$\Gamma_{p'}$ (eV)	Γ_γ (eV)
1.6236	3/2-	12	0.0	0.42
1.6324	3/2-	25	0.0	0.17
1.6460	3/2-	80	0.0	0.45
1.6517	3/2-	400	0.0	0.41
1.6646	3/2-	60	0.0	0.34
1.6681	3/2-	30	0.0	0.32
1.6774	3/2-	7	0.0	0.16
1.6782	3/2-	5	0.0	0.06
1.6822	3/2-	10	0.0	0.11
1.6925	3/2-	10	0.0	0.32
1.7022	1/2-	10	0.0	0.28
1.7303	1/2-	50	0.0	0.13
1.7418	1/2-	15	0.0	0.12
1.7671	1/2-	40	0.0	0.37
1.7797	3/2-	5	0.0	0.51
1.7994	3/2-	7	0.0	0.71
1.8101	1/2-	25	0.0	0.79
1.8170	1/2-	5	0.003	0.23
1.8268	1/2-	15	0.0	0.19
1.8492	1/2-	35	0.002	0.51
1.8648	1/2-	15	0.003	0.46
1.8693	1/2-	25	0.005	0.85
1.8892	1/2-	60	0.0	0.33

Table 2 (Continued)

Ep (MeV)	J^{π}	Γ_p (eV)	$\Gamma_{p'}$ (eV)	Γ_γ (eV)
1.9032	1/2-	10	0.009	0.91
1.9086	1/2-	100	0.006	0.28
1.9207	1/2-	50	0.021	1.61
1.9493	1/2-	75	0.042	0.56
1.9623	1/2-	35	0.008	0.32
1.9688	1/2-	20	0.004	1.38
1.9724	3/2-	7	0.033	1.14
1.9799	1/2-	10	0.038	0.52
1.9937	1/2-	400	0.018	0.29
2.0006	1/2-	35	0.005	0.10
2.0194	1/2-	175	0.010	0.28
2.0273	1/2-	240	0.099	0.40
2.0428	1/2-	53	0.267	0.50
2.0456	1/2-	350	0.207	0.31
2.0489	1/2-	63	0.180	0.61
2.0658	1/2-	242	0.568	0.75
2.0750	1/2-	35	0.068	0.86
2.0932	1/2-	64	0.082	0.28
2.1062	1/2-	19	0.150	0.55
2.1074	1/2-	15	0.220	0.61
2.1200	1/2-	60	0.066	0.29
2.1242	1/2-	30	0.061	0.81
2.1418	1/2-	48	0.016	0.55

Table 2 (Continued)

Ep (MeV)	J^{π}	Γ_p (eV)	$\Gamma_{p'}$ (eV)	Γ_γ (eV)
2.1559	$1/2^-$	40	0.024	0.26
2.1771	$1/2^-$	11	0.165	0.38
2.1992	$1/2^+$	73	0.031	0.60
2.1999	$1/2^+$	10	0.804	0.55
2.2038	$1/2^+$	20	0.329	0.88
2.2217	$1/2^+$	140	0.279	0.92
2.2421	$1/2^+$	130	0.047	0.46
2.2466	$1/2^+$	800	0.718	2.12
2.2562	$1/2^+$	35	0.098	1.16
2.2682	$1/2^+$	13	0.140	0.35
2.2793	$1/2^+$	12	1.658	0.48

Figure 14 The adopted level scheme of ^{45}Sc (Nuclear Data Tables, 1970); the spin assignments for the levels at 1237, 1302, and 1557 KeV are from Rust and Naudé (1972)

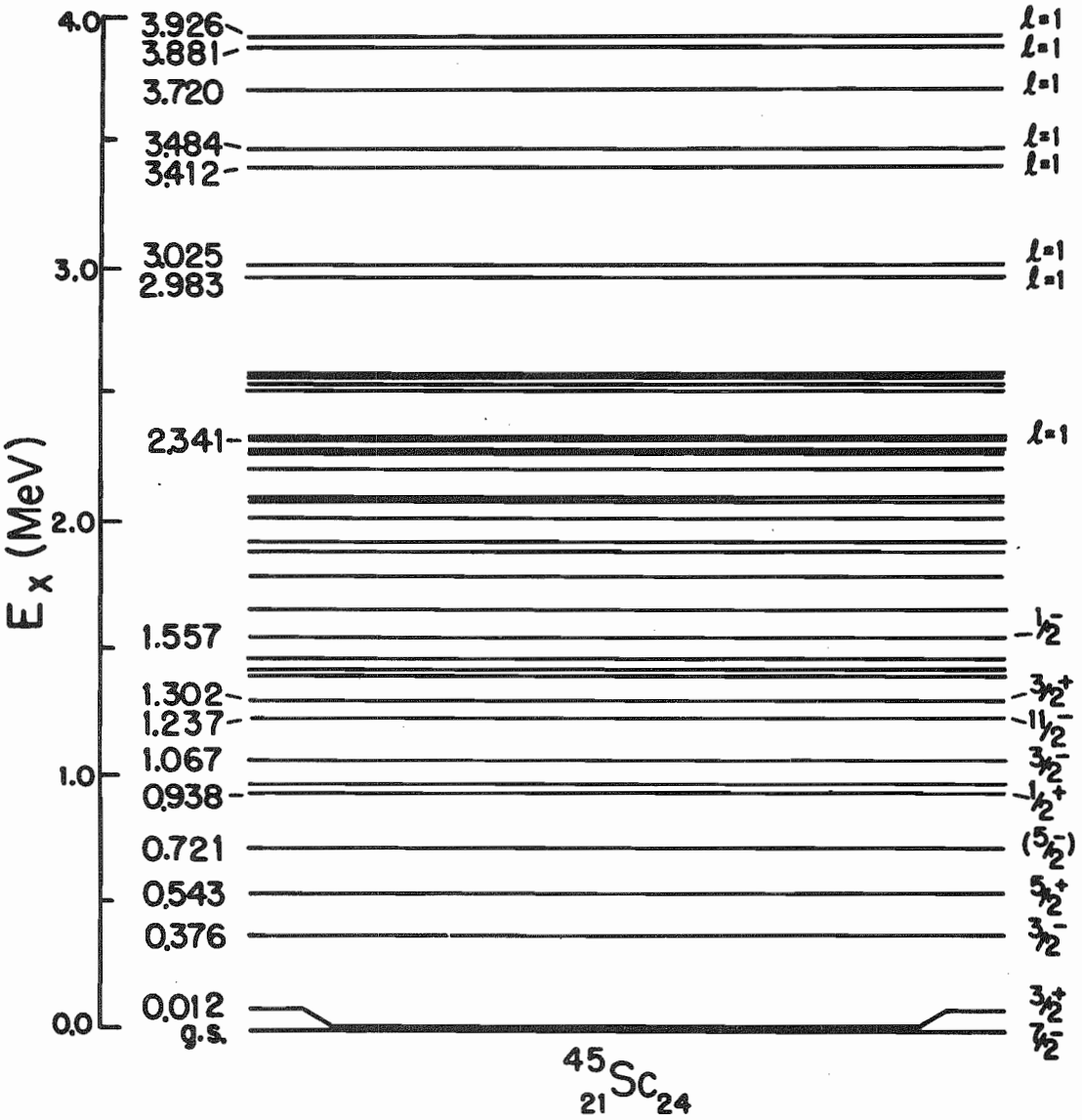
4.0
3.0
2.0
1.0
0.0
E_x (MeV)
3.926
3.881
3.720
3.484
3.412
3.025
2.983
2.341
1.557
1.302
1.237
1.067
0.938
0.721
0.543
0.376
0.012
g.s.
l=1
l=1
l=1
l=1
l=1
l=1
l=1
l=1
$\frac{1}{2}^-$
$\frac{3}{2}^+$
$\frac{11}{2}^-$
$\frac{3}{2}^-$
$\frac{1}{2}^+$
$(\frac{5}{2}^-)$
$\frac{5}{2}^+$
$\frac{3}{2}^-$
$\frac{3}{2}^+$
$\frac{7}{2}^-$
$^{45}_{21}Sc_{24}$

near 2.03 MeV was identified as the fragmented analgoue of the eighth excited state of ^{45}Ca , while the group of $1/2^+$ states centered near 2.23 MeV form the analogue of the tenth excited state of ^{45}Ca (Wilson, 1973).

Figure 15 shows the elastic and capture excitation functions in the region of the analogue state at 1.65 MeV. In these excitation functions note that the number of capture resonances is approximately three to four times the number of observed proton resonances. (The level density can also be compared to earlier work of Erlandsson and Valli (1963) where 34 capture resonances were observed from 1.3 to 2.5 MeV. The difference in observed density can be explained by the difference in beam energy resolution. Erlandsson quotes a resolution of 5 keV at 1.5 MeV while the present experiment was performed with a resolution of 300-350 eV.) Ten resonances were studied with the Ge(Li) detector; these resonances were considered fragments of the 3/2- analogue state.

Figure 16 shows a typical spectrum obtained on a fragment of this 3/2- analogue. As shown in Figure 16, there are several primary transitions. The complexity of this spectrum is typical for spectra obtained from the capture reaction on ^{44}Ca . Gamma-ray partial widths for the direct transitions were obtained following the procedure described above. Figure 17 shows the partial decay widths of the individual fragments of this analogue state. As shown in the level scheme, there is a level at 12.4 keV in ^{45}Sc with $J^\pi = 3/2^+$. The ground state of ^{45}Sc has $J^\pi = 7/2-$, thus transitions from 3/2- states would be expected to decay to the first excited states instead of the ground state. Also, if one assumes the highest energy transitions

Figure 15 Elastic and capture excitation function in the region of the 3/2- analogue state in ^{45}Sc ; the line through the elastic data is a fit to the data (Wilson, 1973), while the line through the capture data is only a visual aid

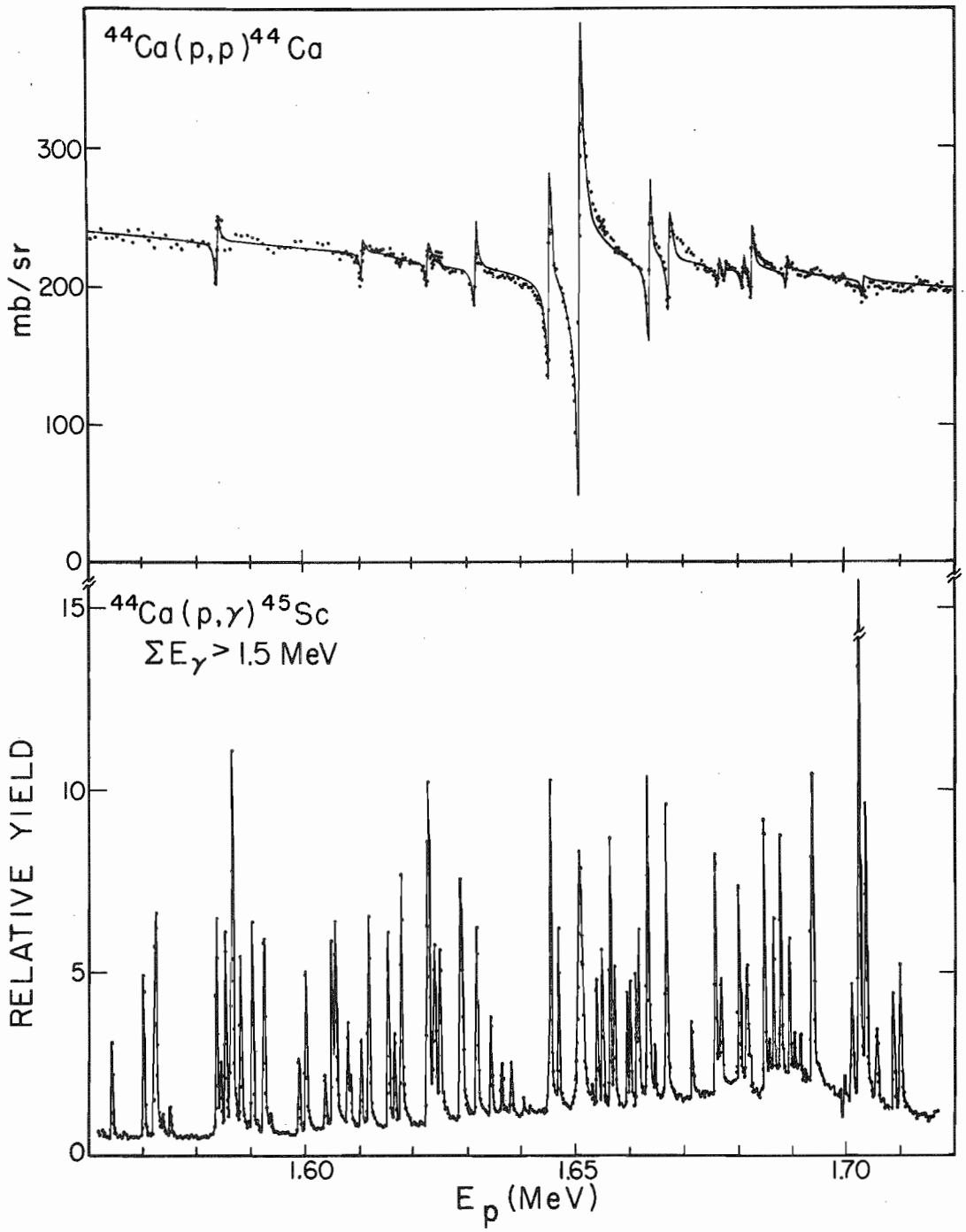
$^{44}Ca(p,p)^{44}Ca$
300
200
100
0
mb/sr
$^{44}Ca(p,\gamma)^{45}Sc$
$\Sigma E_\gamma > 1.5$ MeV
15
10
5
0
RELATIVE YIELD
1.60
1.65
1.70
E_p (MeV)

Figure 16 A typical Ge(Li) spectrum showing the decay of a fragment of the 3/2- analogue state in ^{45}Sc

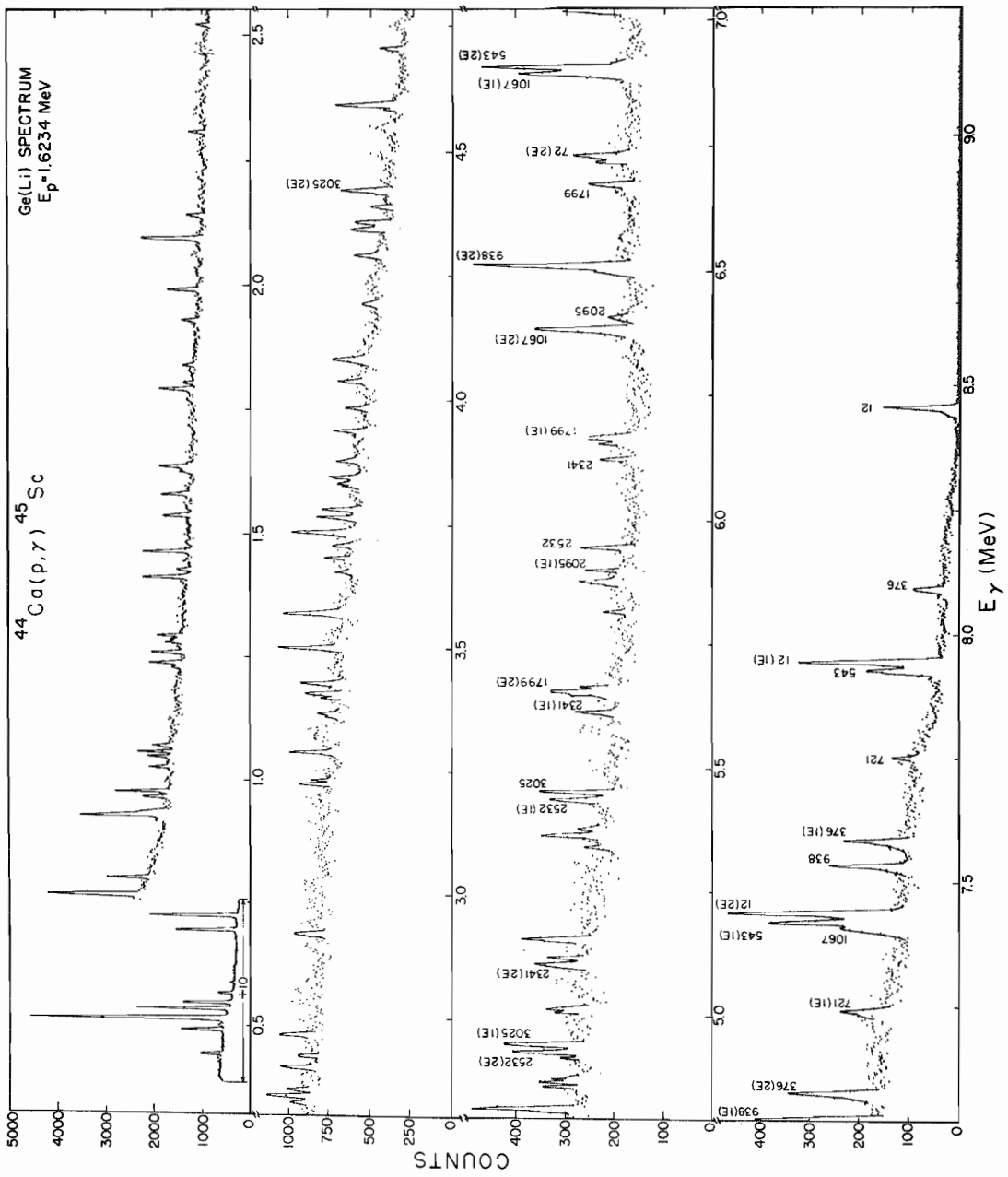
Ge(Li) SPECTRUM
E_p=1.6234 MeV
$^{44}Ca(p,\gamma)^{45}Sc$
COUNTS
E_γ (MeV)
938(1E)
376(2E)
721(1E)
2532(2E)
2541(2E)
3025(1E)
543(2E)
1067(1E)
72(2E)
1799
938(2E)
2095
1067(2E)
1799(1E)
2341
2532
2095(1E)
1799(2E)
2341(1E)
3025
2532(1E)
376(1E)
938
12(2E)
543(1E)
1067
721
543
12(1E)
376
12

Figure 17 Absolute gamma-ray widths for the ten fragments of the 3/2- analogue state in ^{45}Sc ; E_{ex} is the energy of the final state in the transition from the resonance

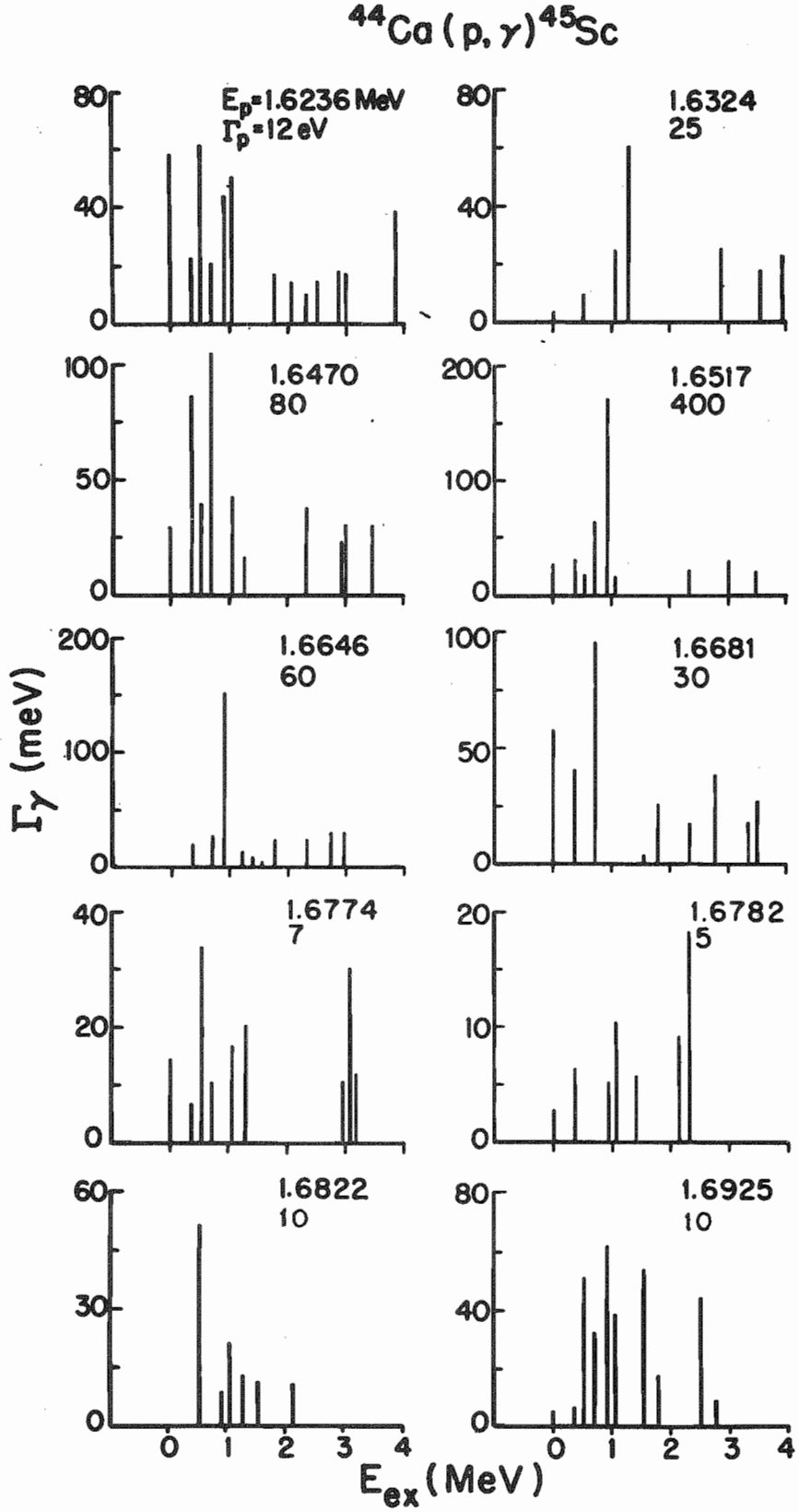
$^{44}Ca(p,\gamma)^{45}Sc$
E_p=1.6236 MeV
Γ_p=12 eV
1.6324
25
1.6470
80
1.6517
400
1.6646
60
1.6681
30
1.6774
7
1.6782
5
1.6822
10
1.6925
10
Γ_γ (meV)
E_{ex} (MeV)

are to the ground state then the energies of transitions to the other low-lying levels are in disagreement by about 12 keV. Therefore, the transition which appears to be a transition to the ground state in Figure 17 is actually a transition to the first excited state. Qualitatively, the states with the largest elastic widths have similar decay patterns. States which are stronger in the elastic channels are also stronger in the capture channel. For example, the 60 and 400 eV states have very similar patterns.

The group of 1/2- states near 2.03 MeV form the analogue of the eighth excited state of ^{45}Ca . The capture and elastic excitation functions are shown in Figure 18. In the energy region from 1.71 to 2.14 MeV, there are a number of 1/2- resonances. Thus, the 1/2- states apparently offer an opportunity to study both analogue and background states of the same spin and parity in the same nucleus. (However, as noted below, there may be a difficulty in making a sharp distinction between analogue and background states.) Therefore a detailed study of all of the 1/2- resonances in this energy region was performed. A total of 38 Ge(Li) spectra were taken on these 1/2- resonances. Figures 19 and 20 show the decay of the 38 1/2- states studied in this energy region. Qualitatively, the stronger fragments have similar decay patterns. The resonances that have the larger elastic widths usually have stronger capture widths and populate fewer final states than the weaker elastic resonances.

The group of $1/2^+$ states near 2.24 MeV are the fragments of the analogue of the tenth excited state of ^{45}Ca . The capture and elastic excitation functions are shown in Figure 21. Note that the analogue state is dominated by a single large resonance. In the capture excitation function, this level appears as a triplet. Ge(Li) spectra were taken on

Figure 18 Capture and elastic excitation functions from 1.70 to 2.14 MeV ; the 1/2- analogue state is centered near 2.03 MeV

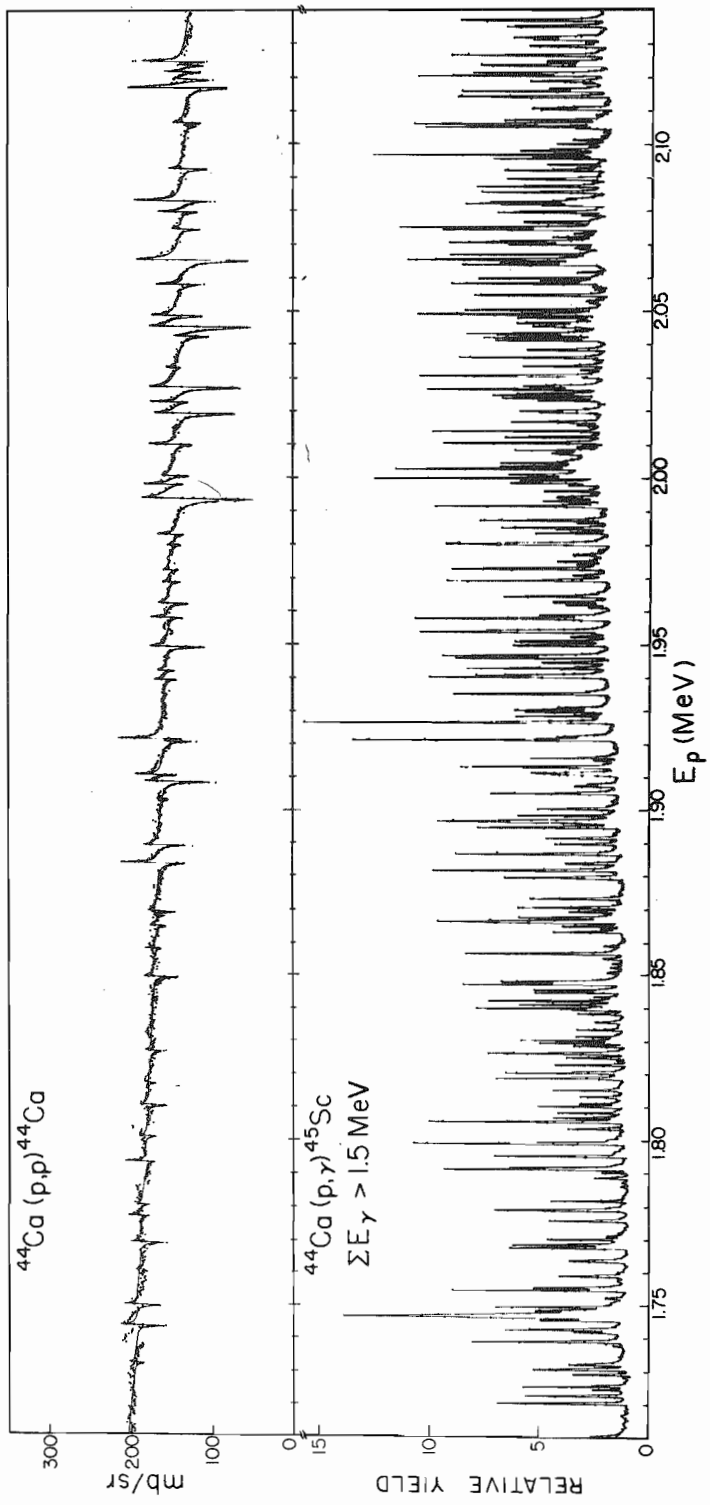
$^{44}Ca\,(p,p)^{44}Ca$
mb/sr
300
200
100
0
$^{44}Ca\,(p,\gamma)^{45}Sc$
$\Sigma E_\gamma > 1.5$ MeV
RELATIVE YIELD
15
10
5
0
1.75
1.80
1.85
1.90
1.95
2.00
2.05
2.10
E_p (MeV)

Figure 19 Absolute gamma-ray widths for the 20 resonances located away from the center of the analogue state at 2.03 MeV

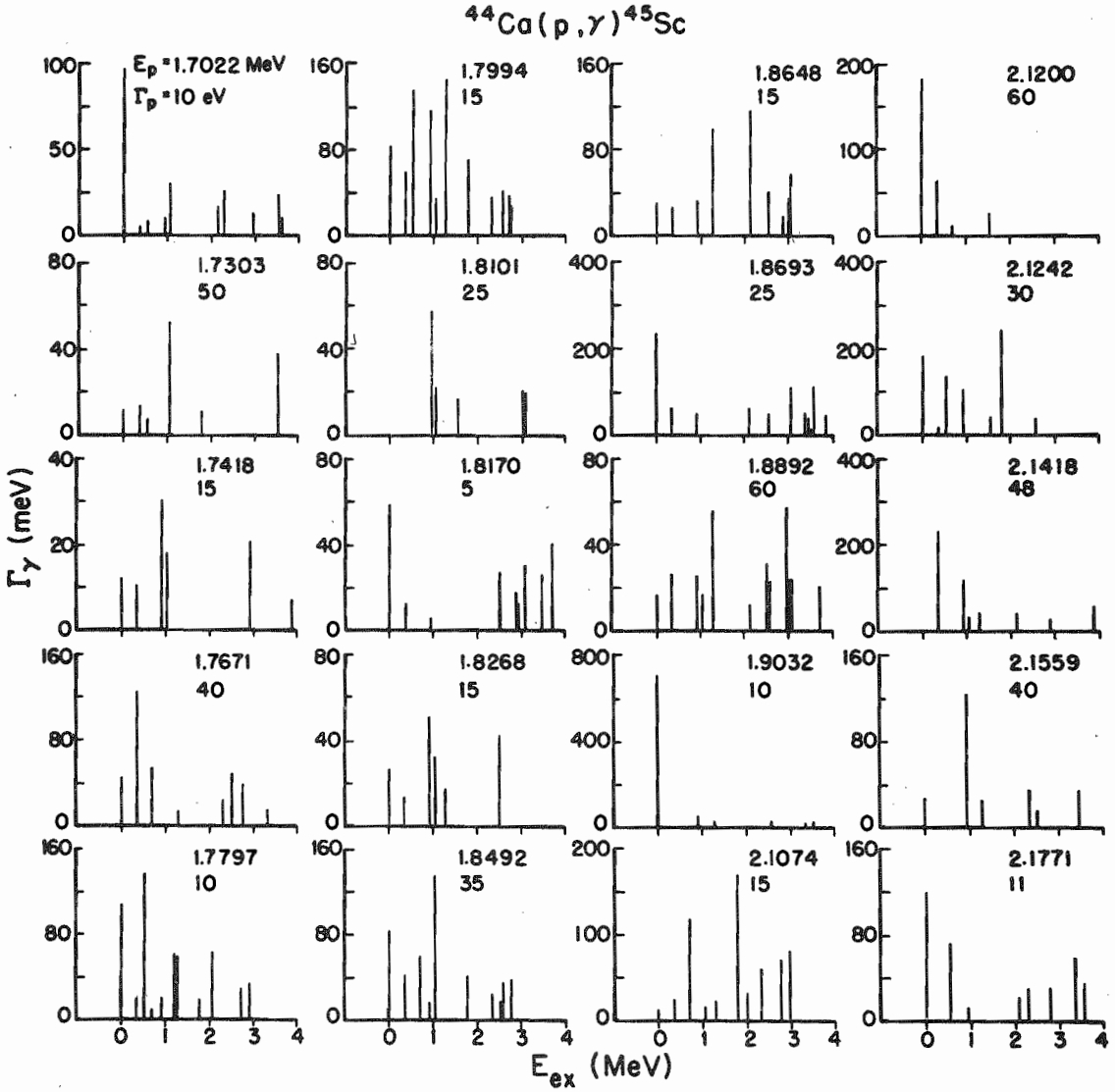
$^{44}Ca(p,\gamma)^{45}Sc$
E_p = 1.7022 MeV
Γ_p = 10 eV
1.7994
15
1.8648
15
2.1200
60
1.7303
50
1.8101
25
1.8693
25
2.1242
30
1.7418
15
1.8170
5
1.8892
60
2.1418
48
1.7671
40
1.8268
15
1.9032
10
2.1559
40
1.7797
10
1.8492
35
2.1074
15
2.1771
11
Γ_γ (meV)
E_{ex} (MeV)

Figure 20 Absolute gamma-ray widths for 18 of the 38 1/2- resonances near the center of the analogue state at 2.03 MeV

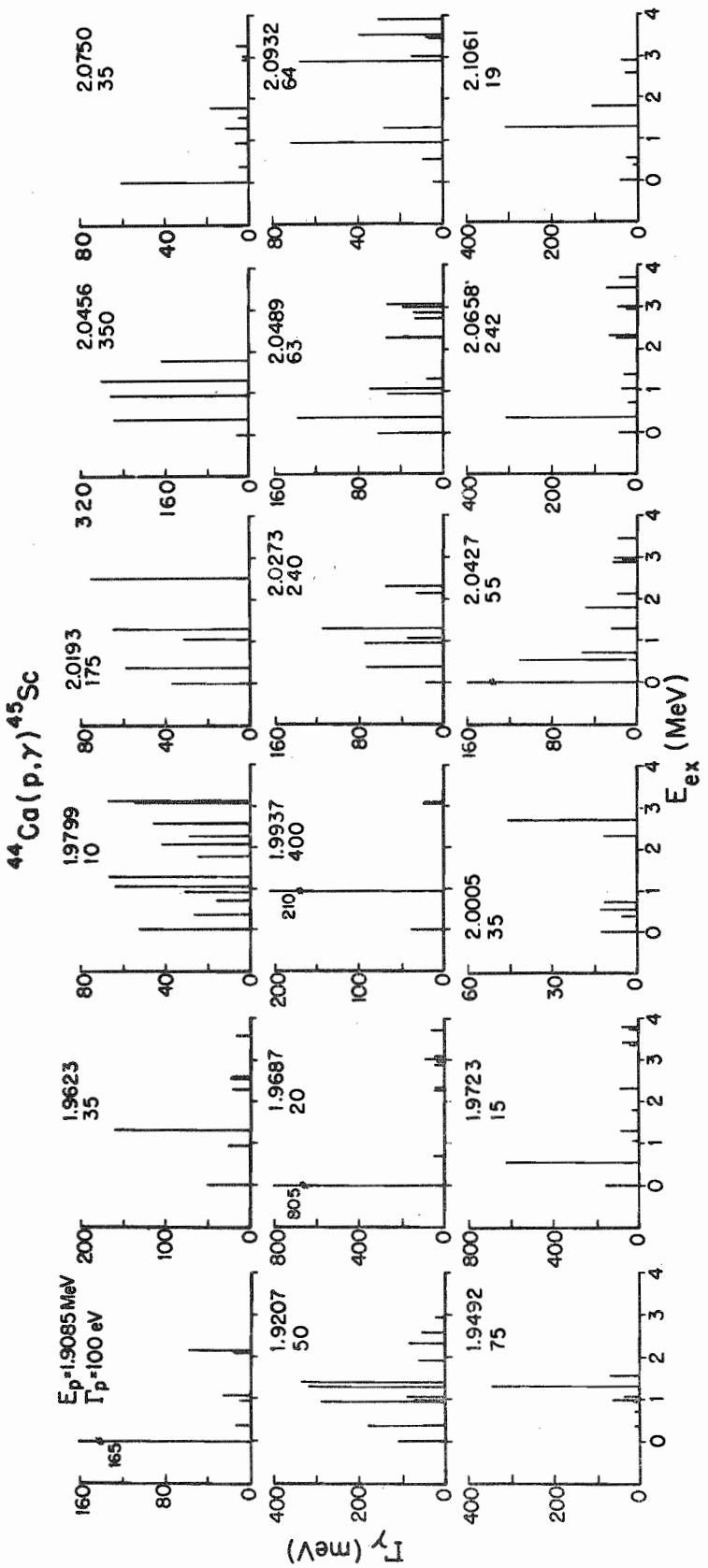
$^{44}Ca(p,\gamma)^{45}Sc$
E_p=1.9085 MeV
Γ_p=100 eV
1.9207
50
1.9492
75
1.9623
35
1.9687
20
1.9723
15
1.9799
10
1.9937
400
2.0005
35
2.0193
175
2.0273
240
2.0427
55
2.0456
350
2.0489
63
2.0658
242
2.0750
35
2.0932
64
2.1061
19
165
805
210
Γ_γ (mev)
E_{ex} (MeV)

Figure 21 Capture and elastic excitation functions from 2.13 to 2.28 MeV; centered near 2.24 MeV is the $1/2^+$ analogue state (note that near 2.24 MeV under the largest elastic resonance the capture data shows a triplet)

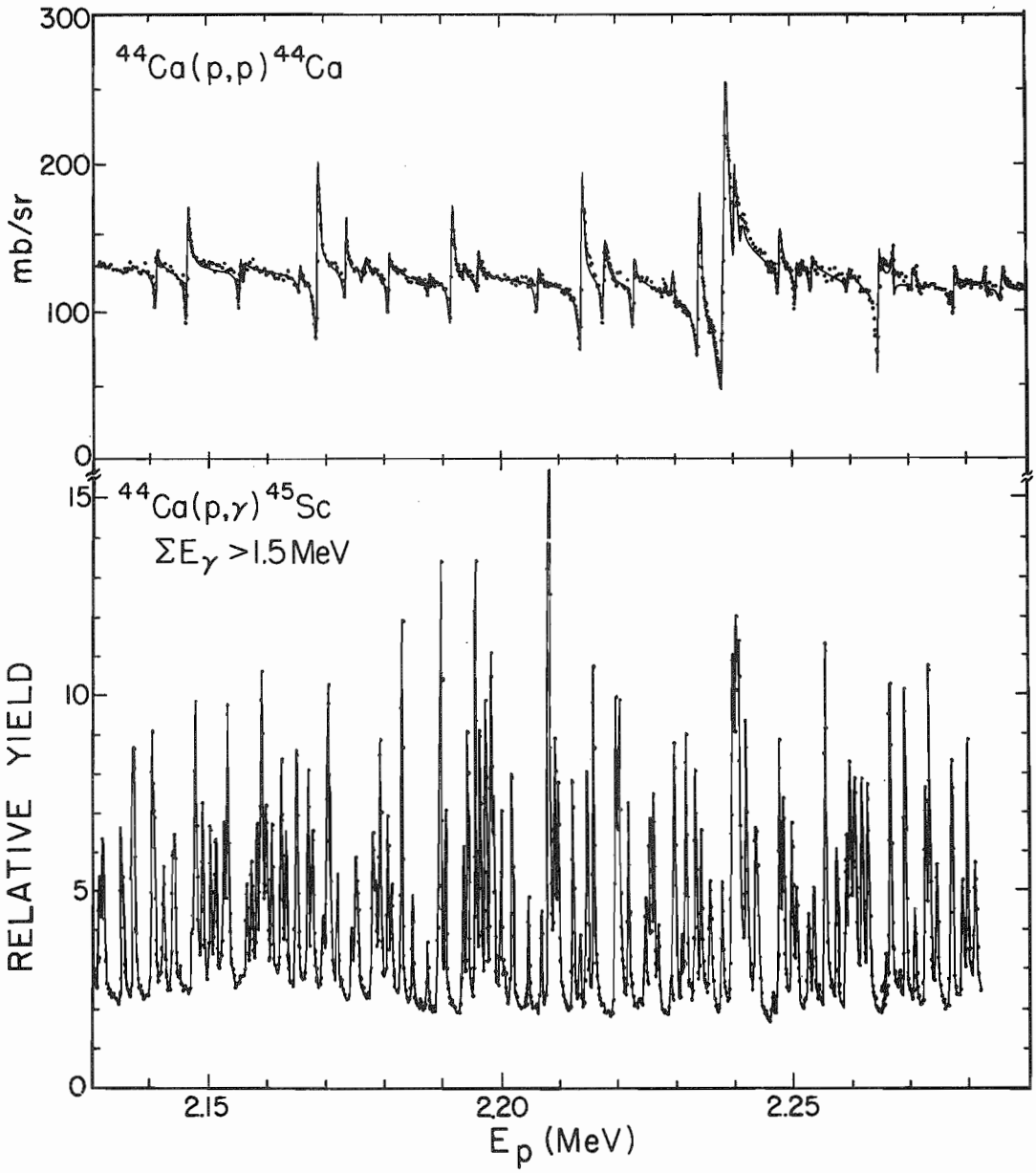
$^{44}Ca(p,p)^{44}Ca$
mb/sr
300
200
100
0
$^{44}Ca(p,\gamma)^{45}Sc$
$\Sigma E_\gamma > 1.5$ MeV
RELATIVE YIELD
15
10
5
0
2.15
2.20
2.25
E_p (MeV)

nine $1/2^+$ resonances in this energy region. Spectra were also taken on the triplet. Because the dominant level of the analogue state is part of this triplet, the partical decay widths for this level may have large errors. The different components of the triplet did not have the same decay patterns. Figure 22 shows the decay of the levels of this analogue state. Since the different components have different decay characteristics, the gamma-ray widths associated with this triplet are presented without any attempt to sort out contributions from different parts of the triplet.

The decay widths for all of the resonances studied in $^{44}Ca(p,\gamma)^{45}Sc$ reaction are tabulated in the Appendix.

$^{62}Ni(p,\gamma)^{63}Cu$

The $^{62}Ni(p,\gamma)^{63}Cu$ excitation function was measured from 2.30 to 2.70 MeV. Browne (1969) had measured the elastic scattering above 2.40 MeV. In the capture experiment elastic data were taken simultaneously at an angle of 135°. These data indicated that some of the resonances previously observed were unresolved doublets which could be resolved with the better resolution now available. Nearest neighbor spacings were not always in agreement with Browne's results. The elastic scattering resonances were remeasured from 2.30 to 2.48 and 2.58 to 2.70 MeV before measuring the decay of the capture resonances with the Ge(Li) detector. The resolution for these data was about 300 eV; more resonances were resolved than in Browne's experiment. However, overall agreement with Browne's results was good. Table 3 lists the elastic scattering parameters. The inelastic proton widths and the total gamma-ray widths listed in Table 3 were determined in the present experiment.

Figure 22 Absolute gamma-ray widths for the nine fragments of the $1/2^+$ analogue state in ^{45}Sc

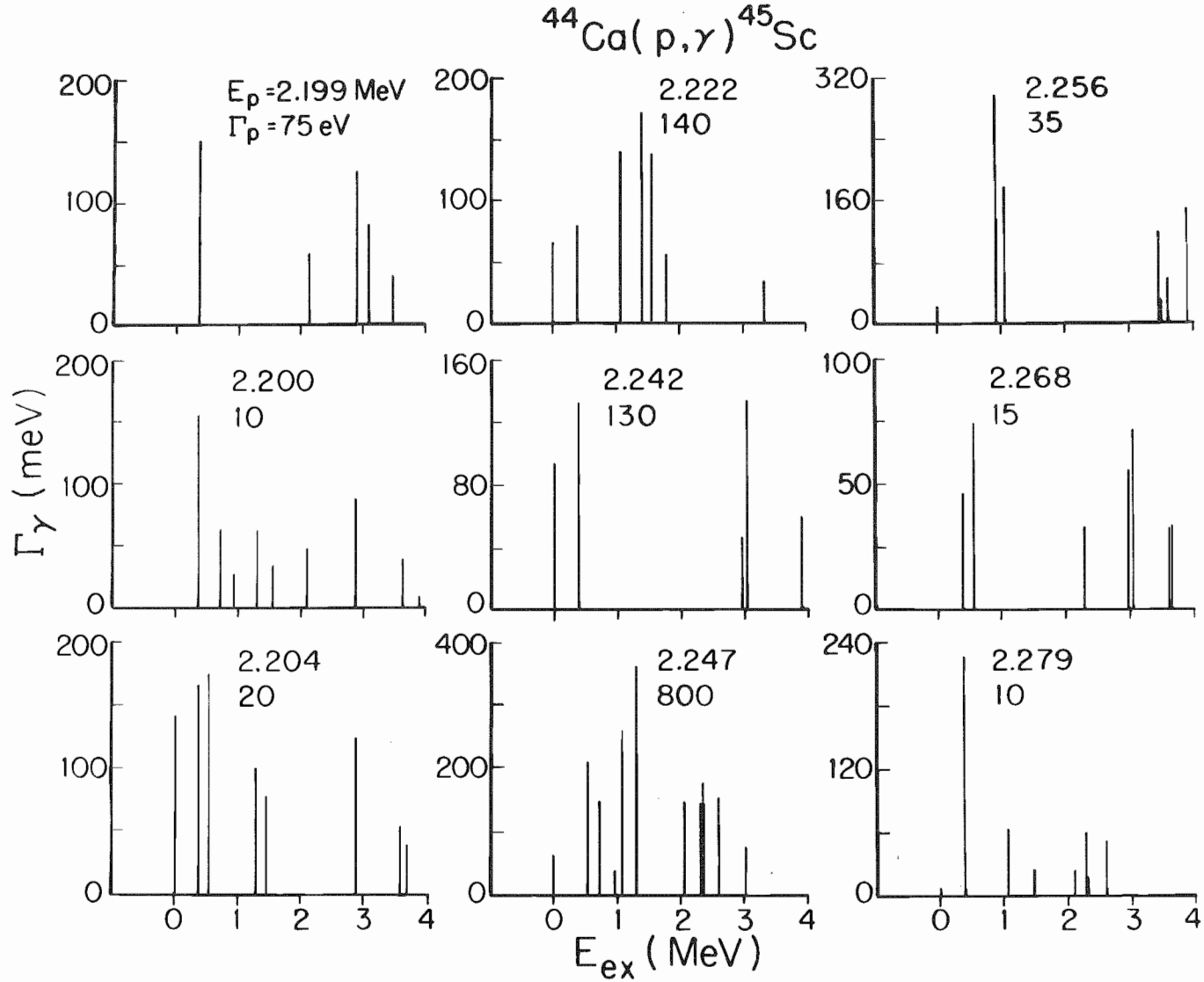
$^{44}Ca(p,\gamma)^{45}Sc$
E_p =2.199 MeV
Γ_p =75 eV
2.222
140
2.256
35
2.200
10
2.242
130
2.268
15
2.204
20
2.247
800
2.279
10
Γ_γ (meV)
E_{ex} (MeV)

Table 3 Resonance parameter for ^{63}Cu

Ep (MeV)	J^{π}	Γ_p (eV)	$\Gamma_{p'}$ (eV)	Γ_γ (eV)
2.3110	$1/2^+$	20	0.019	1.22
2.3203	$1/2^+$	10	0.0	.34
2.3353	$1/2^+$	35	0.0	.37
2.3543	$1/2^+$	15	0.0	.10
2.3603	$1/2^+$	30	0.0	.25
2.3853	$1/2^+$	20	0.022	.15
2.3923	$1/2^+$	8	0.0	.77
2.4043	$1/2^+$	10	0.019	.61
2.4173	$1/2^+$	15	0.0	.31
2.4403	$1/2^+$	115	0.0	.13
2.4443	$1/2^+$	30	0.0	.40
2.4573	$1/2^+$	10	0.023	.11
2.4703	$1/2^+$	35	0.036	.96
2.4783	$1/2^+$	30	0.279	1.10
2.4833	$1/2^+$	135	0.071	.64
2.4953	$1/2^+$	90	0.059	.38
2.5283	$1/2^+$	30	0.020	.10
2.5343	$1/2^+$	10	0.102	.48
2.5485	$1/2^+$	65	0.092	.32
2.5733	$1/2^+$	5	0.177	.19
2.6033	$1/2^+$	25	0.069	.09
2.6123	3/2-	20	0.069	.30
2.6139	3/2-	15	0.119	.21

Table 3 (Continued)

Ep (MeV)	J^{π}	Γ_p (eV)	$\Gamma_{p'}$ (eV)	Γ_γ (eV)
2.6376	3/2-	10	0.101	.40
2.6365	3/2-	5	0.019	.28
2.6390	3/2-	5	0.026	.54
2.6466	3/2-	15	0.225	.60
2.6506	3/2-	10	0.248	.36
2.6536	3/2-	5	0.122	.46
2.6564	3/2-	10	0.278	.22
2.6617	3/2-	40	0.585	.69
2.6631	3/2-	125	1.194	.81
2.6664	3/2-	5	0.195	.24
2.6675	3/2-	20	0.164	.39
2.6704	3/2-	5	0.228	.42

The level scheme for ^{63}Cu is fairly well known (Nuclear Data Sheets, 1967) up to about 2 MeV. Figure 23 shows the adopted level scheme. States that show $\ell = 1$ proton transfer strength in the $^{62}Ni(^{3}He,d)$ reaction are indicated in Figure 23 also.

In the energy region studied there is a highly fragmented 3/2- analogue state at a proton energy of 2.65 MeV. The elastic scattering data indicated fourteen fragments. The capture and elastic excitation functions in the region of this analogue are shown in Figure 24. Ge(Li) spectra were taken on these fourteen resonances. Figure 25 shows a typical Ge(Li) spectrum on a fragment of this analogue. This spectrum was typical of the decay of capture resonances in the ^{62}Ni experiment. The relative simplicity of the spectrum was expected since Peters (1972) had obtained similar results on both ^{54}Cr and ^{58}Fe targets. In retrospect, it is the complexity of the gamma-ray spectra observed in the $^{44}Ca(p,\gamma)^{45}Sc$ reaction that is anomalous.

Figure 26 shows the decay of the individual fragments of this analogue state. As shown in Figure 26, the gamma-ray decay is usually weak on the smaller resonances. On the resonances with small elastic widths, the transition to the ground state is dominant. The resonances at 2.655 and 2.657 MeV have very strong gamma-ray widths. Since these resonances are near the center of the analogue state, this is evidence for enhancement of the gamma-ray decay widths.

In addition to the analogue state, a number of $1/2^+$ background states were studied. These $1/2^+$ states were studied for two reasons. Since there were no 3/2- resonances observed nearby, the $1/2^+$ resonances provided an opportunity to investigate background states in the same nucleus.

Figure 23 The adopted level scheme of ^{63}Cu (Nuclear Data Tables, 1967); levels which have $\ell = 1$ proton stripping patterns in $^{62}Ni(^{3}He,d)$ are also indicated in the figure

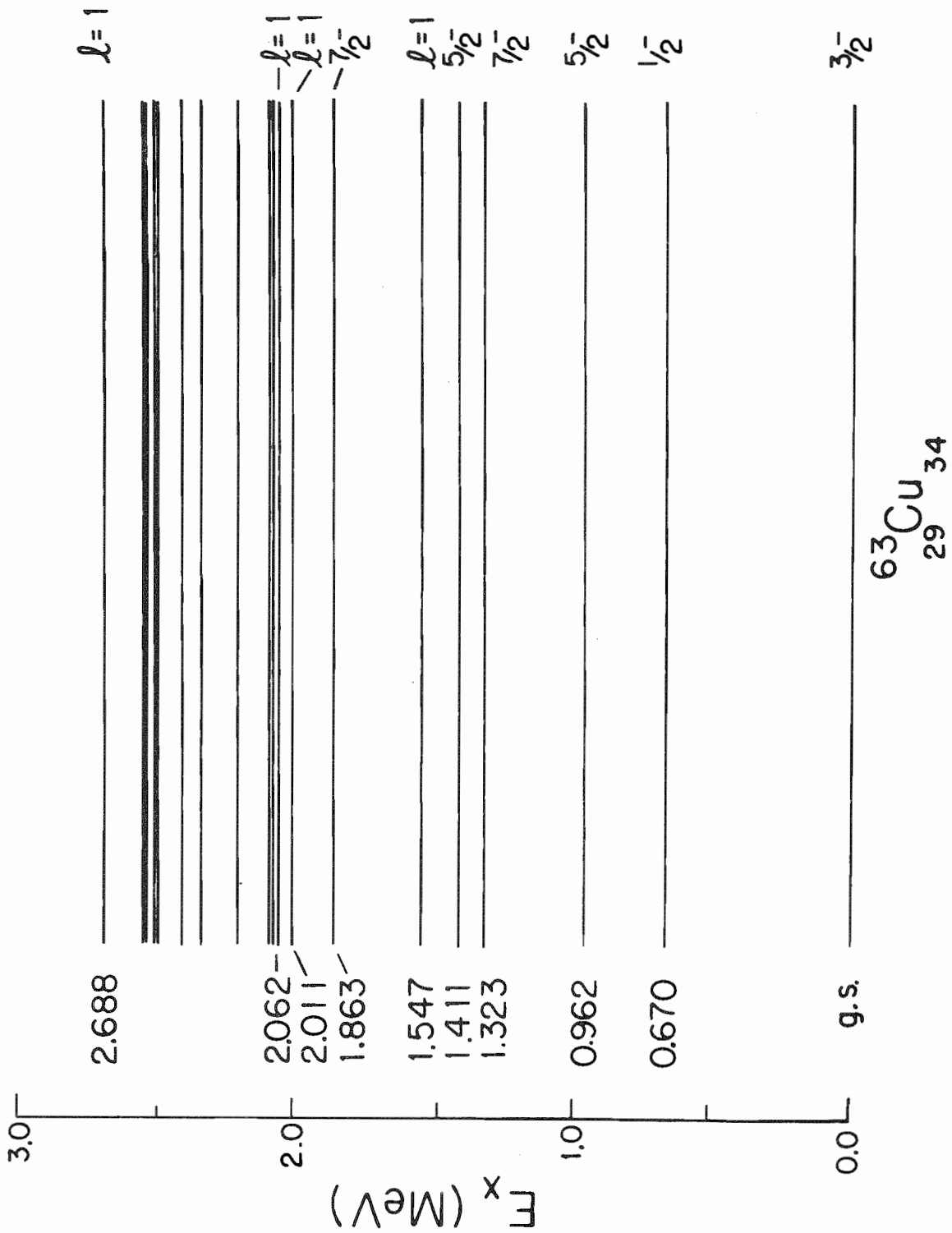
$^{63}_{29}Cu_{34}$
E_x (MeV)
3.0
2.0
1.0
0.0
2.688
2.062
2.011
1.863
1.547
1.411
1.323
0.962
0.670
g.s.
l = 1
l = 1
l = 1
7/2⁻
5/2⁻
7/2⁻
5/2⁻
1/2⁻
3/2⁻

Figure 24 Capture and elastic excitation functions from 2.58 to 2.70 MeV; the 3/2- analogue state in ^{63}Cu is centered at 2.65 MeV (the line through the elastic data is a fit to the data, while the line through the capture data is intended as a visual aid)

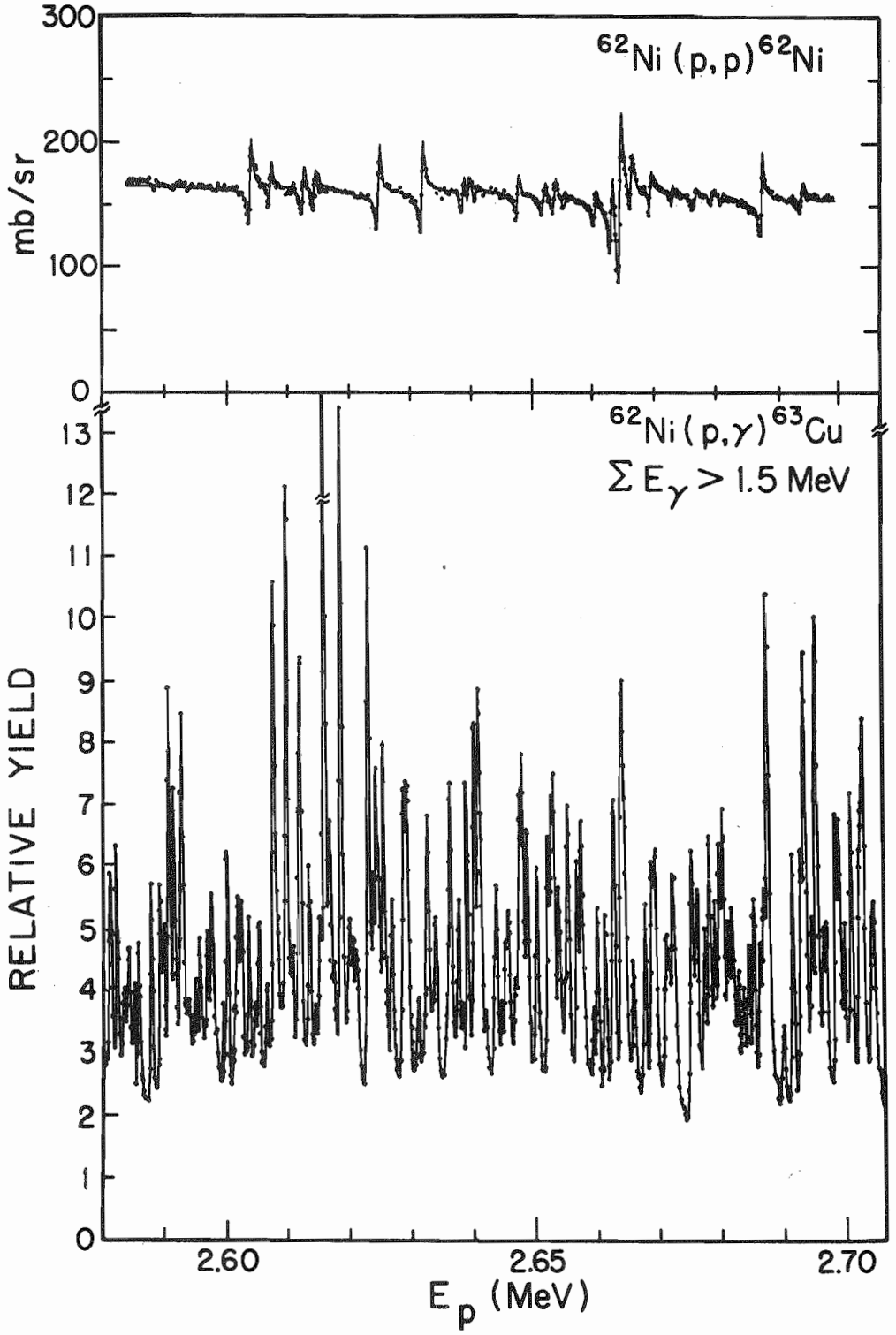
^{62}Ni (p,p) ^{62}Ni
mb/sr
300
200
100
0
^{62}Ni (p,γ) ^{63}Cu
Σ E_γ > 1.5 MeV
RELATIVE YIELD
13
12
11
10
9
8
7
6
5
4
3
2
1
0
2.60
2.65
2.70
E_p (MeV)

Figure 25 Typical Ge(Li) spectrum illustrating the decay of a fragment of the 3/2- analogue in ^{63}Cu

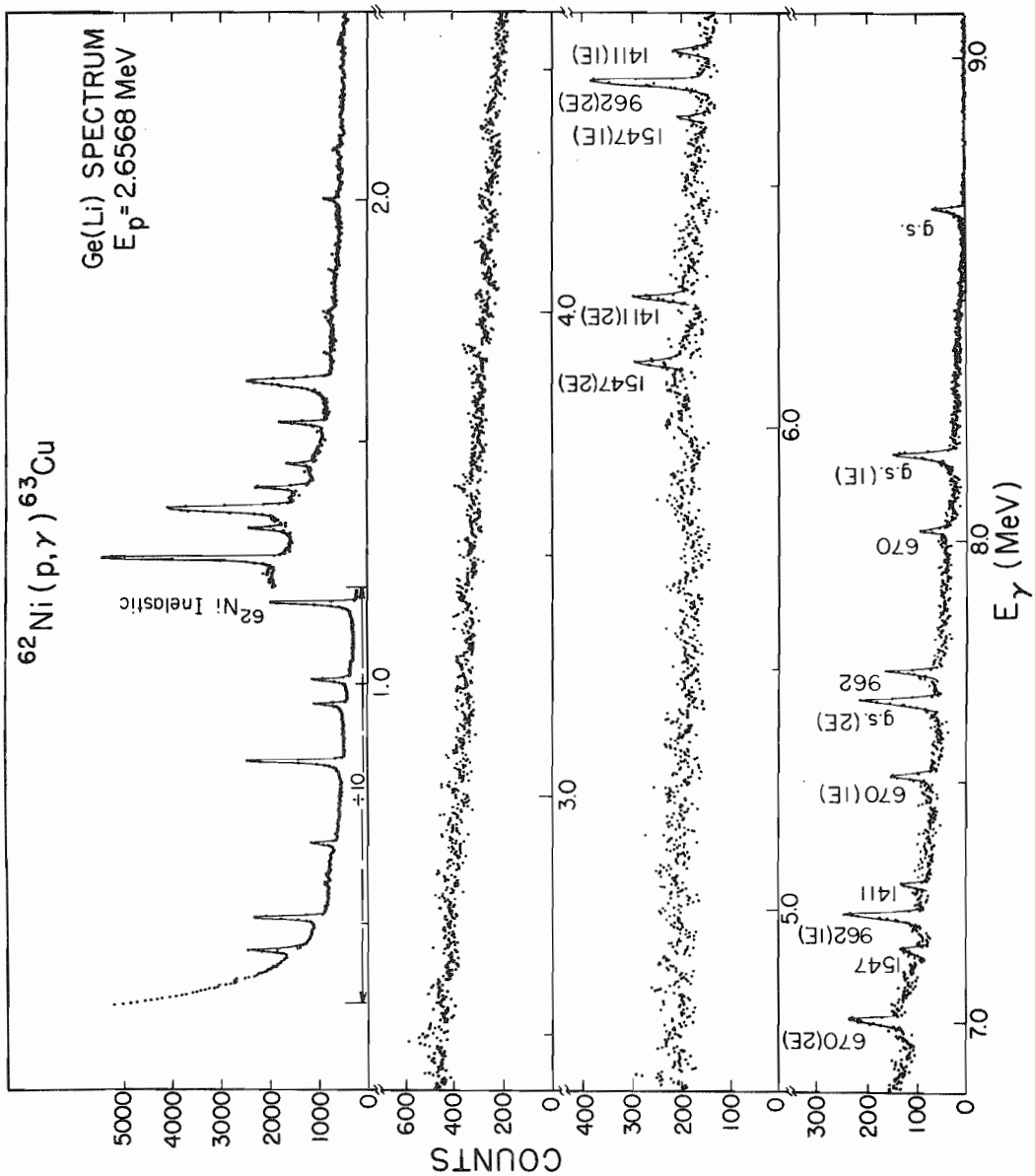
^{62}Ni(p,γ)^{63}Cu
Ge(Li) SPECTRUM
E_p=2.6568 MeV
^{62}Ni Inelastic
÷10
COUNTS
E_γ (MeV)
670(2E)
1547
962(1E)
1411
670(1E)
g.s.(2E)
962
670
g.s.(1E)
1547(2E)
1411(2E)
1547(1E)
962(2E)
1411(1E)
g.s.

Figure 26 Absolute gamma-ray widths for the 14 fragments of the 3/2- analogue state in ^{63}Cu

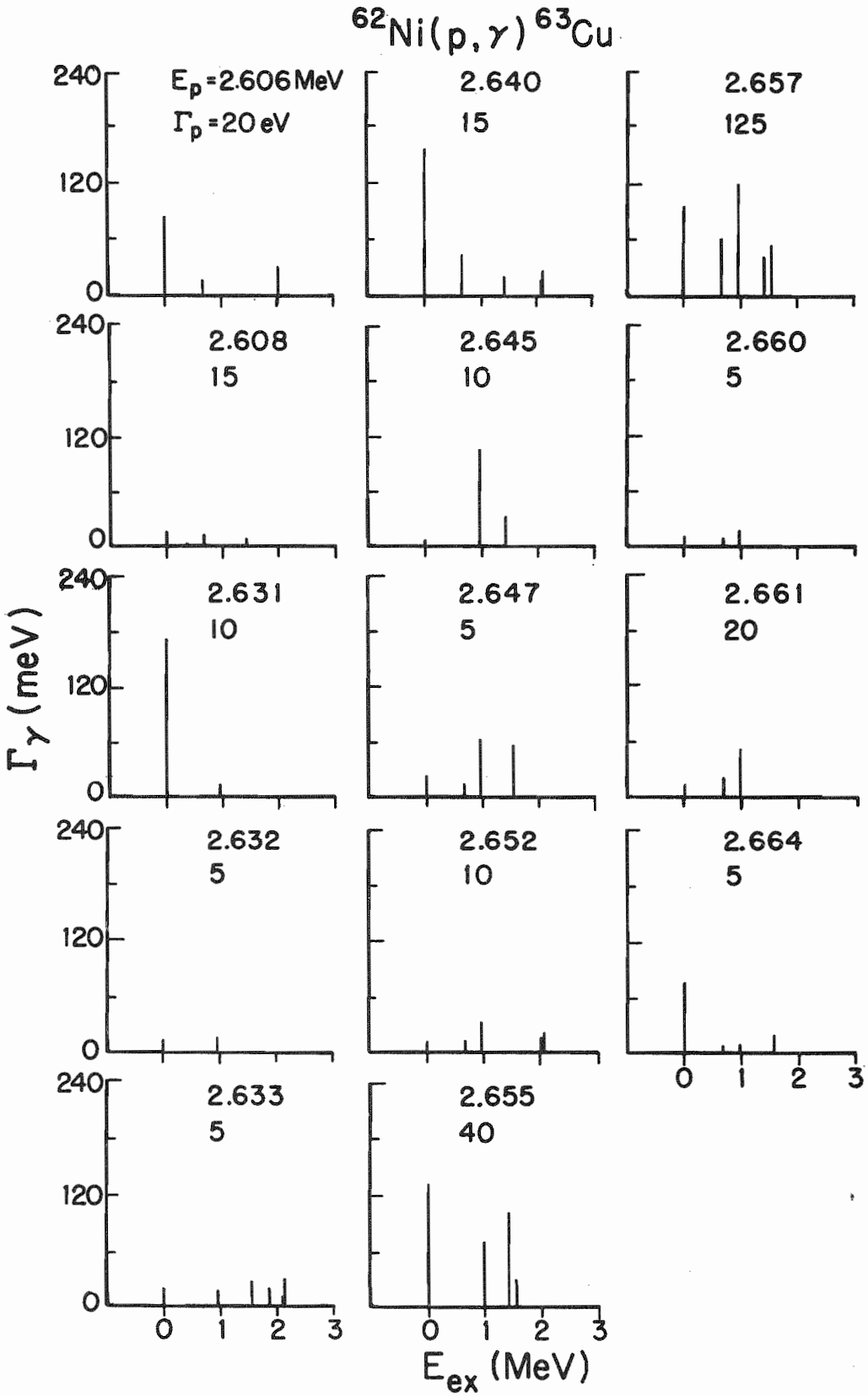
$^{62}Ni(p,\gamma)^{63}Cu$
E_p=2.606MeV
Γ_p=20eV
2.640
15
2.657
125
2.608
15
2.645
10
2.660
5
2.631
10
2.647
5
2.661
20
2.632
5
2.652
10
2.664
5
2.633
5
2.655
40
240
120
0
Γ_γ (meV)
0 1 2 3
E_{ex} (MeV)

Another motivation was to investigate the anomaly observed in the elastic channel for the $1/2^+$ resonances near 2.44 MeV, in order to see if this anomaly also appeared in the capture channel. The capture and elastic excitation functions in the region of 2.30 to 2.60 MeV are shown on Figures 27 and 28. Ge(Li) spectra were measured on the twenty $1/2^+$ resonances in this energy region. Figure 29 shows the decay of these $1/2^+$ states. As expected, there is no obvious pattern in the resonance decay. These data are interpreted in Chapter 5.

The partial decay widths for the $1/2^+$ and the 3/2- resonances in the $^{62}Ni(p,\gamma)^{63}Cu$ are tabulated in the Appendix.

Figure 27 Capture and elastic excitation frunctions from 2.30 to 2.47 MeV; in this energy range there are 15 $1/2^+$ resonances

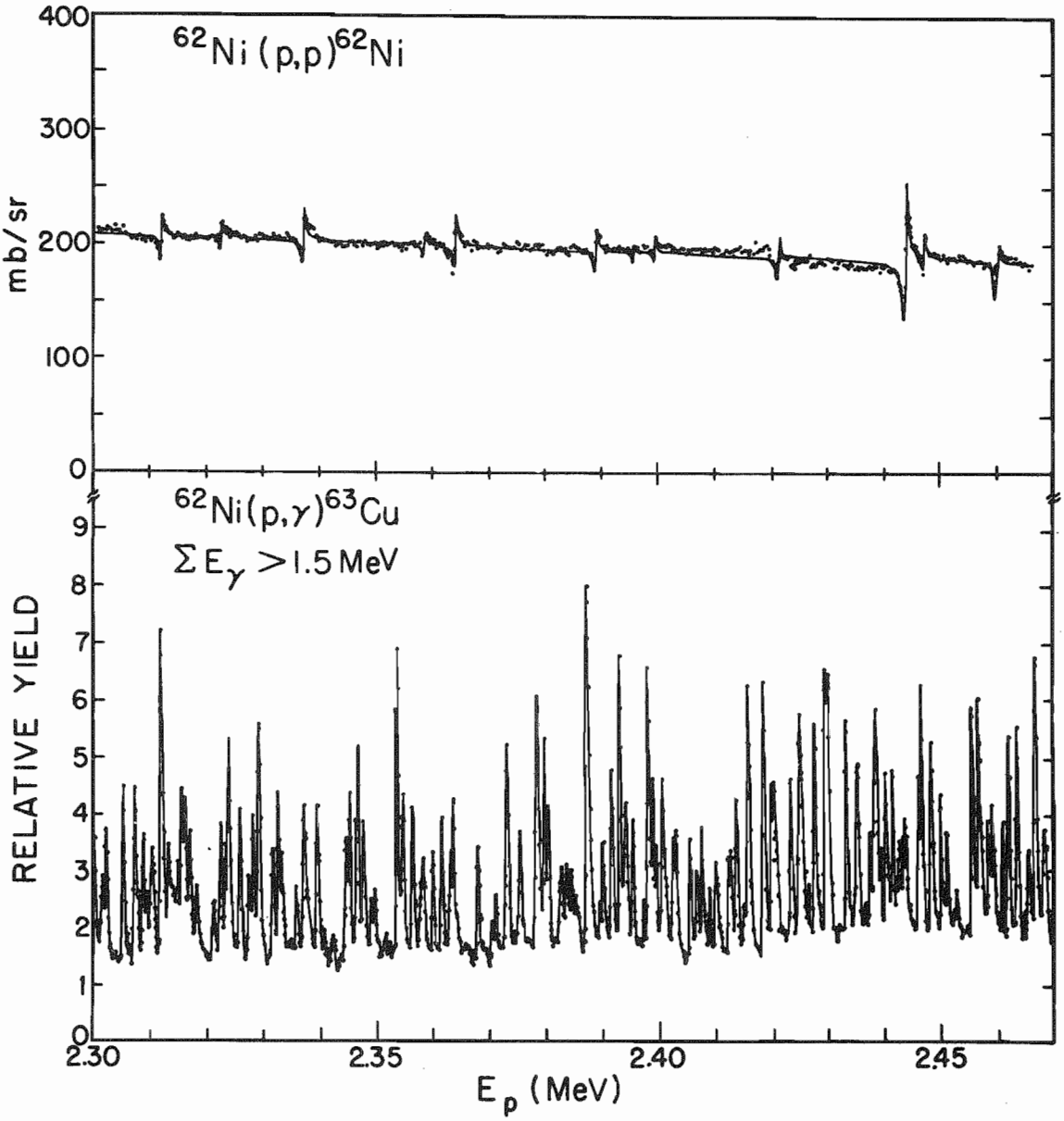
^{62}Ni (p,p)^{62}Ni
mb/sr
400
300
200
100
0
^{62}Ni(p,γ)^{63}Cu
ΣE$_\gamma$ > 1.5 MeV
RELATIVE YIELD
9
8
7
6
5
4
3
2
1
0
2.30
2.35
2.40
2.45
E$_p$ (MeV)

Figure 28 Capture excitation function from 2.46 to 2.60 MeV

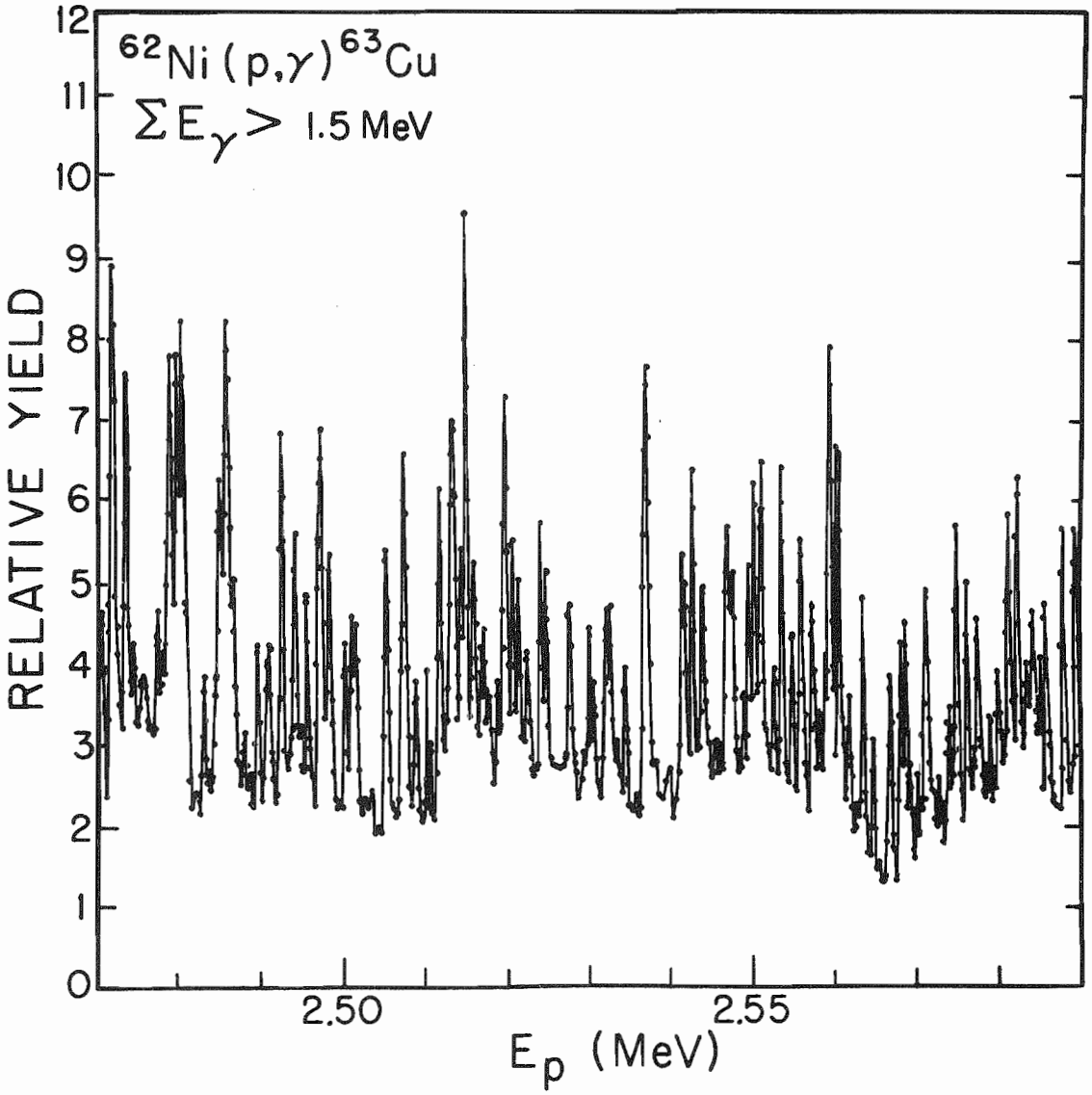
$^{62}Ni(p,\gamma)^{63}Cu$
$\Sigma E_\gamma > 1.5$ MeV
RELATIVE YIELD
0
1
2
3
4
5
6
7
8
9
10
11
12
2.50
2.55
E_p (MeV)

Figure 29 Absolute gamma-ray widths for 20 $1/2^+$ resonances studied in ^{63}Cu

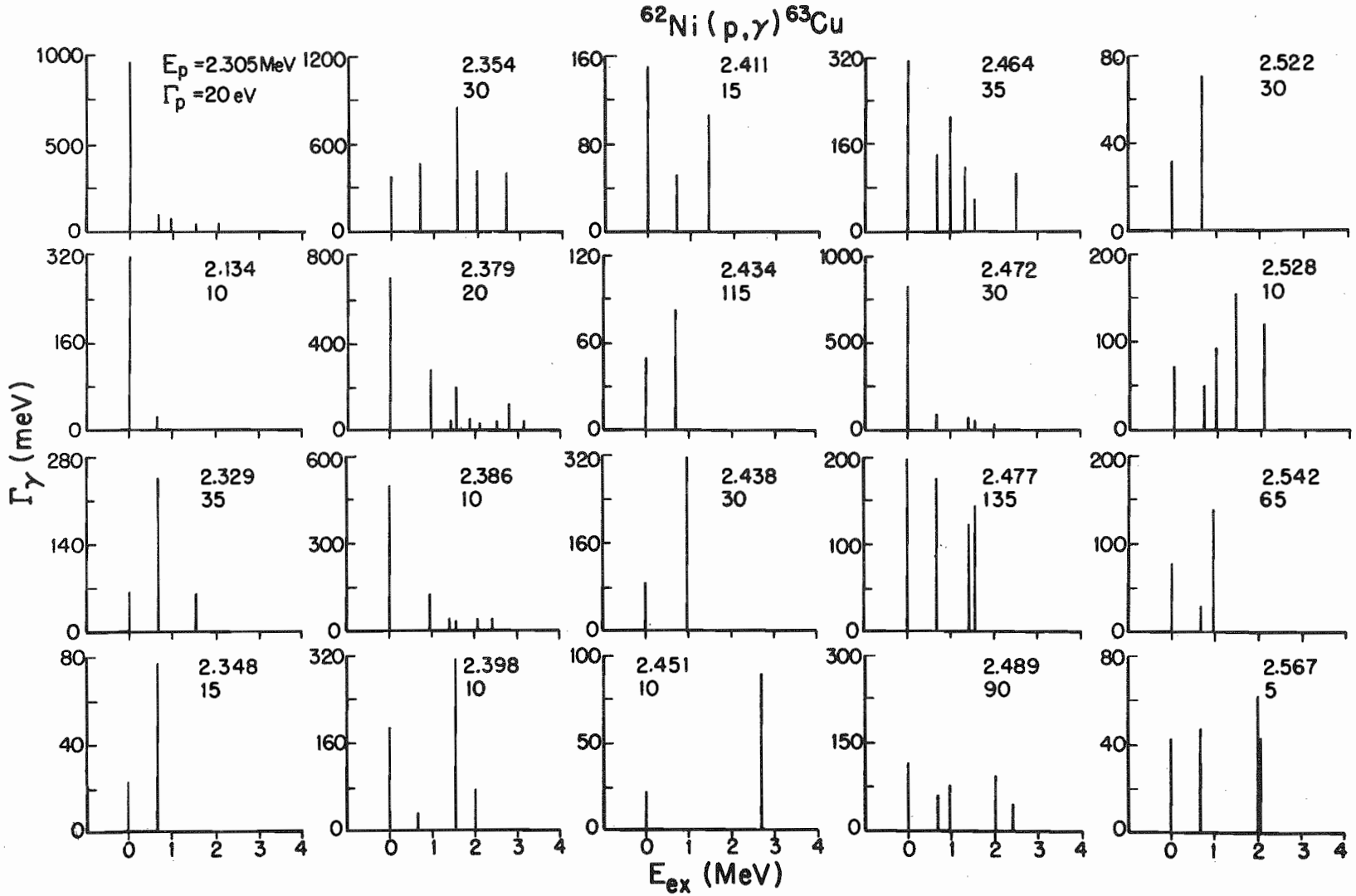
$^{62}Ni(p,\gamma)^{63}Cu$
E_p =2.305MeV
Γ_p =20eV
2.354
30
2.411
15
2.464
35
2.522
30
2.134
10
2.379
20
2.434
115
2.472
30
2.528
10
2.329
35
2.386
10
2.438
30
2.477
135
2.542
65
2.348
15
2.398
10
2.451
10
2.489
90
2.567
5
Γ_γ (meV)
E_{ex} (MeV)

ANALYSIS AND DISCUSSION

In this chapter, both statistical and spectroscopic properties of the data are considered. Partial decay widths in different channels are examined for correlations. The ^{44}Ca and ^{62}Ni proton capture data are examined for possible $(^3He,d)$-(p,γ) correlations between gamma-ray widths and $(^3He,d)$ strengths to the same final states. The total gamma-ray widths are examined (using the maximum likelihood technique) to obtain an effective number of degrees of freedom. Comparisons with other data in this mass region are made: these include comparison with results from both proton capture and neutron capture. Inelastic spectroscopic factors are calculated. In addition to results from this experiment, inelastic spectroscopic factors are also determined from measurements performed by Moses (1970), Prochnow (1971), and Peters (1972).

Correlations

Previous experiments in this mass region involving neutron stripping and neutron capture by the same nucleus have shown a correlation between the spectroscopic factors $((2J+1)C^2S)$ and the gamma decay to the same final states (Lane, 1972). Often these correlations are large, with a linear correlation coefficient (LCC) greater than 0.8. A natural sequel to these experiments is a search for a correspondence between proton stripping and proton capture. As noted in the previous chapter, several $\ell = 1$ states in ^{45}Sc and ^{63}Cu which are strongly populated in the $(^3He,d)$ reaction were also populated in the proton capture reaction. The spectroscopic factors for these $\ell = 1$ states in ^{45}Sc and ^{63}Cu were taken from the literature, Schwartz and Alford (1966) for ^{45}Sc ; Blair

(1965) and Smith et al. (1967) for ^{63}Cu . These spectroscopic factors and the strength of the gamma decay to these states (in W.u.) are tabulated in Tables 4 and 5 for ^{45}Sc and ^{63}Cu , respectively. The linear correlation coefficients between the spectroscopic factors and the transition strengths is 0.45 for ^{45}Sc and 0.96 or 0.99 for ^{63}Cu depending on which spectroscopic factors are used. These correlations are listed in Table 6. If the distribution of gamma-ray widths to these final states is a chi-squared distribution of one degree of freedom, then these correlations are statistically significant at greater than the 90% level for ^{45}Sc and greater than the 95% level for ^{63}Cu.

As mentioned in Chapter 2, analgoue states provide the best case in the search for correlations between partial widths in various channels. Lane (1972) describes the situation as:

> "... an analogue state, because it corresponds to a low-lying state is much simpler than other states ($T_<$-states) near it. In particular, its natural decay widths for open allowed channels will be much greater than those for the $T_<$ states, roughly by the ratio of the level spacings for the two systems. ... Thus the isolated analogue state is a perfect example of a common doorway not just for two but in general for several channels."

Qualitative evidence for enhancement was presented in Chapter 4 where it was pointed out that the stronger fragments of the analogue states have generally stronger decay and usually populate fewer final states. In the case of highly fragmented analogue states, the strength of the analogue state is shared with other nearby resonances of the same spin

Table 4 The strength of the $\ell=1$ levels on ^{45}Sc in the $(^{3}He,d)$ reactions and the (p,γ) reaction

E_{ex} (KeV)	$(2J+1)C^2S$ [a]	M1 Widths on 3/2- A.S. (W.u.)	M1 Widths on 1/2- A.S. (W.u.)	M1 Widths on 1/2- Resonances off Analogue (W.u.)
376	0.56	2.02×10^{-2}	7.49×10^{-2}	6.16×10^{-2}
2067	0.56	2.24	4.34	4.33
1557	0.28	1.09	0.42	1.04
2341	0.12	2.84	3.74	2.80
2983	0.24	1.89	1.09	1.87
3025	0.40	1.45	3.87	2.11
3412	0.08	----	2.22	1.87
3484	0.20	1.04	2.45	2.28
3720	0.20	----	5.53	1.54
3881	0.20	2.	----	4.81
3926	0.40	1.20	----	----

[a] Schwartz and Alford (1966)

Table 5 The strength of the $\ell=1$ levels in ^{63}Cu in the ^{62}Ni$(^{3}He,d)$ reaction and the ^{62}Ni(p,γ) reaction

E_{ex} (KeV)	$(2J+1)C^2S$ [a]	$((2J+1)C^2S)$ [b]	M1 Widths in W.u.
G.S.	2.64	3.14	7.38×10^{-2}
670	1.40	1.42	3.14
2011	----	0.11	1.16
2062	0.46	0.28	0.74

[a] Blair (1965)

[b] Smith et al, (1967)

Table 6 Correlation between the $(^3He,d)$ strengths and the M1 strengths for the $\ell = 1$ low-lying levels in ^{45}Sc and ^{63}Cu

Isotope	Specie of Resonances	Correlation
^{45}Sc	3/2- Analogue Resonances	0.44[a]
	1/2- Analogue Resonances	0.46[a]
	1/2- Non-Analogue Resonances	0.51[a]
^{63}Cu	3/2- Analogue Resonances	0.96[b]
	3/2- Analogue Resonances	0.99[c]

[a] $(^3He,d)$ strengths taken from Schwartz and Alford (1966)

[b] $(^3He,d)$ strengths taken from Blair (1965)

[c] $(^3He,d)$ strengths taken from Smith et al. (1968)

and parity. Thus, if the strength in other channels is shared in the same proportion as the strength in the entrance channel, one will observe correlations between the entrance channel widths and the decay widths to the different open channels. That is, the analogue state is a common doorway for the channels. However, if the other channels are not strongly enhanced then no correlation is expected. The correlations measured between the various sets of widths are presented in the following two subsections.

$^{44}Ca(p,\gamma)^{45}Sc$

Figure 30 shows a plot of the proton widths, total gamma-ray widths, and partial gamma-ray widths for the fragments of the 3/2- analogue near 1.65 MeV. A visual comparison of the various sets of widths in this figure provides a qualitative measure of the correlations between the different channels. A more quantitative measure can be obtained by computing the LCC between the various sets of widths and by using Monte Carlo techniques to determine which of the LCC are statistically significant. (These Monte Carlo calculations are discussed in the Appendix. The definition of significance level is also discussed in this Appendix.) The various LCC are listed in Table 7. The 95% confidence levels for the correlations between the proton widths and other partial decay widths are -0.37 and 0.76. The transitions to the following final states were observed on six or more of the ten resonances of this fragmented analogue (the number in parenthesis is the statistical significance of the measured correlation); 12.4 keV (76%), 376 keV (82%), 543 keV (47%), 721 keV (86%), 938 keV (94%), 1067 keV (56%), and 2341 keV (86%). These significance levels were calculated treating each correlation as independent.

Figure 30 Channel decay widths for the ten fragments of the 3/2- analogue state in ^{45}Sc

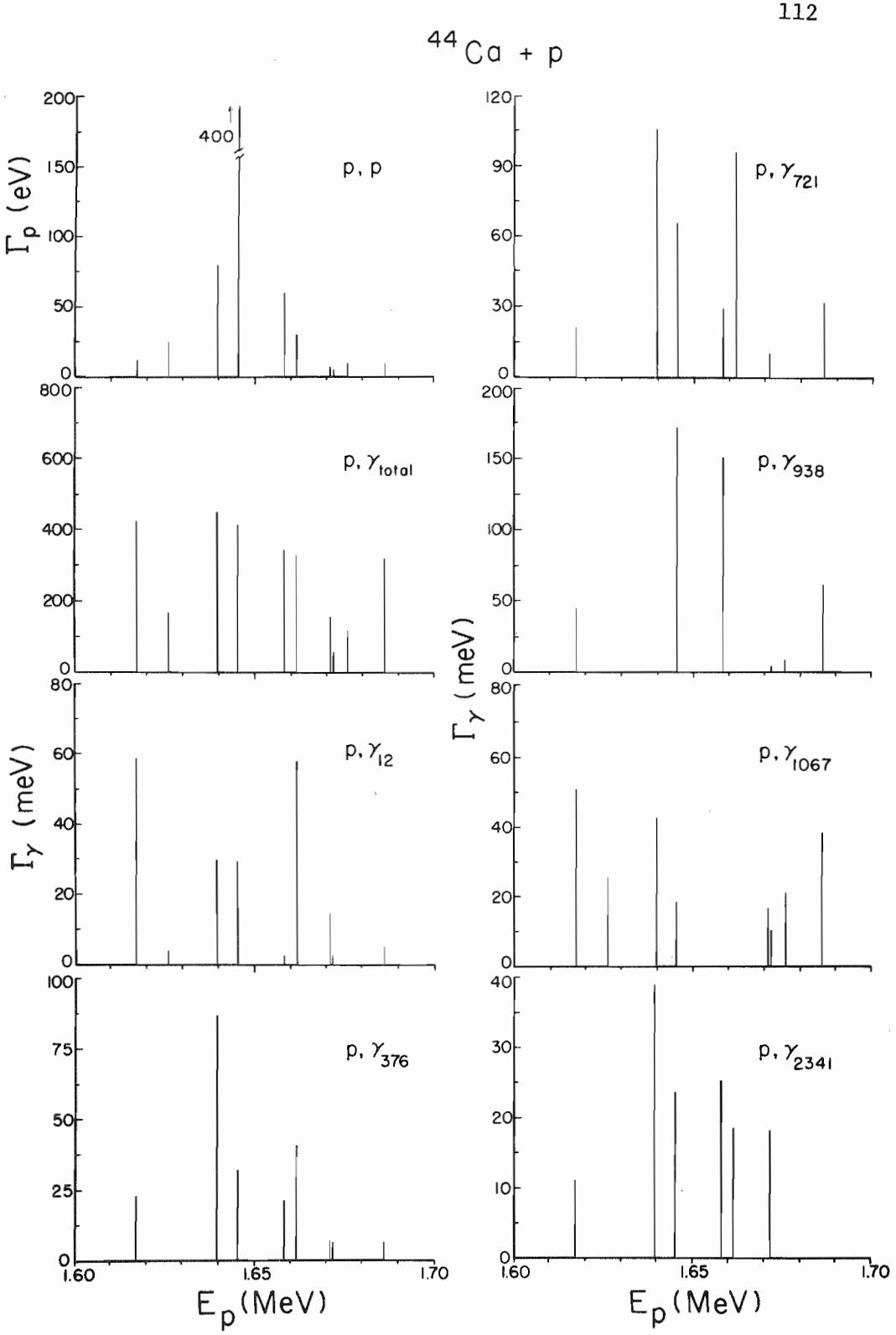
^{44}Ca + p
p, p
p, γ_{721}
p, γ_{total}
p, γ_{938}
p, γ_{12}
p, γ_{1067}
p, γ_{376}
p, γ_{2341}
400
Γ_p (eV)
Γ_γ (meV)
Γ_γ (meV)
E_p (MeV)
E_p (MeV)
1.60
1.65
1.70

Table 7 Channel-channel correlations for the 3/2- analogue state in ^{45}Sc

	P,P	P, γ Total	P, γ_{12}	P, γ_{376}	P, γ_{543}	P, γ_{721}	P, γ_{938}	P, γ_{1067}	P, γ_{2341}
P,P	1.00								
P, γ Total	0.45	1.00							
P, γ_{12}	0.16	0.63	1.00						
P, γ_{376}	0.29	0.71	0.53	1.00					
P, γ_{543}	-0.15	0.23	0.14	0.02	1.00				
P, γ_{721}	0.39	0.73	0.61	0.90	-0.09	1.00			
P, γ_{938}	0.71	0.49	-0.05	0.02	-0.15	0.11	1.00		
P, γ_{1067}	-0.08	0.37	0.22	0.22	0.83	0.02	-0.19	1.00	
P, γ_{2341}	0.42	0.58	0.33	0.85	-0.32	0.72	0.31	-0.09	1.00

Another interesting question is: what is the statistical significance of N out of M correlations having a correlation coefficient greater than a given value r ? Using the Bernoulli distribution, one can calculate this probability. The probability of obtaining exactly N of M correlation greater than r is given by

$$P_M(N) = \binom{N}{M}(1-q)^{M-N} q^N \tag{47}$$

where q is the probability of obtaining a correlation of r and $\binom{N}{M}$ is $N!/M!(N-M)!$. Thus, to determine the probability of obtaining five of seven correlation coefficients significant at levels of 76% or greater one computes the sum $p_7(5)$, $p_7(6)$, and $p_7(7)$. One obtains the result of 0.01, this is interpreted as meaning that there is 1% chance of obtaining the measured results, hence, the results are significant at the 99% level. The correlation between the elastic widths and total gamma widths is 0.41, which is significant at greater than the 90% level.

The decay of the fragments of the analogue state near 2.03 MeV was also examined for correlations. In this case inelastic widths were observed for a number of resonances. Figure 31 shows the elastic, inelastic, total gamma-ray, and other gamma-ray decay widths on the 38 1/2- resonances studied. Visually, the inelastic widths are stronger in the region near the center of the analogue state. This might be taken as evidence of enhancement, although a similar effect would be observed if the penetrabilities were changing rapidly in this energy region. Calculations indicate that the penetrabilities are not changing rapidly enough to account for the observed phenomena. Visually, the inelastic widths do not appear to be correlated with the proton widths.

Figure 31 Channel decay widths for the 38 1/2- resonances studied in ^{45}Sc ; the 1/2- analogue state is centered near 2.03 MeV

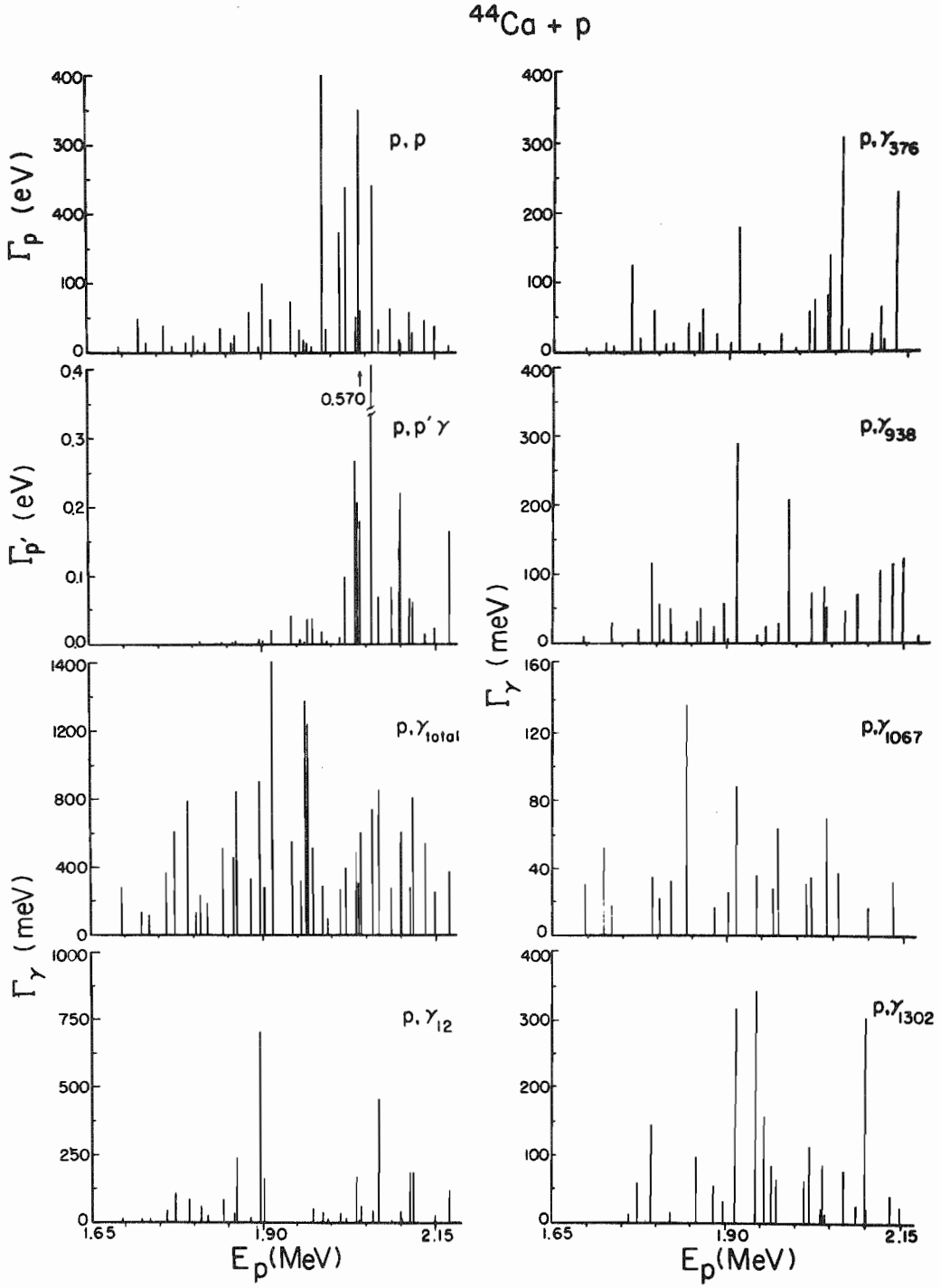
$^{44}Ca + p$
Γ_p (eV)
p, p
$\Gamma_{p'}$ (eV)
0.570
p, p'γ
Γ_γ (meV)
p, γ_{total}
p, γ_{12}
p, γ_{376}
p, γ_{938}
p, γ_{1067}
p, γ_{1302}
1.65
1.90
2.15
E_p(MeV)

Since data were taken both on the analogue and far from the analogue, some procedure must be adopted to classify the states. Based on an article by Lane (1969), one can show that 90% of the strength is within three times the spreading width of the analogue. Using the results of Wilson (1973), there are 24 fragments of this analogue state within 135 keV (three times the spreading width) of the centroid of the analogue state.

For the 38 resonances studied in this energy region, linear correlation coefficients were calculated as follows: first, on all resonances which were measured, second, on those 24 resonances that were within $\pm$ 135 keV of the centroid, and third, on those 14 resonances more than 135 keV from the centroid of the analogue state.

Table 8 lists the correlations in the region of the 24 fragments of the analogue state. The transitions to the following final states were observed on more than half of these 24 resonances (the number in parenthesis is the statistical significance of the measured correlation); 12.4 keV (87%), 376 keV (83%), 938 keV (87%), and 1302 keV (39%). Elastic widths were also correlated with the inelastic widths; the significance level was 83%. Thus, four of these five correlations are significant at a level greater than or equal to 83%. The statistical significance of four of five being significant at 83% level is greater than 98%. That is, about two percent of the time, four of the five correlations would be significant at a level of 83% or larger. The correlation of the elastic widths with the total capture widths is -0.28; significant at greater than the 90% level. Since this is of the opposite sign of the usual result for analogue states, this correlation between the elastic and total capture widths was examined very closely. Another measure of the total capture width is the area of the resonance

Table 8 Channel-channel correlations for the 1/2- analogue state in ^{45}Sc

	P,P	P, γ Total	P, γ_{12}	P, γ_{376}	P, γ_{938}	P, γ_{1067}	P, γ_{1302}	P, γ_{1799}	P, P'γ
P, P	1.00								
P, γ Total	-0.28	1.00							
P, γ_{12}	-0.27	0.55	1.00						
P, γ_{376}	0.25	0.25	-0.20	1.00					
P, γ_{938}	0.30	0.27	-0.17	0.25	1.00				
P, γ_{1067}	-0.04	0.41	-0.22	0.56	0.31	1.00			
P, γ_{1302}	-0.11	0.30	-0.19	0.03	0.22	0.35	1.00		
P, γ_{1799}	-0.22	0.18	0.13	-0.20	-0.05	-0.27	-0.02	1.00	
P, P'γ	0.26	0.01	-0.17	0.51	-0.26	0.04	-0.16	0.12	1.00

observed in the NaI excitation function. These areas were correlated with the elastic widths, yielding a value of -0.35, in agreement with the above result.

Table 9 lists the correlations for 14 1/2- resonances located more than 135 keV from the centroid of the analogue state. These correlations are consistent with a purely statistical behavior.

Table 10 lists the correlations for the 38 resonances studied in the region of this analogue state. The significant correlations are between the elastic and the inelastic widths and between elastic and partial gamma-ray widths to the levels at 376 and 938 keV. These are the same correlations that were statistically significant for the 24 resonances within 135 keV of the centroid of the analogue state; all are significant at greater than the 95% level. These results for all the 1/2- resonances simply reflect the dominance of the analogue state; the same correlations which were significant for resonances near the center of the analogue state, are also significant when the correlations are computed using data for all the 1/2- resonances.

The various widths for the $1/2^+$ states in the ^{45}Sc are shown in Figure 32. Note the visual correlation between the total gamma-ray widths and the elastic widths. This is quantitatively confirmed by evaluation of the LCC. Table 11 lists these correlations. The correlation between the elastic and total gamma-ray widths is 0.87, significant at the 96% level. It should be noted that the correlation is due to the large widths for both the elastic and gamma-ray near the center of the analogue state. Recalling that this level is a triplet in the capture channel, the total

Table 9 Channel-channel correlations for the 14 1/2- resonances away from the 1/2- analogue state in ^{45}Sc

	P,P	P, Total	P, γ_{12}	P, γ_{376}	P, γ_{938}	P, γ_{1067}	P, γ_{1302}	P, γ_{1799}	P, P'γ
P, P	1.00								
P, γ Total	-0.22	1.00							
P, γ_{12}	-0.27	0.72	1.00						
P, γ_{376}	0.33	0.29	-0.11	1.00					
P, γ_{938}	-0.30	0.51	0.28	0.0	1.00				
P, γ_{1067}	0.31	-0.12	-0.21	-0.03	-0.07	1.00			
P, γ_{1302}	-0.13	0.47	0.04	0.18	0.61	-0.18	1.00		
P, γ_{1799}	-0.02	0.41	-0.06	0.24	0.52	0.52	0.58	1.00	
P, P'γ	-0.29	0.65	0.88	-0.11	0.11	-0.20	-0.05	-0.19	1.00

Table 10 Channel-channel correlations for the 38 1/2- resonances in ^{45}Sc

	P, P	P, γ Total	P, γ_{12}	P, γ_{376}	P, γ_{938}	P, γ_{1067}	P, γ_{1302}	P, γ_{1799}	P, P'γ
P, P	1.00								
P, γ Total	-0.15	1.00							
P, γ_{12}	-0.20	0.59	1.00						
P, γ_{376}	0.29	0.27	-0.16	1.00					
P, γ_{938}	0.31	0.32	-0.07	0.25	1.00				
P, γ_{1067}	-0.03	0.18	-0.22	0.34	0.18	1.00			
P, γ_{1302}	-0.01	0.35	-0.13	0.08	0.28	0.16	1.00		
P, γ_{1799}	-0.12	0.24	0.10	-0.13	0.03	-0.10	0.07	1.00	
P, P'γ	0.37	0.10	-0.10	0.51	-0.16	-0.01	-0.03	0.20	1.00

Table 11 Channel-channel correlations for the $1/2^+$ analogue state in ^{45}Sc

	P,P	P, γ_{12}	P, γ_{376}	P, γ_{543}	P, γ_{1067}	P, γ_{1302}	P, γ_{3025}	P, P'γ	P, γ Total
P, P	1.00								
P, γ_{12}	0.21	1.00							
P, γ_{376}	-0.52	0.03	1.00						
P, γ_{543}	0.64	0.52	-0.30	1.00					
P, γ_{1067}	0.73	0.05	-0.68	0.33	1.00				
P, γ_{1302}	0.91	0.29	-0.39	0.83	0.61	1.00			
P, γ_{3025}	0.41	0.24	-0.29	0.21	0.0	0.24	1.00		
P, P'γ	0.09	-0.24	0.47	0.03	0.14	0.20	-0.27	1.00	
P, γ Total	0.87	0.28	-0.63	0.65	0.88	0.86	0.07	0.03	1.00

Figure 32 Channel decay widths for the nine fragments of the $1/2^+$ analogue state in ^{45}Sc

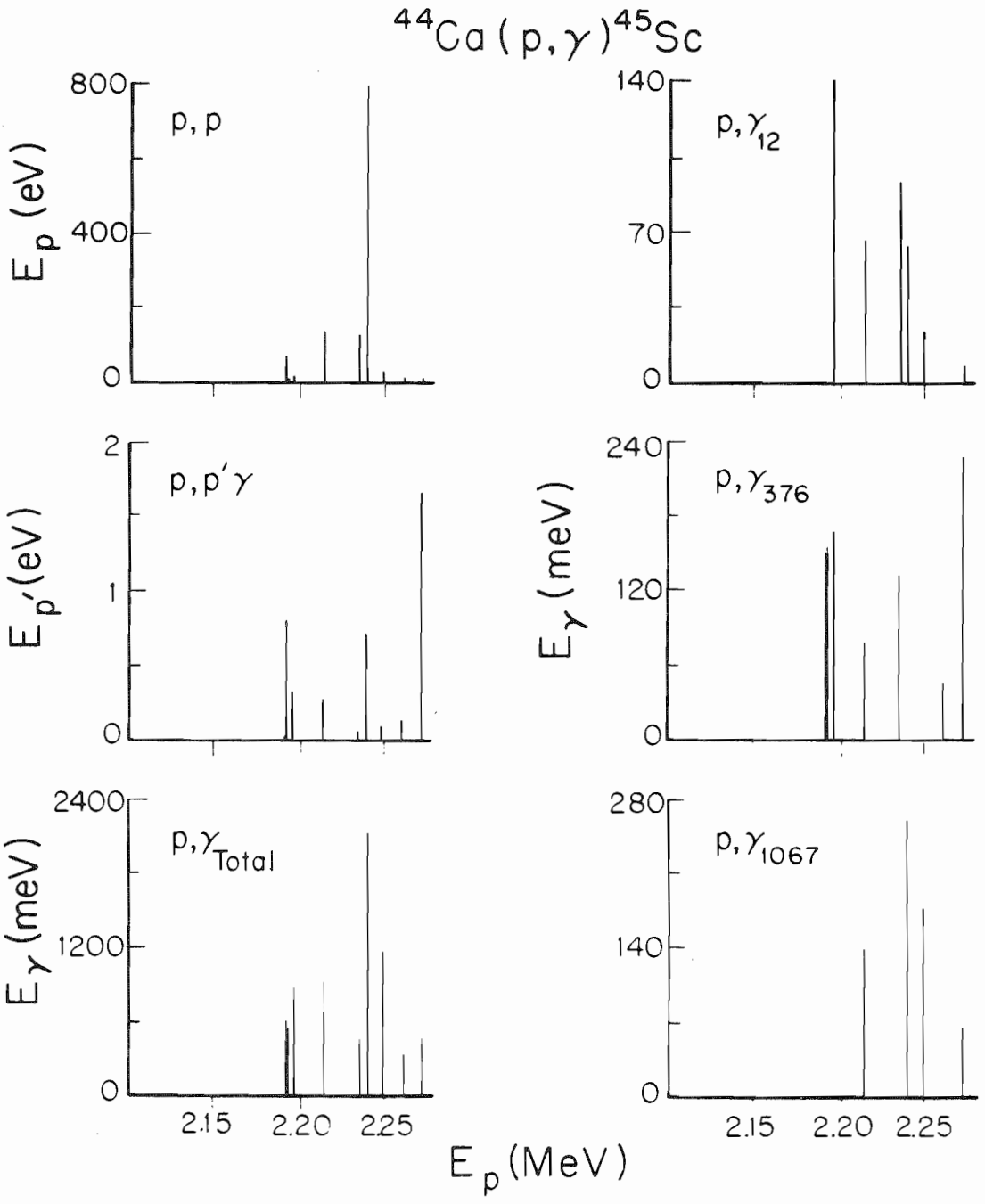
$^{44}Ca(p,\gamma)^{45}Sc$
p, p
E_p (eV)
800
400
0
p, γ_{12}
140
70
0
p, p'γ
$E_{p'}$(eV)
2
1
0
p, γ_{376}
E_γ (meV)
240
120
0
p, γ_{Total}
E_γ (meV)
2400
1200
0
p, γ_{1067}
280
140
0
2.15
2.20
2.25
E_p (MeV)

gamma-ray width may have a large error; if this resonance is omitted then the correlation is not statistically significant. Correlations between elastic widths and widths in other channels are not significant.

$^{62}Ni(p,\gamma)^{63}Cu$

As shown in the previous chapter, the decay of capture resonances in ^{63}Cu are simpler than the decay of capture resonances in ^{45}Sc . The decay of the s-wave resonance showed no definite characteristic patterns, while the stronger fragments of the 3/2- analogue state showed stronger gamma-ray widths than the weaker fragments of the analogue state.

These data were examined for correlations between the widths of various open channels. Figure 33 shows the elastic, inelastic, total gamma-ray, and partial gamma-ray widths associated with the $1/2^+$ resonances in ^{63}Cu . Visually there is little evidence for correlations between the elastic widths and any partial widths in other channels. Calculations of the LCC confirm this observation. Correlations between the various sets of widths are listed in Table 12. The correlations between the elastic channels and other channels are not statistically significant. There is visually a correlation between the total gamma-ray widths and the widths of the transitions to the ground state. The LCC is 0.74, statistically significant at greater than the 95% level. Since the ground state transition is usually the strongest transition and has a large fraction of the total capture width, it modulates the total gamma-ray widths.

Figure 34 shows the various widths for the analogue state at 2.65 MeV. In this case the similarity between the elastic and inelastic widths is

Figure 33 Channel decay widths for the 21 $1/2^+$ resonances studied in ^{63}Cu ; note that a large fraction of the total capture width is in the ground state branch

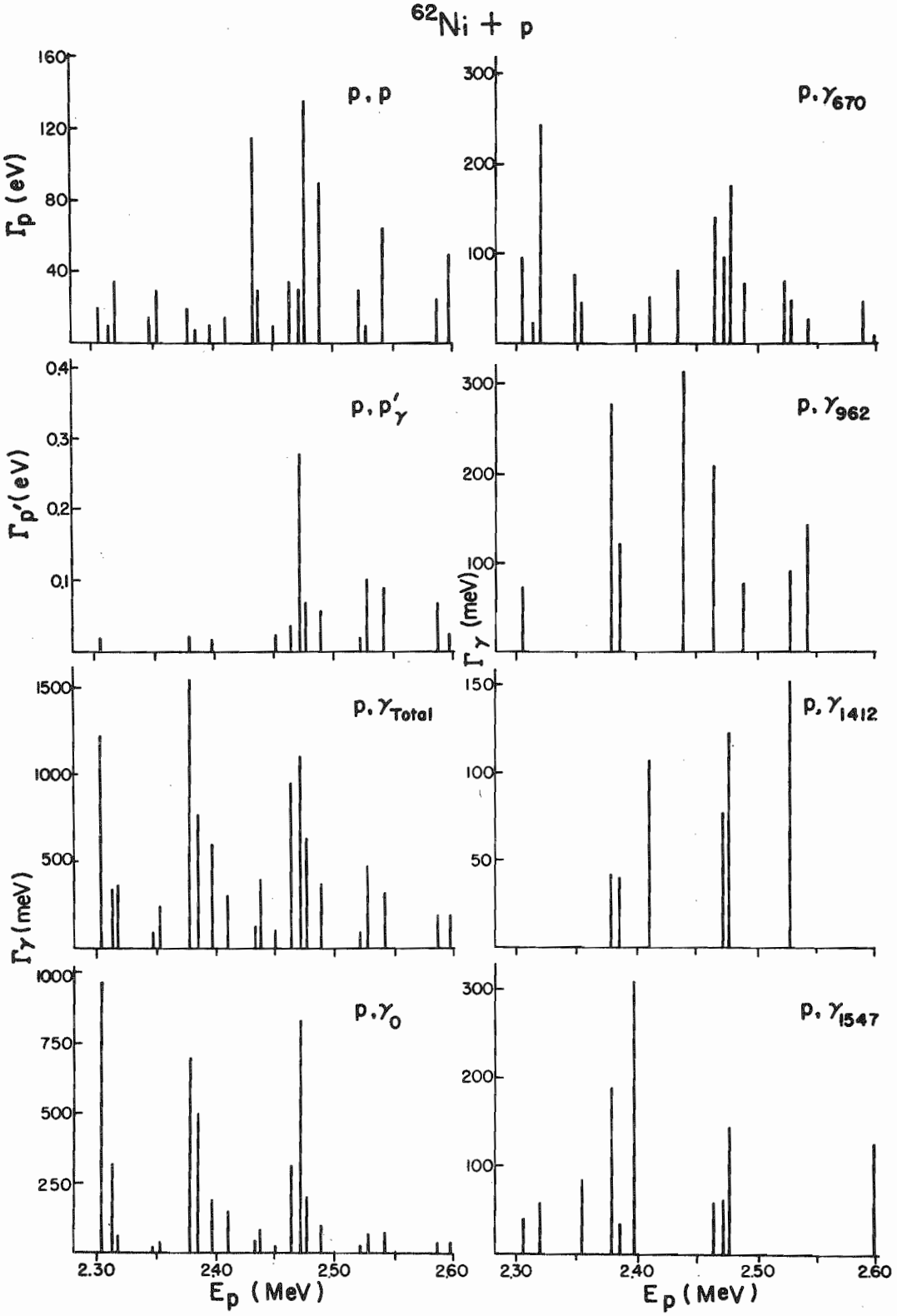
$^{62}Ni + p$
p, p
p, γ_{670}
p, p'_γ
p, γ_{962}
p, γ_{Total}
p, γ_{1412}
p, γ_0
p, γ_{1547}
Γ_p (eV)
$\Gamma_{p'}$ (eV)
Γ_γ (meV)
E_p (MeV)
2.30
2.40
2.50
2.60

Table 12 Channel-channel correlations for the 20 $1/2^+$ resonances in ^{63}Cu

	P, P	P, P'γ	P, γ G.S.	P, γ Total
P, P	1.00			
P, P'γ	0.11	1.00		
P, γ G.S.	-0.21	0.36	1.00	
P, γ Total	-0.06	0.44	0.74	1.00

Figure 34 Channel decay widths for the 14 fragments of the 3/2- analogue state in ^{63}Cu at 2.65 MeV

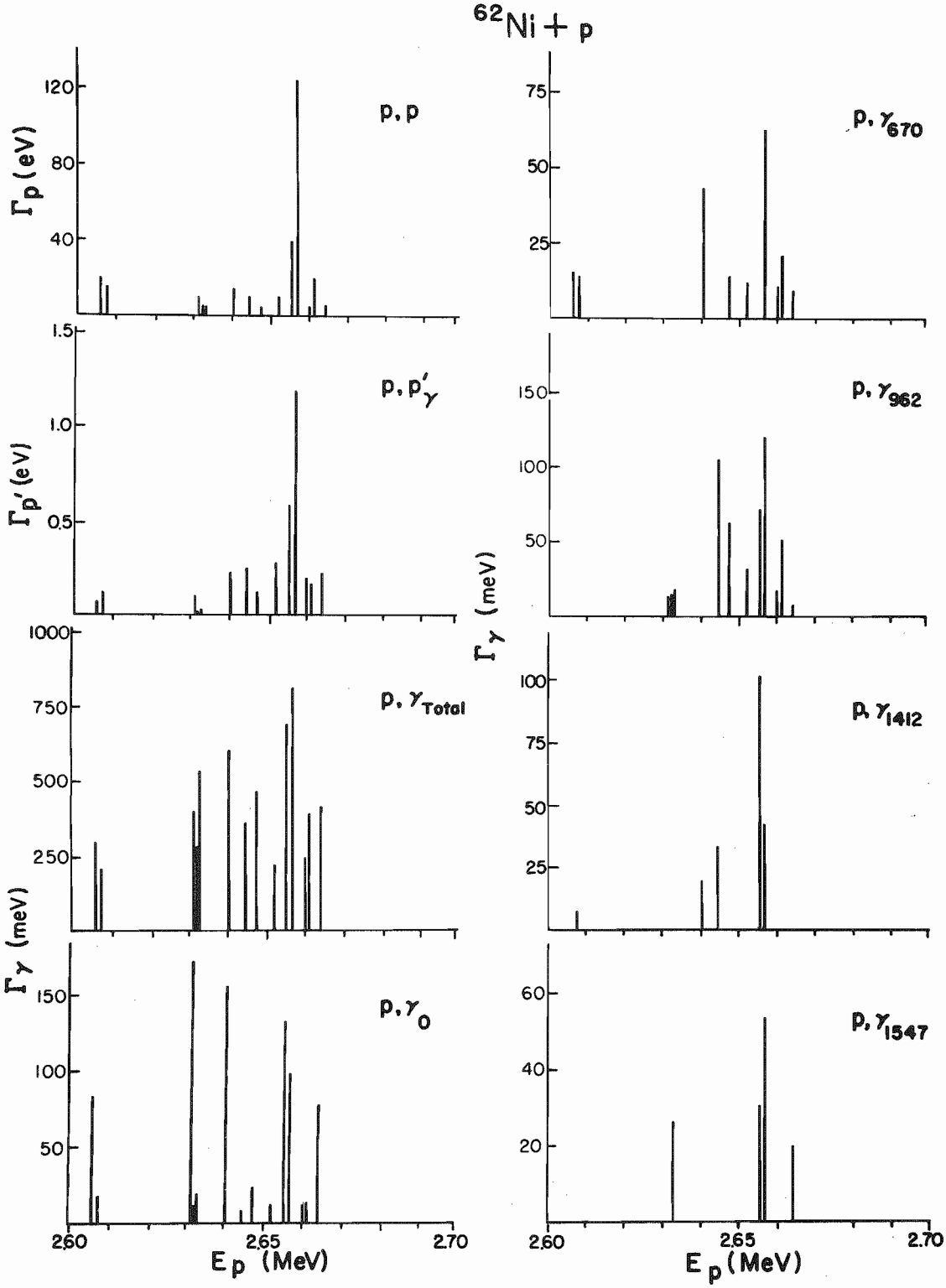
$^{62}Ni + p$
p, p
p, γ_{670}
p, p'_γ
p, γ_{962}
p, γ_{Total}
p, γ_{1412}
p, γ_0
p, γ_{1547}
Γ_p (eV)
$\Gamma_{p'}$ (eV)
Γ_γ (meV)
E_p (MeV)
2.60
2.65
2.70

very striking. Also, there is evidence for correlations with other channels. The LCC are tabulated in Table 13. The transitions to the following final states were observed on nine of more of the resonances of this fragmented analogue state (the number in parenthesis is the statistical significance of the measured correlation); g.s. (87%), 670 keV (98%), and 962 keV (94%). The correlations between the elastic widths and the inelastic widths is significant at the 99% level, and the correlation between the elastic and total gamma-ray widths is significant at the 98% level. The fact that all the measured correlations with the elastic widths are positive and significant at greater than the 80% level is very unusual. The chance for this event is on the order of one in 10^8. In fact, all the correlations in Table 13 are positive, save one which is almost zero. An estimate of the probability of this event occuring is on the order of one in 10^{10}. Indeed this analogue state displays non-statistical behavior!

Multipole Transitions

Transitions observed in these experiments (where the final state spin and parity are known) can be categorized by their multipolarity. Most of the transitions observed were of E1 or M1 character. Since the mixing ratios are assumed to be zero, the computed widths (in W.u.) represent upper limits for the various transitions.

In the ^{44}Ca capture data, the multipolarity of approximately 300 transitions was identified. Of these transitions about 250 are E1 and M1. Figure 35 shows the distribution of these E1 and M1 transitions of the various species of resonances studied. The shaded portion of the M1

Table 13 Channel-channel correlations for the 3/2- analogue state in ^{63}Cu

	P, P	P, γ Total	P, P'γ	P, γ G.S.	P, γ_{670}	P, γ_{962}	P, γ_{1412}	P, γ_{1547}
P, P	1.00							
P, γ Total	0.73	1.00						
P, P'γ	0.93	0.78	1.00					
P, γ G.S.	0.34	0.70	0.31	1.00				
P, γ_{670}	0.76	0.53	0.67	0.28	1.00			
P, γ_{962}	0.60	0.56	0.72	-0.08	0.28	1.00		
P, γ_{1412}	0.49	0.74	0.63	0.40	0.09	0.57	1.00	
P, γ_{1547}	0.51	0.58	0.57	0.09	0.34	0.56	0.35	1.00

Figure 35 Distribution of the E1 and M1 transition strengths for the $3/2^-$, $1/2^-$ and $1/2^+$ resonances studied in ^{45}Sc

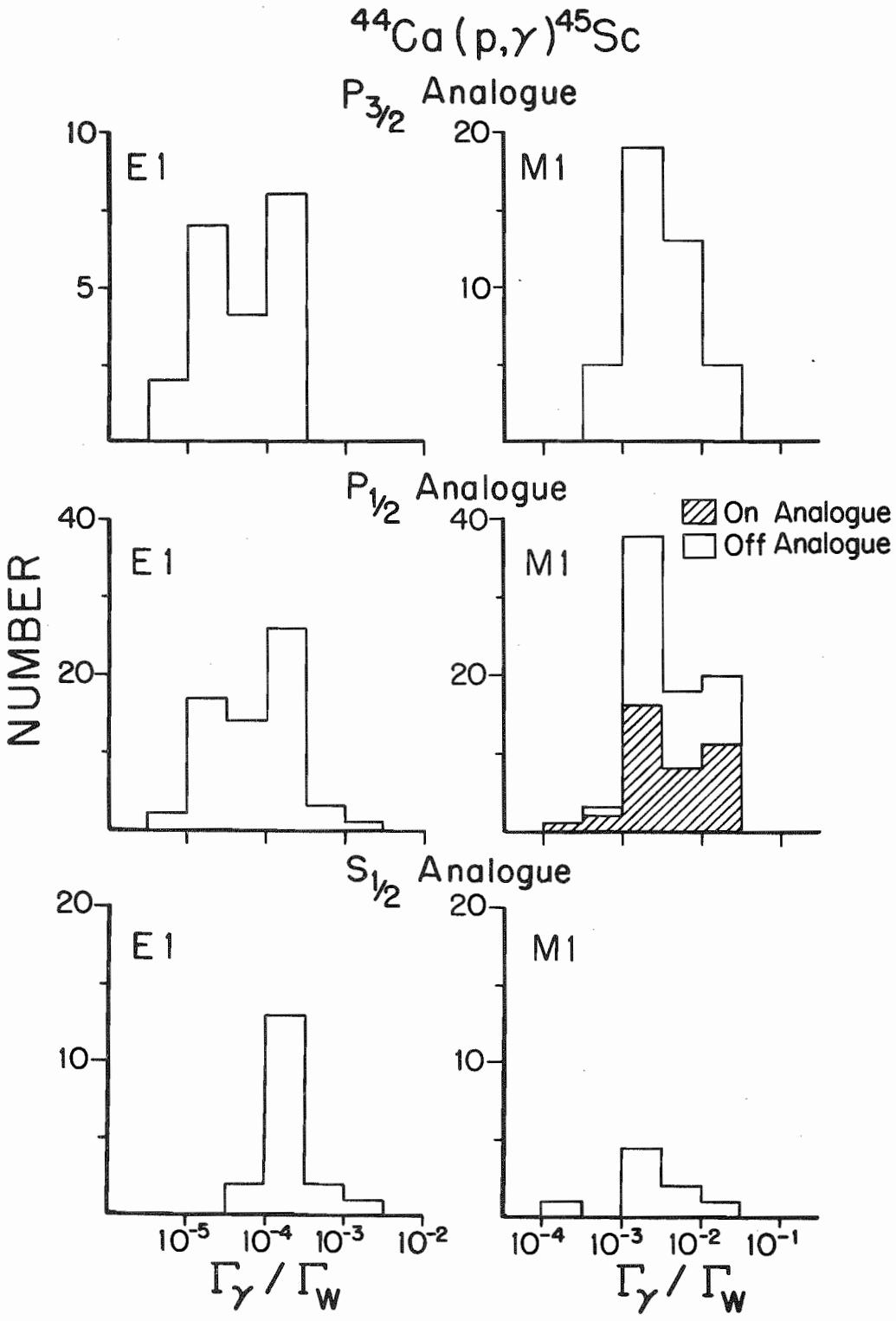
$^{44}Ca(p,\gamma)^{45}Sc$
$P_{3/2}$ Analogue
E1
M1
10
5
20
10
$P_{1/2}$ Analogue
On Analogue
Off Analogue
NUMBER
40
20
$S_{1/2}$ Analogue
10^{-5} 10^{-4} 10^{-3} 10^{-2}
10^{-4} 10^{-3} 10^{-2} 10^{-1}
Γ_γ / Γ_W

strength on the 1/2- analogue state is from the central portion of the analogue state. General trends observed on the figure are:

1) the average E1 strength is about 2×10^{-4} W.u., and
2) the average M1 strength is about 5×10^{-3} W.u.

Figure 36 summarizes the experimental data in this mass region involving M1 transitions from analogue states. Most of these data involve analogue to anti-analogue state transitions, therefore transitions to levels with the same spin and parity. A direct comparison of these data with the decay of fragmented analogue states may not be straightforward. For comparison purposes only, transitions which may be to states with the same spin and parity are considered.

The sum of the M1 strength on the 3/2- analogue state near 1.65 MeV in $^{44}Ca + p$ is 0.22 W.u. This sum does not contain any transitions to states known to be other than 3/2-. Since no background states of spin and parity 3/2- are nearby, the background strength is unknown. Therefore the sum of M1 strength is an upper limit for the strength on this analogue. Comparison of this value with data presented on Figure 36 shows that the M1 strength is of the right order of magnitude.

The sum of the M1 strength for the 38 1/2- levels studied is 0.59 W.u. Of this strength 0.05 W.u. is known to consist of transitions to states with spin and parity other than 1/2-. The fourteen resonances more than 135 keV from the centroid of the analogue state have an upper limit of 0.11 W.u. for the transitions to states with spin and parity 1/2-. This gives an estimate of 0.18 W.u. for the background for 24 levels. An estimate of 0.25 W.u. is obtained for the M1 strength above background for

Figure 36 **Analogue to** anti-analogue M1 transition strengths in W.u. (squares indicate 7/2- to 7/2- transitions; circles 3/2- to 3/2- transitions; triangles $9/2^{+}$ to $9/2^{+}$ transitions); the open symbols are experimental data (Endt, 1967, and 1969; Maripuu *et al.* 1970; Maripuu, 1970a and 1970b; Klapdor, 1971); the filled symbols are values for the single-particle transitions with a spinless core calculated with Schmidt g-factors (Maripuu, 1969)

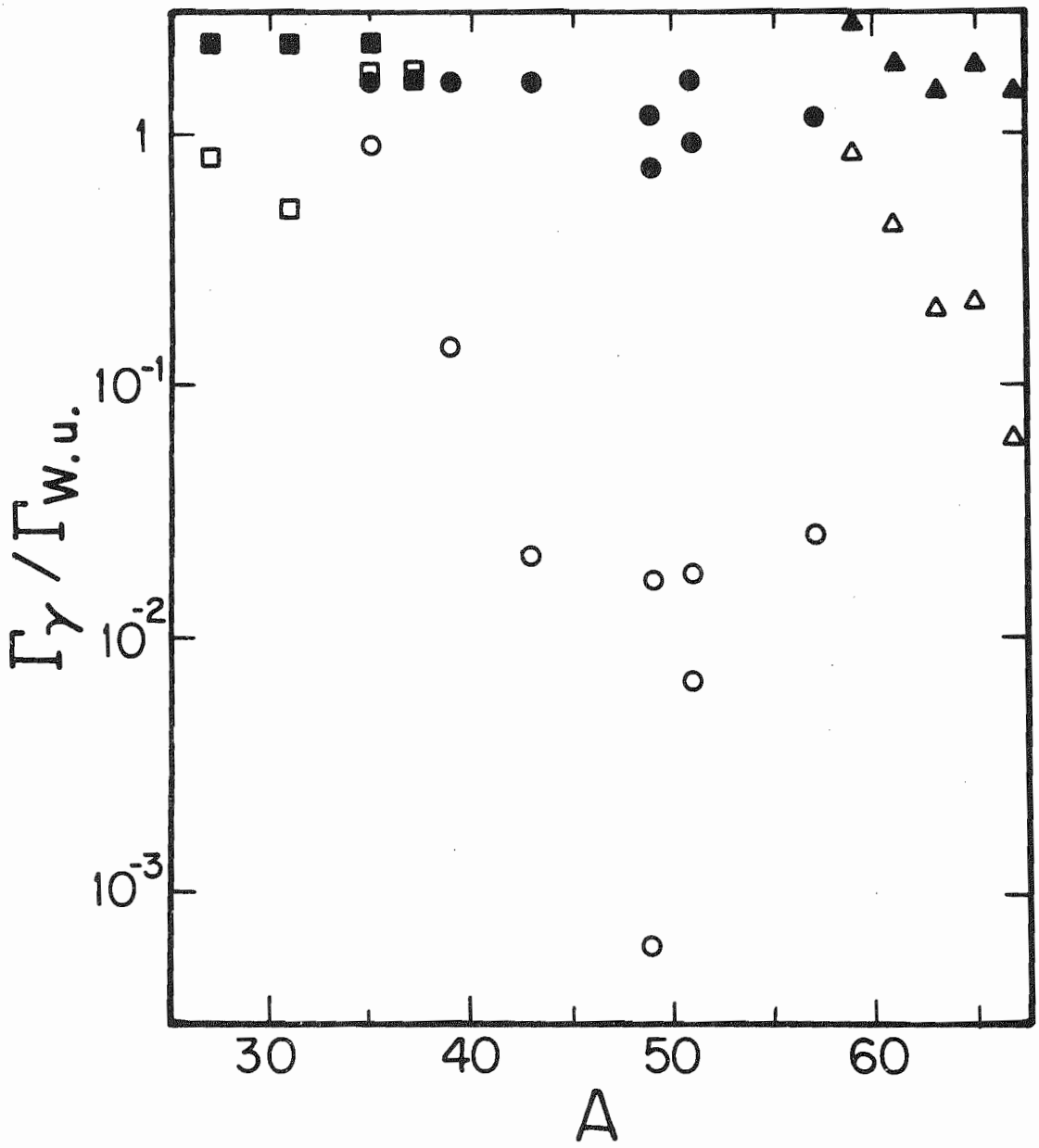
1
10^{-1}
10^{-2}
10^{-3}
$\Gamma_\gamma / \Gamma_{W.u.}$
30
40
50
60
A

the 24 levels within $\pm$ 135 keV of the centroid of the analogue state. This seems clear evidence for enhancement of the M1 strength on this analogue state.

For the $1/2^+$ states studied near the analogue state the sum of the M1 strength is 5.49×10^{-2} W.u. There are only two transitions which are to states with $J = 1/2^+$. One of these transitions is especially large, 2.65×10^{-2} W.u. This large transition strength is from a level adjacent to the strongest level in the analogue state. This indicates that the M1 strength is appreciable near the center of the analogue state. Note that the M1 strength for this analogue state is smaller than the M1 strength for the two $\ell = 1$ analogue states in this nucleus.

There are only a few higher multipole transitions observed on these analogue states. The higher multipoles are predominantly M2. These M2 transitions are usually observed on some of the smaller resonances in the elastic channel. In fact, some of the M2 transitions are very large and may indicate misassigned J values. For example, the resonance at 1.9724 MeV with a proton width of 15 eV has an M2 transition of about 90 W.u. If the spin is 3/2- then the transition would be E1 multipolarity and have a width of about 10^{-3} W.u. This information can be very helpful in determining spins. The spins of some of these weak resonances are very important to statistical studies of proton resonances. Thus the capture data complement the elastic scattering data.

In the study of the proton capture on resonances in $^{62}Ni(p,\gamma)^{63}Cu$ the multipolarities of about 125 transitions were identified. Approximately 100 of these transitions are E1 and M1. About fifteen M2 transitions were observed. These results were summarized in Figure 37.

Figure 37 Distribution of M1 strength on the 3/2- analogue in ^{63}Cu and distributions of E1 and M2 strengths on the $1/2^+$ resonances in ^{63}Cu (see text for explanation of the large M2 transitions)

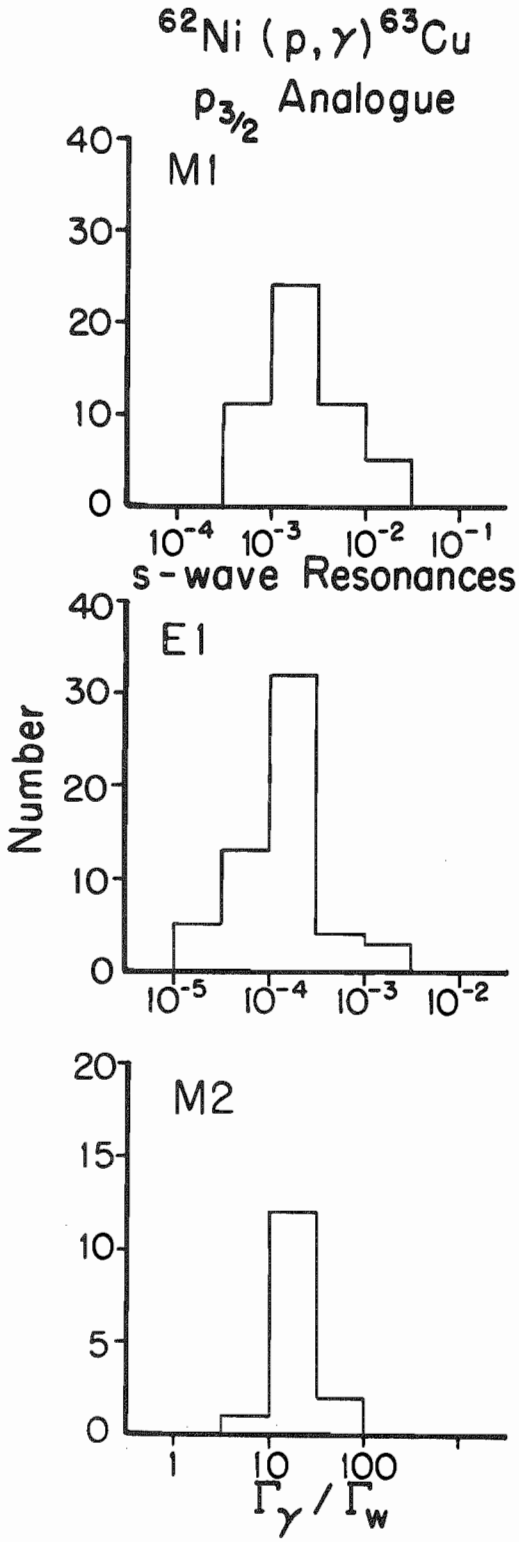
$^{62}Ni\ (p,\gamma)^{63}Cu$
$p_{3/2}$ Analogue
M1
40
30
20
10
0
10^{-4} 10^{-3} 10^{-2} 10^{-1}
s-wave Resonances
Number
E1
40
30
20
10
0
10^{-5} 10^{-4} 10^{-3} 10^{-2}
M2
20
15
10
5
0
1
10
100
Γ_γ / Γ_w

The average E1 strength is about 2.5 X 10^{-4} W.u., about the same as the ^{45}Sc data. The average M1 strength on the analogue state is about 4.3 X 10^{-3} W.u.

The sum of the M1 strength from the 3/2- analogue state near 2.65 MeV is about 0.23 W.u. As in the case of the 3/2- analogue in ^{45}Sc there are no nearby background levels to give an indication of the background strength. Subtracting transition strength to states known to be not 3/2- one obtains an upper limit of 0.10 W.u. This is in agreement with the M1 strength from a 9/2 + analogue state in ^{63}Cu (Fodor et al., 1970; Szentpetery et al., 1972; Maripuu et al., 1972).

On the $1/2^+$ resonances studied in this nucleus there were a number of M2 transitions observed. Recalling the level density observed in the capture excitation function for ^{62}Ni(p,γ)^{63}Cu it is clear there may be unresolved resonances in the capture channel. If there are unresolved doublets, with a resonance of higher J value near the $1/2^+$ state, one may observe transitions which are considered M2. With these possibilities in mind, the data from $1/2^+$ were carefully examined for evidence of doublets. Several of the $1/2^+$ resonances having M2 transitions were near other levels, although some of the resonances appeared to be single. On these resonances angular distributions were measured. Although these measurements are preliminary, they do indicate a non-isotropic decay. This would imply higher spin states mixed with the $1/2^+$ resonances. Other work in ^{62}Ni(p,γ)^{63}Cu in this energy region has indicated similar difficulties (Garg and Bokharee, 1973). Although these ambiguities are probably also present on the analogue state at 2.65 MeV the correlations observed are believed to be real. As shown above, the observed

correlations on the 3/2- analogue state are already highly significant. Contributions from higher spin states would tend to weaken these correlations.

Distribution of Gamma-Ray Widths

The maximum likelihood technique was used to determine the number of degrees of freedom of the assumed chi-square distribution of the gamma-ray widths. For example, the decay to any given final state would be expected to have $\nu = 1$ while the distribution of total gamma-ray widths would be quite different. The results are consistent with these expectations; transitions to a particular final state yield ν values of about 1.5 ± 0.5. Specific values of ν are 1.88 ± 0.84 for transitions in ^{45}Sc and 1.57 ± 0.45 for transitions in ^{63}Cu. For such a limited sample, this result is not considered to be in disagreement with the expected result of one degree of freedom. The total gamma-ray widths were examined for the effective number of degrees of freedom. The results in ^{45}Sc are 4.50 ± 0.75 and in ^{63}Cu 3.57 ± 0.99 . In the case of ^{63}Cu this agrees with the number of primary transitions, while in ^{45}Sc this is about half of the number of primary transitions. This discrepancy between the number of observed transitions and the effective number of degrees of freedom indicates that on the average the transitions to various final states in ^{45}Sc are not equal.

Inelastic Spectroscopic Factors

The parent state inelastic spectroscopic factors are calculated using equation

$$S_{pp'} = \frac{(2T_o+1)\Gamma^A_{p'}}{\Gamma^{sp}_{p'}} . \qquad [(42)]$$

For fragmented analogue states the width is obtained by summing the inelastic widths observed on the different fragments of the analogue state. Background corrections are not made since the inelastic widths off the analogue state are very small.

For the inelastic decay of analogue states in this mass region the single particle widths are calculated using three different methods: the B-matrix method of Thompson, Adams and Robson (1968) (hereafter referred to as TAR), the shell model methods of Zaidi, Darmodjo and Harney (1967) (ZDH) and Mekjian and MacDonald (1968) (MM). These methods are discussed by Harney and Weidenmüller (1969) and incorporated into a computer code written by Harney (1969).

The use of this code to calculate single particle widths involves two steps. The first step is to input the proton optical model parameters, the analogue state parameters, and the parent state parameters (the neutron binding energy and the number of modes in the neutron wave function, i.e., the major shell number). The proton optical model parameters are those used to calculate the elastic spectroscopic factors. In the first calculation the neutron optical model parameters are varied until the parent state binding energy matches Bn. A more accurate proton well depth is then obtained by adding to this neutron well depth the symmetry potential:

(48) $$U_{sym} = \{\frac{(2T_o+1)}{2}\} \cdot \frac{125}{A} \text{MeV}$$

This is the isospin dependent term of the optical potential. The new proton parameters are used for the final calculation. The single particle widths calculated from this code are tabulated in Table 14. Note that the calculation from the two shell models (ZDH and MM) are almost identical and significantly different from the R-matrix value (TAR).

The spectroscopic factors calculated for several analogue states in this mass region are listed in Table 15. These results show that the inelastic spectroscopic factors are often comparable to the elastic spectroscopic factors. The results are consistent with the work of Kern et al. (1973).

Table 14 Calculated single particle widths for inelastic scattering on selected analogue states in mass 45-63 region

Parent	E_p^{Lab} (MeV)	J^{π}	U_n (MeV)	U_p (MeV)	$\Gamma^{TAR}_{S.P.(2T_o+1)^{-1}}$ (eV)	$\Gamma^{ZDH}_{S.P.(2T_o+1)^{-1}}$ (eV)	$\Gamma^{MM}_{S.P.(2T_o+1)^{-1}}$ (eV)
^{45}Ca	2.034	1/2-	-53.40	-60.34	6.05	12.55	12.69
	2.233	$1/2^+$	-71.271	-78.214	174.4	315.1	318.6
^{47}Ti	2.894	3/2-	-46.505	-50.58	3733	8636	8701
^{49}Ti	2.951	3/2-	-44.765	-51.275	2698	4320	4868
^{51}Cr	3.150	$(5/2)^+$	-64.644	-68.800	1477	3157	3178
^{55}Cr	1.995	3/2-	-46.990	-55.100	56.65	84.88	85.86
^{59}Fe	2.226	3/2-	-43.694	-51.817	23.40	36.61	37.06
^{63}Ni	2.650	3/2-	-44.271	-51.321	10.18	17.43	17.63

$$U_p = U_n - [(2T_o+1)/2]\frac{125}{A}$$

$$R_r = R_C = 1.25\ A^{1/3}\ \text{fm}$$

$a_r = 0.65$ fm

$a_s = 0.47$ fm

$V_{so} = -8.0$ MeV

Table 15 Spectroscopic factors for inelastic scattering from selected analogue states in the mass 45-63 region

Isobaric Pair	E_x of Parent (MeV)	E_p^{Lab} MeV	J^π	$\Sigma\Gamma_{p'}$ (eV)	$S_{pp'}^{TAR}$	$S_{pp'}^{ZDH}$	$S_{pp'}^{MM}$	S_{pp}
^{45}Ca-^{45}Sc	2.251	2.034	1/2-	2.36	0.39	0.19	0.19	0.22[a]
	2.396	2.233	$1/2^+$	4.10	0.02	0.01	0.01	0.03[a]
^{47}Ti-^{47}V[b]	3.913	2.894	3/2-	780	0.21	0.09	0.09	0.05[b]
^{49}Ti-^{49}V[b]	3.261	2.951	3/2-	455	0.17	0.09	0.09	0.13[b]
^{51}Cr-^{51}Mn[c]	4.070	3.150	$(5/2)^+$	1875[g]	1.27	0.59	0.59	0.20[c]
^{55}Cr-^{55}Mn[d]	0	1.995	3/2-	2.49	0.04	0.03	0.03	0.31[c]
^{59}Fe-^{59}Co[d]	0	2.226	3/2-	5.15	0.22	0.14	0.14	0.27[e]
^{63}Ni-^{63}Cu	0.158	2.650	3/2-	3.57	0.35	0.20	0.20	0.11[f]

a Wilson (1973)

b Prochnow (1971)

c Moses (1970)

d Peters (1972)

e Lindstrom (1970)

f Browne (1969)

g Based on the inelastic scattering off the analogue state between 10 and 20% of this is attributed to background

SUMMARY AND CONCLUSIONS

Capture excitation functions are measured on ^{44}Ca (1.56 to 2.28 MeV) and ^{62}Ni (2.30 to 2.70 MeV). Using an 80 cm^3 Ge(Li) detector spectra were taken on 57 resonances in ^{45}Sc and 35 resonances in ^{63}Cu. The partial gamma-ray widths (and inelastic widths when observable) were extracted for these 92 resonances. The analysis of these data was directed primarily toward correlations between partial widths in different channels. On the 3/2- and 1/2- analogue states in ^{45}Sc and on the 3/2- analogue state in ^{63}Cu statistically significant correlations between various channels were found.

In particular, for the 1/2- analogue state in ^{45}Sc and the 3/2- analogue state in ^{63}Cu, the elastic widths are strongly correlated with the inelastic widths. This strong correlation between the elastic and inelastic widths is consistent with results for a highly fragmented 3/2- analogue state in ^{49}V (Prochnow, 1971) and for analogue states in ^{55}Mn and ^{59}Co experiments the correlation between elastic and inelastic widths off analogue states were not statistically significant. One concludes that for all of these analogue states, the analogue is a common doorway for both the elastic and inelastic channels.

The correlation between elastic widths and total capture widths on the four analogue states studied in ^{45}Sc and ^{63}Cu were all statistically significant. These results agree with the results of Vingiani et al. (1971a, 1968b), and Peters (1972). In ^{45}Sc the correlation between the total capture widths and the elastic widths on fourteen 1/2- resonances off the analogue state is -0.13. If one assumes

that the total widths are distributed according to a chi-squared distribution with five degrees of freedom (as the data indicate), then -0.13 is the most probable value for the correlation of the elastic widths with the total capture widths. Similar results were obtained on twenty s-wave resonances in ^{63}Cu . It is clear that the analogue state strongly modulates the total capture widths. With one exception (the $1/2^+$ analogue state in ^{45}Sc) elastic widths are also correlated with particular partial gamma-ray widths to low-lying final states.

The strengths of the $\Delta J = 0$ M1 transitions on the analogue states, although indicating an enhancement of the M1 strength on the analogue, are still small compared to the M1 strengths observed in the s - d shell. The M1 strengths on the 3/2- analogue states are inhibited by a factor of 10-100. These inhibitions have been observed for other analogue states in this mass region. Maripuu (1970c) and Hirata (1970) have explained these inhibitions in terms of core polarization effects in the f - p shell. The observed M1 strength of the 3/2- analogue in ^{45}Sc is approximately the same as the M1 strength for the 1/2- analogue in ^{45}Sc . The M1 strength from the 1/2- analogue state is expected to be reduced ty 20 (Maripuu, 1970b). If this were true, the present results would imply an M1 strength for the 3/2- analogue of the order of a W.u., or essentially the same as observed in the s - d shell. Thus, the result for the two $\ell = 1$ analogue states in ^{45}Sc may indicate core polarization effects are much stronger for $J = 3/2$ than for $J = 1/2$ in this shell.

These experiments have shown non-statistical behavior for different analogue state exit channels. The large and significant correlations between widths in different channels demonstrate that the analogue state is

a common doorway for these channels, and thus confirm Lane's predictions. Decay from non-analogue resonances seems consistent with the usual compound nuclear model. From these present results, it seems clear that high resolution studies of the proton capture reaction on analogue states will continue to provide exacting tests for understanding of analogue state phenomena.

LIST OF REFERENCES

Anderson, J.D. and C. Wong. 1961. Phys. Rev. Letters 7, 250.

Anderson, J.D. and C. Wong. 1962. Phys. Rev. Letters 8, 442.

Anderson, J.D., C. Wong, and J.W. McClure. 1962. Phys. Rev. 126, 2170.

Anderson, J.D., C. Wong, and J.W. McClure. 1963. Phys. Rev. 129, 2718.

Barkas, W.H. and M.J. Berger. 1964. NAS-NRC Publication 1133, Nuclear Science Series, Report 39, 103.

Bevington, P.R. 1969. Data Reduction and Error Analysis for the Physical Sciences. McGraw-Hill Co., New York, New York.

Blair, A.G. 1965. Phys. Rev. 140, E648.

Blatt, J.M. and V.F. Weisskopf. 1952. Theoretical Nuclear Physics. John Wiley and Sons, Inc., New York, New York.

Bondelid, R.O. and C.A. Kennedy. 1958. A two-meter positive-ion beam electrostatis analyzer. Naval Research Laboratory, Washington, D.C.

Browne, J.C. 1969. Fine structure of analog states in ^{61}Cu, ^{63}Cu and ^{65}Cu. Unpublished Ph.D. dissertation. Duke University, Durham, N.C., Department of Physics. University Microfilms, Ann Arbor, Michigan.

Browne, J.C., G.A. Keyworth, P. Wilhjelm, D.P. Lindstrom, J.D. Moses, H.W. Newson, and E.G. Bilpuch. 1968. Phys. Letters 28B, 26.

Browne, J.C., H.W. Newson, E.G. Bilpuch, and G.E. Mitchell. 1970. Nucl. Phys. A153, 481.

Bohr, N. 1936. Nature, London, England. 137, 344.

Camp, D.C. and G.L. Meredith. 1971. Nucl. Phys. A166, 349.

Chasman, C., K.W. Jones, R.A. Ristenen, and J.T. Sample. 1967. Phys. Rev. Letters 18, 219.

Chilosi, G., R.A. Ricci, and G.B. Vingiani. 1968. Phys. Rev. Letters 20, 159.

Coker, W.R. and C.F. Moore. 1969. Phys. Today 22, No. 4, 53.

Endt, P.M. 1966. Second symposium on the structure of low-medium mass nuclei. P. Goldhammer and L.W. Seagondollar, editors. Department of Physics, N.C. State Univ., Raleigh, N.C., p. 58.

Endt, P.M. 1967. Nuclear Structure. A. Hossain et al., editors. North Holland Publishing Company, Amsterday, Holland, p. 58.

Endt, P.M. 1968. Third symposium of the structure of low-medium mass nuclei. J.P. Davidson, Editor. Univerisity Press of Kansas, Lawrence, Kansas, p. 73.

Endt, P.M. 1969. Nuclear Isospin. J.D. Anderson, S.D. Bloom, J. Cerny, and W.W. True, Editors. Academic Press, New York, New York, p. 51.

Erlandsson, B. and K. Valli. 1963. Arkiv Pysik 25, 143.

Erne, F.C., W.A.M. Veltman and J.A.J. Wintermans. 1966. Nucl. Phys. 88, 1.

Fodor, I., I. Szentpetery, and J. Szucs. 1970. Phys. Letters 32B, 689.

Fox, J.D., C.F. Moore and D. Robson. 1964. Phys. Rev. Letters 12, 198.

Gaarde, C., P. Wilhjelm, and P.B. Jorgensen. 1966. Phys. Letters 22, 466.

Gove, H.E. 1959. Nuclear Reactions, Vol. 1. P.M. Endt and M. Emeur, Editors. North Holland Publishing Company, Amsterdam, Holland, p. 302.

Hanna, S.S. 1969. Isospin in Nuclear Physics. D.H. Wilkinson, Editor. North Holland Publishing Company, Amsterdam, Holland, p. 591.

Harney, H.L. 1969. Unpublished Computer Code.

Harney, H.L. and H.A. Weidenmuller. 1969. Nucl. Phys. A118, 241.

Harris, G.I. and J.J. Ferizo. 1970. Phys. Rev. C2, 1347.

Heisenberg, W. 1932. Z. Physik 77, 1.

Henley, E.M. 1969. Isospin in Nuclear Physics. D.H. Wilkinson, Editor. North Holland Publishing Company, Amsterdam, Holland, p. 15.

Hirata, M. 1970. Phys. Letters 32B, 656.

I.B.M. 1959. Data Processing Techniques: Random Number Generation and Testing.

Jackson, J.D. 1962. Classical Electrodynamics. John Wiley and Sons, Inc., New York, New York.

Kern, B.D. and F.D. Snyder. 1973. Phys. Rev. 8C, 2267.

Keyworth, G.A. 1968. A high resolution study of isobaric analog states in ^{41}K and ^{23}Na. Unpublished Ph.D. Dissertation. Duke University, Durham, N.C., Department of Physics. University Microfilms, Ann Arbor, Michigan.

Keyworth, G.A., G.C. Kyker, E.G. Eilpuch, and H.W. Newson. 1966a. Phys. Letters 20, 281.

Keyworth, G.A., G.C. Kyker, E.G. Eilpuch, and H.W. Newson. 1966b. Phys. Letters 89, 590.

Klapdor, H.V. 1971a. Phys. Letters 35B, 405.

Klapdor, H.V. 1971b. Gamma spectroscopy of T=3/2 - 7/2 analogue states of nuclei in the f-p shell. Unpublished Ph.D. Dissertation. Department of Physik. Max Planck Institute fur Kernphysik, Hidelberg, Germany. University Microfilms, Ann Arbor, Michigan.

Lane, A.M. 1962. Nucl. Phys. 35, 676.

Lane, A.M. 1969. Isospin in Nuclear Physics. D.H. Wilkinson, Editor. North Holland Publishing Company, Amsterdam, Holland p. 509.

Lane, A.M. 1972. Statistical Propertics of Nuclei. 1972. J. B. Garg, Editor. Plenum Press, New York, New York, p. 271.

Lane, A.M. and J.M. Soper. 1962. Nucl. Phys. 37, 506.

Lindstrom, D.P. 1970. Fine structure of analog states in ^{55}Co, ^{57}Co, and ^{59}Co. Unpublished Ph.D. Dissertation. Duke University, Durham, N.C., Department of Physics. University Microfilms, Ann Arbor, Michigan.

Marion, J.B. 1960. Nuclear Data Tables 3 NAS-NRC, 160.

Marion, J.B. and F.C. Young. 1968. Nuclear Reaction Analysis. North Holland Publishing Company, Amsterdam, Holland.

Maripuu, S. 1969. Nucl. Phys. A123, 357.

Maripuu, S. 1970a. Nucl. Phys. A149, 593.

Maripuu, S. 1970b. Nucl. Phys. A153, 183.

Maripuu, S. 1970c. Phys. Letters 31B, 181.

Mekjian, A. and W.M. MacDonald. 1968. Nucl. Phys. A121, 385.

Mello, P.A. 1967. Ann. Phys. 45, 240.

Mitchell, G.E., E.G. Bilpuch, W.C. Peters, J.D. Moses and N.H. Prochnow. 1972. Statistical Properties of Nuclei. J.B. Garg, Editor. Plenum Press, New York, New York, p. 299.

Moore, C.F., S.A.A. Zaidi and J.J. Kent. 1967. Phys. Rev. Letters 18, 345.

Morpurgo, G. 1958. Phys. Rev. 110, 721.

Morrison, G.C. 1969. Nuclear Isospin. J.D. Anderson, S.D. Bloom, J. Cerny and W.W. True, Editors. Academic Press, New York, New York, p. 435.

Morse, P.M. and H. Feshbach. 1953. Methods of Theoretical Physics. McGraw-Hill Book Company, New York, New York.

Moses, J.D. 1970. A high resolution study of isobaric analog resonances in ^{51}Mn, ^{53}Mn, and ^{55}Mn. Unpublished Ph.D. Dissertation. Duke University, Durham, N.C., Department of Physics. University Microfilms, Ann Arbor, Michigan.

Nuclear Data. 1967. K. Way, Editor. B2.

Nuclear Data. 1970. K. Way, Editor. B4.

Parks, P.B., H.W. Newson, and R.M. Williamson. 1958. Rev. Sci. Instr. 29, 834.

Parks, P.B., P.M. Beard, E.G. Bilpuch, and H.W. Newson. 1964. Rev. Sci. Instr. 35, 549.

Peters, W.C. 1972. Electromagnetic decay of fragmented analogue states in ^{55}Mn and ^{59}Co. Unpublished Ph.D. Dissertation. Duke University, Durham, N.C. Department of Physics. University Microfilms, Ann Arbor, Michigan.

Peters, W.C., E.G. Bilpuch, and G.E. Mitchell. 1973. Nucl. Phys. A207, 626.

Peters, W.C., E.G. Bilpuch, G.E. Mitchell and G.L. Morgan. 1971. Bull. Am. Phys. Soc. 16.

Porter, C.E. and R.G. Thomas. 1956. Phys. Rev. 104, 483.

Preston, M.A. 1962. Physics of the Nucleus. Addison-Wesley Publishing Company, New York, New York.

Prochnow, N.H. 1971. A high resolution study of proton resonances in ^{47}V, ^{49}V, and ^{51}V. Unpublished Ph.D. Dissertation, Duke University, Durham, N.C. University Microfilms, Ann Arbor, Michigan.

Robson, D. 1965. Phys. Rev. 137, 535.

Robson, D. 1969. Nuclear Isospin. J.D. Anderson, S.D. Bloom, J. Cerny, and W.W. True, Editors. Academic Press, New York, New York, p. 385.

Richard, P., C.F. Moore, J.D. Fox and D. Robson. 1964. Phys. Rev. Letters 13, 343.

Rust, N.J.A. and W.J. Naude. 1972. Annual Research Report. (Compiled by W.R. McMurray) Southern Universities Nuclear Institute, Faur E. Cape Providence, South Africa.

Schwartz, J.J. and W.P. Alford. 1966. Phys. Rev. 149, 820.

Seibel, F.T. Jr. 1968. Neutron Resonances in ^{34}S, ^{40}A, and ^{48}Ca. Unpublished Ph.D. Dissertation. Duke University, Durham, N.C., Department of Physics. University Microfilms, Ann Arbor, Michigan.

Smith, D.L., H.Y. Chen and H.A. Enge. 1968. Nucl. Phys. A107, 639.

Stein, N. 1969. Nuclear Isospin. J.D. Anderson, S.D. Bloom, J. Cerny and W.W. True, Editors. Academic Press, New York, New York, P. 481.

Szentpetery, I. and J. Szucs. 1972. Phys. Rev. Letters 28, 378.

Talmi, I. and I. Unna. 1960. Annual Review of Nuclear Science. Vol. 10. E. Segre, G. Friedlander and W. E. Meyerhot, Editors. Annual Reviews, Inc., Palo Alto, California, p. 353.

Thompson, W.J., J.L. Adams and D. Robson. 1968. Phys. Rev. 173, 975.

Toller, A. L. 1954. Neutron resonances in sodium, aluminum, and potassium. Unpublished Ph.D. Dissertation, Duke University, Durham, N.C. University Microfilms, Ann Arbor, Michigan.

Trainer, L.E.N. 1952. Phys. Rev. 85, 962.

Vingiani, G.B., G. Chilosi and W. Eruyenstein. 1968. Phys. Letters 26B, 285.

Vingiani, G.B., G. Chilosi and C. Rossi-Alvarez. 1971a. Phys. Letters 34B, 597.

Vingiani, G.B. and R.A. Ricci. 1971b. Topical Conference on The Structure of 1f7/2 Nuclei. R.A. Ricci, Editor. Editrice Compositori, Bologna, Germany, p. 304.

Vingiani, G.B., R.A. Ricci, R. Giacomich, and G. Poiani. 1968. Nuovo Cimento 57, 453.

Walinga, J., J.C. Manthuruthil, and C.P. Poirier. 1969. Phys. Rev. 185, 1439.

Warburton, E.K. 1966. Isobaric Spin in Nuclear Physics. J.D. Fox and D. Robson, Editors. Academic Press, New York, New York, p. 173.

Watson, D.D., J.C. Manthuruthil and F.D. Lee. 1967. Phys. Rev. 164, 1399.

Wigner, E.P. 1937. Phys. Rev. 51, 106.

Wilhjelm, P., G.A. Keyworth, J.C. Browne, W.P. Beres, M. Divadeenam, H.W. Newson, and E.G. Bilpuch. 1969. Phys. Rev. 177, 1553.

Wilkinson, D.H. 1969. Isospin in Nuclear Physics. D.H. Wilkinson, Editor. North Holland Publishing Company, Amsterdam, Holland.

Wilson, W.M. 1973. A high resolution study of proton resonances in ^{41}Sc, ^{43}Sc, and ^{45}Sc. Unpublished Ph.D. Dissertation, Duke University, Durham, N.C., Department of Physics. University Microfilms, Ann Arbor, Michigan.

Zaidi, S.A.A. and S. Darmodjo. 1967. Phys. Rev. Letters 19, 1446.

Zelen, M. and N.C. Severo. 1964. Handbook of Mathematical Functions with Formulas, Graphs, and Mathematical Tables. M. Abramowitz and I.A. Stegun, Editors. U.S. Government Printing Office, Washington, D.C.

FOOTNOTES

Garg, J.B. and S. Bokharee. 1973. Private communications.

Maripuu, S., J.C. Manthuruthil, and C.P. Poirier. 1972. Private communications.

Wilson, W.M. 1974. Private communications.

APPENDIX

Gamma-Ray Widths for ^{45}Sc and ^{63}Sc

The partial gamma-ray widths for ^{45}Sc and ^{63}Cu are tabulated on the following pages. Resonant energies quoted are the laboratory energies Ep of the incident proton. The estimated uncertainty in the gamma-ray and inelastic widths is 30% for widths greater than 50 meV, 50% for widths between 10 and 50 meV, and 100% for widths less than 10 meV. The limit of observability for the gamma-ray widths is about 5 meV.

In Tables 16, 17, and 18, the gamma-ray widths for resonances studied in ^{45}Sc are listed. Tables 19 and 20 list the widths for the resonances studied in ^{63}Cu. In each table the following notations are adopted: if the spin assignment is uncertain, the J-value is enclosed in parenthesis (J). For resonances which are very close to another resonance observed in the capture excitation function, the resonant is shown with a dagger (+). If the spin and parity of the final state is unknown, then no multipolarity is shown.

Scattering Chamber

A new scattering chamber was designed for use in capture experiments. The capture work on ^{62}Ni was performed using an older scattering chamber (shown in Figure 7). A number of difficulties were experienced with this chamber; the most serious problem was the vacuum system. The relatively poor vacuum shortened the effective life of targets and permitted occasional arcing from the target to the walls of the chamber. In the new design priority was given to the vacuum system.

Table 16 Partial gamma-ray widths for the 3.2- analogue state in ^{45}Sc

E_p (MeV)	J^π	Γ_p (eV)	$\Gamma_{p'}$ (eV)	E_f (keV)	Γ_γ (meV)	Multi-polarity	Γ_γ (W.u.)
1.6236	(3/2-)	12	0.0	12	58.8	E1	0.115E-03
				376	23.0	M1	0.209E-02
						E2	0.890E-01
				543	61.7	E1	0.147E-03
				721	21.3	M1	0.221E-02
						E2	0.103E-00
				938	45.1	E1	0.125E-03
				1067	50.8	M1	0.603E-02
						E2	0.307E-00
				1799	17.7		
				2095	14.9		
				2531	15.1		
				2341	11.0	M1	0.231E-02
						E2	0.171E-00
				2907	18.6		
				3025	17.9	M1	0.534E-02
						E2	0.501E-00
				3881	40.2	M1	0.200E-01
						E2	0.265E-01
				4739	26.7		
1.6324	3/2-	25	0.0	12	4.1	E1	0.795E-05
				543	10.0	E1	0.239E-04
				1067	25.3	M1	0.298E-02
						E2	0.150E-00
				1302	60.4		
				2893	25.4	M1	0.703E-02
						E2	0.628E-00
				3546	18.2		
				3929	23.4	M1	0.120E-01
						E2	0.162E-01
1.6460	3/2-	80	0.0	12	30.0	E1	0.585E-04
				376	86.9	M1	0.785E-02
						E2	0.332E-00
				543	40.5	E1	0.960E-04
				721	105.4	M1	0.108E-01
						E2	0.500E-00
				1067	42.9	M1	0.506E-02
						E2	0.256E-00
				1302	16.7		
				2341	38.7	M1	0.806E-02

Table 16 (Continued)

Ep (MeV)	J^{π}	Γ_p (eV)	$\Gamma_{p'}$ (eV)	E_f (keV)	Γ_γ (meV)	Multi-polarity	Γ_γ (W.u.)
						E2	0.596E-00
				2960	23.8		
				3025	30.7	M1	0.905E-02
						E2	0.842E-00
				3484	31.1	M1	0.119E-01
						E2	0.132E-01
1.6517	3/2-	400	0.0	12	29.4	E1	0.572E-04
				376	32.1	M1	0.290E-02
						E2	0.122E-00
				543	19.7	E1	0.455E-04
				721	65.7	M1	0.674E-02
						E2	0.310E-00
				938	172.3	E1	0.475E-03
				1067	18.2	M1	0.214E-02
						E2	0.108E-00
				2341	23.6	M1	0.490E-02
						E2	0.361E-00
				3025	31.3	M1	0.919E-02
						E2	0.854E-00
				3463	21.4		
1.6646	3/2-	60	0.0	12	2.9	E1	0.555E-05
				376	21.3	M1	0.191E-02
						E2	0.804E-01
				721	29.0	M1	0.296E-02
						E2	0.136E-00
				938	151.4	E1	0.415E-03
				1237	15.2		
				1411	9.4		
				1557	5.8	M1	0.825E-03
						E2	0.475E-01
				1799	24.8		
				2341	25.2	M1	0.520E-02
						E2	0.381E-00
				2750	31.0		
				2983	31.2	M1	0.888E-02
						E2	0.808E-00
1.6681	3/2-	30	0.0	12	58.4	E1	0.113E-03
				376	40.8	M1	0.366E-02
						E2	0.154E-00
				721	96.3	M1	0.982E-02
						E2	0.450E-00
				1557	4.2	M1	0.608E-03

Table 16 (Continued)

E_p (MeV)	J^π	Γ_p (eV)	$\Gamma_{p'}$ (eV)	E_f (keV)	Γ_γ (meV)	Multi-polarity	Γ_γ (W.u.)
						E2	0.351E-01
				1799	26.2		
				2341	18.5	M1	0.381E-02
						E2	0.279E-00
				2779	38.9		
				3346	18.5		
				3484	27.5	M1	0.104E-01
						E2	0.115E-01
1.6774	(3/2-)	7	0.0	12	14.5	E1	0.280E-04
				376	7.0	M1	0.624E-03
						E2	0.262E-01
				543	33.9	E1	0.795E-04
				721	10.5	M1	0.187E-02
						E2	0.491E-01
				1067	16.9	M1	0.198E-02
						E2	0.985E-01
				1302	20.4		
				2960	10.5		
				3090	30.3		
				3177	12.0		
1.6782	(3/2-)	5	0.0	12	2.8	E1	0.546E-05
				376	6.4	M1	0.569E-03
						E2	0.239E-01
				938	5.2	E1	0.142E-04
				1087	10.4	M1	0.121E-02
						E2	0.607E-01
				1411	5.8		
				2148	9.2		
				2341	18.2	M1	0.407E-02
						E2	0.315E-00
1.6822	(3/2-)	10	0.0	543	51.8	E1	0.121E-03
				938	9.2	E1	0.249E-04
				1067	21.2	M1	0.246E-02
						E2	0.123E-00
				1302	13.1		
				1557	11.4	M1	0.177E-02
						E2	0.107E-00
				2148	11.0		
1.6925	(3/2-)	10	0.0	12	5.5	E1	0.105E-04
				376	6.6	M1	0.589E-03
						E2	0.247E-01

Table 16 (Continued)

Ep (MeV)	J^{π}	Γ_p (eV)	$\Gamma_{p'}$ (eV)	E_f (keV)	Γ_γ (meV)	Multi-polarity	Γ_γ (W.u.)
				543	51.2	E1	0.119E-03
				721	32.3	M1	0.326E-02
						E2	0.149E-00
				938	62.1	E1	0.189E-03
				1067	38.5	M1	0.446E-02
						E2	0.223E-00
				1557	54.0	M1	0.774E-02
						E2	0.445E-00
				1799	17.4		
				2531	44.0		
				2779	8.8		

Table 17 Partial gamma-ray widths for the 1.2- resonances in ^{45}Sc between E_p=1.70 and 2.18 MeV

Ep (MeV)	J^π	Γ_p (eV)	$\Gamma_{p'}$ (eV)	E_f (keV)	Γ_γ (meV)	Multi-polarity	Γ_γ (W.u.)
1.7022	(1/2-)	10	0.0	0	97.4	M3	0.278E-05
						E4	0.212E-08
				12	14.1	E1	0.271E-04
				378	5.7	M1	0.505E-03
						E2	0.211E-01
				543	9.3	M2	0.153E-01
						E3	0.101E-03
				938	11.1	E1	0.300E-04
				1067	30.9	M1	0.356E-02
						E2	0.177E-00
				2148	17.6		
				2291	26.2		
				2960	14.0		
				3589	24.9		
				3609	11.6		
				4478	21.5		
1.7303	1/2-	50	0.0	12	12.1	E1	0.229E-04
				376	13.5	M1	0.119E-02
						E2	0.493E-01
				543	7.5	M2	0.123E-01
						E3	0.809E-02
				1067	52.6	M1	0.607E-02
						E2	0.297E-00
				1799	11.1		
				3539	37.9		
1.7418	(1/2-)	15	0.0	12	12.4	E1	0.235E-04
				376	10.6	M1	0.931E-03
						E2	0.386E-01
				938	30.4	E1	0.812E-04
				1067	18.2	M1	0.208E-02
						E2	0.103E-00
				2944	21.1		
				3905	7.5		
				4050	15.4		
1.7671	1/2-	40	0.0	12	45.3	E1	0.852E-04
				376	125.2	M1	0.109E-01
						E2	0.448E-00
				721	54.4	E2	0.240E-00
				1302	14.7		
				2341	25.2	M1	0.497E-02
						E2	0.354E-00

Table 17 (Continued)

Ep (MeV)	J^{π}	Γ_p (eV)	$\Gamma_{p'}$ (eV)	E_f (KeV)	Γ_γ (meV)	Multi-polarity	Γ_γ (W.u.)
				2531	49.3		
				2779	39.3		
				3346	16.7		
1.7797	(3/2-)	5	0.0	12	98.7	E1	0.185E-03
				376	18.4	M1	0.159E-02
						E2	0.652E-01
				543	125.1	E1	0.283E-03
				721	9.4	M1	0.924E-03
						E2	0.414E-01
				938	18.9	E1	0.497E-04
				1237	56.6		
				1302	54.1		
				1799	17.9		
				2095	57.4		
				2750	27.0		
				2944	31.1		
1.7994	(3/2-)	7	0.0	12	76.2	E1	0.142E-03
				376	54.0	M1	0.463E-02
						E2	0.189E-00
				543	122.8	E1	0.276E-03
				938	105.1	E1	0.275E-03
				1067	31.7	M1	0.353E-02
						E2	0.172E-00
				1302	131.6		
				1799	64.1		
				2341	32.5	M1	0.630E-02
						E2	0.444E-00
				2590	38.0		
				2740	33.3		
				2779	25.3		
1.8101	1/2-	25	0.0	938	57.5	E1	0.150E-03
				1067	22.1	M1	0.246E-02
						E2	0.119E-00
				1557	16.8		
				3025	20.5		
				3090	19.6		
1.8170	(1/2-)	5	0.003	12	58.9	E1	0.109E-03
				376	12.7	M1	0.108E-02
						E2	0.440E-01
				938	6.2	E1	0.162E-04
				2531	27.0		

Table 17 (Continued)

Ep (MeV)	J	p (eV)	p′ (eV)	Ef (KeV)	r (meV)	Multi-polarity	r (W.u.)
				2893	18.0	M1	0.456E-02
						E2	0.384E-00
				2944	12.6		
				3090	30.1		
				3484	25.6	M1	0.893E-02
						E2	0.930E-00
				3720	40.4		
1.8268	(1/2-)	15	0.0	12	26.9	E1	0.496E-04
				376	13.9	M1	0.118E-02
						E2	0.481E-01
				938	51.5	E1	0.133E-03
				1067	32.9	M1	0.363E-02
						E2	0.175E-00
				1302	17.8		
				2531	42.9		
1.8492	1/2-	35	0.002	0	12.2	M3	0.310E-04
						E4	0.232E-07
				12	83.6	E1	0.153E-03
				376	42.1	M1	0.355E-02
						E2	0.143E-00
				721	61.5	E2	0.259E-00
				938	18.0	E1	0.461E-04
				1067	136.7	M1	0.149E-01
						E2	0.711E-00
				1799	41.9		
				2531	18.2		
				2590	36.3		
				2779	38.6		
				2341	25.2	M1	0.479E-02
						E2	0.333E-00
1.8648	(1/2-)	15	0.003	12	31.6	E1	0.575E-04
				376	27.3	M1	0.229E-02
						E2	0.921E-01
				938	32.8	E1	0.836E-04
				1302	99.4		
				2148	116.7		
				2562	42.3		
				2893	18.7		
				3025	34.7	M1	0.195E-02
						E2	0.790E-00
				3068	57.4		

Table 17 (Continued)

Ep (MeV)	J	p (eV)	p′ (eV)	Ef (KeV)	r (meV)	Multi-polarity	r (W.u.)
1.8693	1/2-	25	0.005	12	236.8	E1	0.430E-03
				376	62.4	M1	0.522E-02
						E2	0.210E-00
				938	51.2	E1	0.130E-03
				2143	63.4		
				2590	50.4		
				3090	112.0		
				3412	52.8	M1	0.171E-01
						E2	0.169E-01
				3484	41.1	M1	0.139E-01
						E2	0.142E-01
				3881	48.4	M1	0.206E-01
						E2	0.245E-01
				3539	15.1		
				3609	112.0		
1.8892	1/2-	60	0.0	12	16.5	E1	0.297E-04
				376	26.5	M1	0.220E-02
						E2	0.881E-01
				938	25.7	E1	0.649E-04
				1067	17.1	M1	0.184E-02
						E2	0.877E-01
				1302	55.9		
				2140	12.6		
				2531	31.1		
				2599	22.9		
				2960	56.9		
				3025	23.6	M1	0.613E-02
						E2	0.525E-00
				3090	23.8		
				3720	20.7	M1	0.791E-02
						E2	0.877E-00
1.9032	(1/2-)	10	0.009	12	706.3	E1	0.127E-02
				938	58.1	E1	0.146E-03
				1302	33.6		
				2599	28.7		
				2590	29.2		
				3346	13.4		
				3362	13.4		
				3539	27.9		
1.9086+	1/2-	100	0.006	12	163.6	E1	0.293E-03
				376	13.9	M1	0.116E-02
						E2	0.464E-01

Table 17 (Continued)

Ep (MeV)	J	p (eV)	p′ (eV)	Ef (keV)	r (meV)	Multi-polarity	r (W.u.)
				938	8.1	E1	0.202E-04
				1067	25.7	M1	0.275E-02
						E2	0.131E-00
				2106	15.2		
				2148	57.7		
1.9207	1/2-	50	0.021	12	108.4	E1	0.194E-03
				376	179.4	M1	0.148E-01
						E2	0.587E-00
				938	290.3	E1	0.725E-03
				974	71.7	E3	0.965E-03
						M4	0.132E-10
				1067	88.7	M1	0.943E-02
						E2	0.445E-00
				1302	318.9		
				1411	334.5		
				1936	62.6		
				2341	84.7	M1	0.155E-01
						E2	0.106E-01
				2590	54.3		
				2944	20.8		
1.9493	1/2-	75	0.042	12	6.5	E1	0.116E-04
				376	12.3	M1	0.101E-02
						E2	0.397E-01
				721	10.8	E2	0.429E-01
				938	13.1	E1	0.324E-04
				974	61.8	E3	0.813E-03
						M4	0.111E-10
				1067	36.7	M1	0.386E-02
						E2	0.181E-00
				1302	345.3		
				1573	69.4		
1.9623	1/2-	35	0.008	12	51.2	E1	0.902E-04
				938	26.2	E1	0.645E-04
				1302	159.8		
				2291	21.6		
				2562	23.8		
				2590	22.7		
				3592	18.1		
1.9688	1/2-	20	0.004	12	804.9	E1	0.141E-02
				721	50.5	E2	0.197E-00
				2291	50.1		

Table 17 (Continued)

Ep (MeV)	J	p (eV)	p′ (eV)	Ef (keV)	r (meV)	Multi-polarity	r (W.u.)
				2341	47.3	M1	0.851E-02
						E2	0.570E-00
				2893	48.7		
				2960	36.5		
				3025	94.8	M1	0.237E-01
						E2	0.198E-01
				3090	47.4		
				3720	66.1	M1	0.242E-01
						E2	0.260E-01
				4180	33.6		
				4619	33.6		
				5084	66.1		
1.9724	(3/2-)	7	0.033	12	143.6	E1	0.252E-03
				543	573.0	E1	0.121E-02
				1067	25.2	M1	0.262E-02
						E2	0.122E-00
				1302	77.7		
				1799	25.4		
				2303	80.9		
				3362	32.7		
				3412	65.2	M1	0.200E-01
						E2	0.190E-01
				3720	40.7	M1	0.149E-01
						E2	0.160E-01
				3779	70.9		
1.9799+	(1/2-)	10	0.038	12	52.5	E1	0.920E-04
				376	26.6	M1	0.215E-02
						E2	0.842E-01
				721	15.8	E2	0.615E-01
				938	30.9	E1	0.754E-04
				1067	64.2	M1	0.668E-02
						E2	0.310E-00
				1302	66.8		
				1799	24.7		
				2095	41.6		
				2291	29.0		
				2590	45.5		
				3090	54.6		
				3136	67.4		
1.9937	1/2-	400	0.018	12	37.2	E1	0.648E-04
				938	209.2	E1	0.508E-03

Table 17 (Continued)

Ep (MeV)	J	p (eV)	p′ (eV)	Ef (keV)	r (meV)	Multi-polarity	r (W.u.)
				3068	24.6		
				3090	23.6		
2.0006+	1/2-	35	0.005	12	12.8	E1	0.223E-04
				376	5.6	M1	0.447E-03
						E2	0.174E-01
				543	13.2	M2	0.183E-01
						E3	0.113E-03
				721	11.8	E2	0.453E-01
				2341	11.7	M1	0.208E-02
						E2	0.138E-00
				2719	45.8		
2.0194	1/2-	175	0.010	12	36.9	E1	0.638E-04
				376	58.8	M1	0.457E-02
						E2	0.182E-00
				1067	31.4	M1	0.321E-02
						E2	0.148E-00
				1302	64.9		
				2521	75.1		
				2531	9.0		
2.0273	1/2-	240	0.099	12	17.6	E1	0.304E-04
				376	73.8	M1	0.586E-02
						E2	0.227E-00
				938	75.1	E1	0.180E-03
				1067	35.3	M1	0.361E-02
						E2	0.166E-00
				1302	115.4		
				2140	26.0		
				2303	54.5		
2.0428	1/2-	53	0.267	12	167.3	E1	0.288E-03
				543	100.5	M2	0.151E-02
						E3	0.927E-03
				721	51.8	E2	0.196E-00
				1302	23.9		
				1799	48.5		
				2140	18.3		
				2893	22.1		
				2944	13.5		
				2983	21.4	M1	0.516E-02
						E2	0.421E-00
				3463	17.8		

Table 17 (Continued)

Ep (MeV)	J	p (eV)	p′ (eV)	Ef (keV)	r (meV)	Multi-polarity	r (W.u.)
2.0456	1/2-	350	0.207	12	8.5	E1	0.146E-04
				376	80.7	M1	0.637E-02
						E2	0.247E-00
				938	82.8	E1	0.198E-03
				1302	88.1		
				1799	51.9		
2.0489	1/2-	63	0.180	12	61.9	E1	0.106E-03
				376	138.9	M1	0.110E-01
						E2	0.424E-00
				938	53.0	E1	0.126E-03
				1067	70.1	M1	0.712E-02
						E2	0.326E-00
				1302	15.9		
				2291	53.3		
				2303	36.8		
				2750	26.2		
				2880	27.7		
				3009	37.6		
				3090	52.2		
				4761	39.0		
2.0658	1/2-	242	0.568	0	6.9	M3	0.148E-04
						E4	0.180E-07
				12	42.4	E1	0.722E-04
				376	308.7	M1	0.242E-01
						E2	0.932E-00
				721	21.2	E2	0.783E-01
				1067	37.6	M1	0.379E-02
						E2	0.173E-00
				1411	32.0		
				2291	49.6		
				2341	65.8	M1	0.113E-01
						E2	0.738E-00
				2970	24.7	M1	0.576E-02
						E2	0.459E-00
				3025	45.3	M1	0.108E-01
						E2	0.874E-00
				3484	72.7	M1	0.221E-01
						E2	0.211E-01
				3720	42.0	M1	0.145E-01
						E2	0.151E-01
2.0750+	1/2-	35	0.068	12	454.2	E1	0.772E-03
				376	32.8	M1	0.256E-02

Table 17 (Continued)

Ep (MeV)	J	p (eV)	p′ (eV)	Ef (keV)	r (meV)	Multi-polarity	r (W.u.)
						E2	0.984E-01
				938	48.7	E1	0.115E-03
				1302	79.1		
				1557	34.4	M1	0.420E-02
						E2	0.218E-00
				1799	135.6		
				2944	19.8		
				3025	18.0	M1	0.431E-02
						E2	0.349E-00
				3286	41.6		
2.0932	1/2-	64	0.082	12	4.8	E1	0.805E-05
				543	9.9	M2	0.131E-01
						E3	0.794E-02
				938	72.4	E1	0.198E-03
				1302	27.9		
				2907	68.0		
				3025	14.9	M1	0.352E-02
						E2	0.284E-00
				3463	7.0		
				3484	8.1	M1	0.242E-02
						E2	0.229E-00
				3539	39.9		
				3905	30.5		
2.1062	1/2-	19	0.150	12	40.1	E1	0.675E-04
				376	9.1	M1	0.701E-03
						E2	0.267E-01
				543	24.9	M2	0.328E-01
						E3	0.198E-03
				1302	307.3		
				1799	106.3		
				2590	26.9		
				2893	35.9		
2.1074	(1/2-)	15	0.220	12	13.3	E1	0.233E-04
				376	25.3	M1	0.196E-02
						E2	0.748E-01
				721	117.8	E2	0.426E-00
				1067	17.2	M1	0.171E-02
						E2	0.772E-01
				1302	23.4		
				1799	170.5		
				2025	31.9		
				2341	60.9	M1	0.103E-01

Table 17 (Continued)

Ep (MeV)	J	p (eV)	p′ (eV)	Ef (keV)	r (meV)	Multi-polarity	r (w.u.)
						E2	0.663E-00
				2779	71.6		
				2983	81.9	M1	0.187E-01
						E2	0.147E-01
2.1200	1/2-	60	0.066	12	182.6	E1	0.303E-03
				376	64.4	M1	0.490E-02
						E2	0.185E-00
				721	13.7	E2	0.484E-01
				1557	27.0	M1	0.320E-02
						E2	0.163E-00
2.1242	1/2-	30	0.061	12	183.5	E1	0.304E-03
				376	17.4	M1	0.132E-02
						E2	0.499E-01
				543	136.7	M2	0.175E-02
						E3	0.105E-04
				938	105.9	E1	0.243E-03
				1557	43.4	M1	0.515E-02
						E2	0.262E-00
				1799	244.6		
				2590	39.9		
				5309	25.1		
				4309	20.4		
2.1418	1/2-	48	0.016	376	230.0	M1	0.174E-01
						E2	0.654E-00
				938	117.1	E1	0.267E-03
				1067	32.5	M1	0.316E-02
						E2	0.141E-00
				1302	42.9		
				2140	40.5		
				2907	29.1		
				3881	57.4	M1	0.207E-01
						E2	0.221E-01
2.1559	1/2-	40	0.024	12	27.0	E1	0.443E-04
				938	123.4	E1	0.280E-03
				1302	25.3		
				2341	34.4	M1	0.566E-02
						E2	0.357E-00
				2531	16.6		
				3463	34.9		

Table 17 (Continued)

Ep (MeV)	J	p (eV)	p′ (eV)	Ef (keV)	r (meV)	Multi-polarity	r (W.u.)
2.1771	(1/2-)	11	0.165	12	119.7	E1	0.195E-03
				543	71.6	M2	0.891E-01
						E3	0.527E-03
				938	13.0	E1	0.293E-04
				2095	22.1		
				2303	30.2		
				2779	31.2		
				3362	58.4		
				3548	35.6		

Table 18 Partial gamma-ray widths for the $1/2^+$ analogue state in ^{45}Sc

Ep (MeV)	J^π	Γ_p (eV)	$\Gamma_{p'}$ (eV)	E_f (keV)	Γ_γ (meV)	Multi-polarity	Γ_γ (W.u.)
2.1992	$1/2^+$	73	0.031	376	149.3	E1	0.276E-03
				2138	58.0		
				2893	124.8		
				3090	81.1		
				3484	39.8	E1	0.279E-03
				3484	39.8	E1	0.279E-03
				3463	39.8		
				4135	34.3		
				4414	36.3		
2.1999	$1/2^+$	10	0.804	376	153.5	E1	0.284E-03
				721	62.1	M2	0.866E-01
						E3	0.536E-03
				938	26.4	M1	0.242E-02
						E2	0.103E-00
				1302	60.6		
				1557	33.0	E1	0.994E-04
				1557	33.0	E1	0.944E-04
				2095	45.9		
				2884	85.3		
				3640	37.1		
				3905	8.4		
2.2038	$1/2^+$	20	0.329	12	141.1	M1	0.935E-02
						E2	0.322E-00
				376	165.6	E1	0.306E-03
				543	175.3	E2	0.540E-00
				1302	99.8		
				2893	124.6		
				1474	77.7		
				3720	38.8	E1	0.309E-03
				3609	54.0		
2.2217	$1/2^+$	140	0.279	0	58.6	E3	0.278E-03
						M4	0.328E-09
				12	66.4	M1	0.438E-02
						E2	0.150E-00
				376	78.7	E1	0.146E-03
				1067	138.6	E1	0.326E-03
				1411	171.0		
				1557	136.8	E1	0.389E-03
				1557	136.8	E1	0.389E-03

Table 18 (Continued)

Ep (MeV)	J^{π}	Γ_p (eV)	$\Gamma_{p'}$ (eV)	E_f (keV)	Γ_γ (meV)	Multi-polarity	Γ_γ (W.u.)
				1799	55.4		
				3346	34.6		
				4050	44.8		
2.2421	$1/2^+$	130	0.047	12	93.9	M1	0.615E-02
						E2	0.210E-00
				376	131.4	E1	0.240E-03
				2960	46.0		
				3025	133.0		
				3905	59.3		
2.2466+	$1/2^+$	800	0.718	12	63.2	M1	0.412E-02
						E2	0.141E-00
				543	211.1	E2	0.637E-00
				721	147.7	M2	0.200E-02
						E3	0.122E-04
				974	37.5	M3	0.156E-05
						E4	0.126E-08
				1067	259.0	E1	0.604E-03
				1302	362.0		
				2062	145.8		
				2303	145.2		
				2341	177.4	E1	0.697E-03
				2341	177.4	E1	0.697E-03
				2583	154.3		
				2590	100.6		
				3025	77.2		
				4424	59.5		
2.2562	$1/2^+$	35	0.098	12	23.3	M1	0.151E-02
						E2	0.515E-01
				938	295.0	M1	0.265E-01
						E2	0.112E-01
				1067	175.6	E1	0.408E-03
				3463	115.9		
				3484	26.8	E1	0.183E-03
				3484	26.8	E1	0.183E-03
				3609	56.7		
				3905	146.9		
				3926	146.9	E1	0.128E-02
				3926	146.9	E1	0.128E-02
2.2682	$1/2^+$	13	0.140	376	45.9	E1	0.830E-04
				543	73.8	E2	0.220E-00

Table 18 (Continued)

Ep (MeV)	J^{π}	Γ_p (eV)	$\Gamma_{p'}$ (eV)	E_f (keV)	Γ_γ (meV)	Multi-polarity	Γ_γ (W.u.)
				2291	33.3		
				2960	55.8		
				3025	71.8		
				3609	32.9		
				3640	33.3		
2.2793	$1/2^+$	12	1.658	12	7.4	M1	0.480E-03
						E2	0.163E-01
				376	226.7	E1	0.408E-03
				1067	64.0	E1	0.147E-03
				2095	24.4		
				1474	25.5		
				2303	17.8		
				2291	59.6		
				2590	51.7		

Table 19 Partial gamma-ray widths for the $1/2^+$ resonances in ^{63}Cu

Ep (MeV)	J^π	Γ_p (eV)	$\Gamma_{p'}$ (eV)	E_f (keV)	Γ_p (meV)	Multi-polarity	Γ_γ (W.u.)
2.3110	$1/2^+$	20	0.019	0	965.1	E1	0.154E-02
				670	96.6	E1	0.198E-03
				961	74.4	M2	0.142E-02
						E3	0.692E-03
				1547	41.4	E1	0.122E-03
				2062	46.9		
2.3203$^+$	$1/2^+$	10	0.0	0	318.9	E1	0.509E-03
				670	24.5	E1	0.501E-04
2.3353$^+$	$1/2^+$	35	0.0	0	62.5	E1	0.991E-04
				670	245.0	E1	0.498E-03
				1547	59.6	E1	0.174E-03
2.3543	$1/2^+$	15	0.0	0	22.4	E1	0.353E-04
				670	77.1	E1	0.156E-03
2.3603	$1/2^+$	30	0.0	0	37.6	E1	0.590E-04
				670	46.4	E1	0.935E-04
				1547	84.8	E1	0.245E-03
				2011	41.6	E1	0.148E-03
				2697	39.7		
2.3853	$1/2^+$	20	0.022	0	694.3	E1	0.108E-02
				961	278.8	M2	0.508E-02
						E3	0.242E-04
				1411	42.2	M2	0.105E-02
						E3	0.564E-03
				1547	188.9	E1	0.539E-03
				1863	65.6	E3	0.139E-04
						M4	0.223E-10
				2092	30.2		
				2497	51.7		
				2778	130.0		
				3126	56.6		
2.3923	$1/2^+$	8	0.0	0	496.9	E1	0.773E-03
				961	123.1	M2	0.223E-02
						E3	0.106E-04
				1411	40.0	M2	0.987E-01
						E3	0.532E-03
				1547	35.1	E1	0.100E-03
				2062	38.5		
				2403	40.2		

Table 19 (Continued)

Ep (MeV)	J^{π}	Γ_p (eV)	$\Gamma_{p'}$ (eV)	E_f (keV)	Γ_γ (meV)	Multi-polarity	Γ_γ (W.u.)
2.4043	$1/2^+$	10	0.019	0	189.5	E1	0.294E-03
				670	32.6	E1	0.648E-04
				1547	322.3	E1	0.916E-03
				2011	75.9	E1	0.266E-03
2.4173^+	$1/2^+$	15	0.0	0	150.8	E1	0.232E-03
				670	52.5	E1	0.103E-03
				1411	107.5	M2	0.260E-02
						E3	0.139E-04
2.4403	$1/2^+$	115	0.0	0	50.6	E1	0.774E-04
				670	83.2	E1	0.163E-03
2.4443	$1/2^+$	30	0.0	0	86.3	E1	0.132E-03
				961	316.9	M2	0.505E-02
						E3	0.261E-04
2.4573^+	$1/2^+$	10	0.023	0	22.3	E1	0.339E-04
				2688	89.2		
2.4703	$1/2^+$	35	0.036	0	315.2	E1	0.477E-03
				670	141.8	E1	0.274E-03
				961	211.3	M2	0.364E-02
						E3	0.170E-04
				1323	119.6	E3	0.136E-04
						M4	0.200E-10
				1547	60.0	E1	0.165E-03
				2497	107.7		
2.4783^+	$1/2^+$	30	0.279	0	829.1	E1	0.125E-02
				670	95.8	E1	0.184E-03
				1411	78.0	M2	0.181E-02
						E3	0.953E-03
				1547	63.3	E1	0.174E-03
				2011	37.1	E1	0.125E-03
2.4833^+	$1/2^+$	135	0.071	0	198.5	E1	0.299E-03
				670	177.5	E1	0.341E-03
				1411	123.5	M2	0.286E-02
						E3	0.150E-04
				1547	144.3	E1	0.395E-03
2.4953	$1/2^+$	90	0.059	0	100.9	E1	0.151E-03

Table 19 (Continued)

Ep (MeV)	J^{π}	Γ_p (eV)	$\Gamma_{p'}$ (eV)	E_f (keV)	Γ_γ (meV)	Multi-polarity	Γ_γ (W.u.)
				670	67.7	E1	0.129E-03
				961	78.1	M2	0.132E-02
						E3	0.612E-03
				2011	93.4	E1	0.312E-03
				2403	38.0		
2.5283	$1/2^+$	30	0.020	0	31.8	E1	0.472E-04
				670	70.6	E1	0.133E-03
2.5343	$1/2^+$	10	0.102	0	69.4	E1	0.103E-03
				670	49.3	E1	0.929E-04
				961	91.8	M2	0.151E-02
						E3	0.694E-03
				1411	152.6	M2	0.340E-02
						E3	0.176E-04
				2062	118.4		
2.5485	$1/2^+$	65	0.092	0	77.2	E1	0.114E-03
				670	28.6	E1	0.537E-04
				961	143.5	M2	0.234E-02
						E3	0.107E-04
2.5733	$1/2^+$	5	0.177	0	45.6	E1	0.667E-04
				670	34.6	E1	0.644E-04
				961	75.0	M2	0.121E-02
						E3	0.549E-03
				1547	64.1	E1	0.169E-03
2.6033	$1/2^+$	25	0.069	0	42.9	E1	0.626E-04
				670	47.4	E1	0.879E-04
				2011	61.9	E1	0.199E-03
				2062	42.9		

Table 20 Partial gamma-ray widths for the 3/2- analogue state in ^{63}Cu

Ep (MeV)	J	Γ_p (eV)	$\Gamma_{p'}$ (eV)	E_f (keV)	Γ_γ (meV)	Multi-polarity	Γ_γ (W.u.)
2.6123	3/2-	20	0.069	0	83.0	M1	0.609E-02
						E2	0.142E-00
				670	15.3	M1	0.143E-02
						E2	0.393E-01
				2011	30.4	M1	0.491E-02
						E2	0.194E-00
2.6139	3/2-	15	0.119	0	17.3	M1	0.127E-02
						E2	0.295E-01
				670	13.9	M1	0.130E-02
						E2	0.357E-01
				1411	6.9	M1	0.859E-03
						E2	0.286E-01
2.6376	(3/2-)	10	0.101	0	172.3	M1	0.126E-01
						E2	0.291E-00
				961	13.4	M1	0.138E-02
						E2	0.405E-01
2.6385	(3/2-)	5	0.019	0	11.2	M1	0.814E-03
						E2	0.189E-01
				961	15.0	M1	0.155E-02
						E2	0.455E-01
2.6390	(3/2-)	5	0.026	0	18.1	M1	0.132E-02
						E2	0.306E-01
				961	17.1	M1	0.183E-02
						E2	0.537E-01
				1547	26.2	M1	0.343E-02
						E2	0.118E-00
				1863	20.1	E2	0.113E-00
				2081	12.1		
				2092	31.7		
2.6466$^+$	3/2-	15	0.225	0	156.4	M1	0.114E-01
						E2	0.263E-00
				670	43.5	M1	0.401E-02
						E2	0.109E-00
				1411	19.2	M1	0.237E-02
						E2	0.782E-01
				2062	15.6		
				2081	26.1		
2.6508	3/2-	10	0.248	0	8.6	M1	0.622E-03
						E2	0.144E-01

Table 20 (Continued)

Ep (MeV)	J	Γ_p (eV)	$\Gamma_{p'}$ (eV)	E_f (keV)	Γ_γ (meV)	Multi-polarity	Γ_γ (W.u.)
				961	105.5	M1	0.109E-01
						E2	0.317E-00
				1411	33.1	M1	0.408E-02
						E2	0.134E-00
2.6536$^+$	(3/2-)	5	0.122	0	23.4	M1	0.170E-02
						E2	0.392E-01
				670	14.3	M1	0.132E-02
						E2	0.357E-01
				961	62.5	M1	0.643E-02
						E2	0.188E-00
				1547	56.3	M1	0.731E-02
						E2	0.250E-00
2.6584	(3/2-)	10	0.278	0	12.4	M1	0.895E-03
						E2	0.207E-01
				670	12.1	M1	0.112E-02
						E2	0.303E-01
				961	31.8	M1	0.326E-02
						E2	0.951E-01
				2011	16.9	M1	0.267E-02
						E2	0.104E-00
				2062	19.8		
2.6617	3/2-	40	0.585	0	132.1	M1	0.954E-02
						E2	0.220E-00
				961	72.1	M1	0.739E-02
						E2	0.215E-00
				1411	101.9	M1	0.125E-01
						E2	0.410E-00
				1547	30.5	M1	0.395E-02
						E2	0.135E-00
2.6631	3/2-	125	1.194	0	97.1	M1	0.702E-02
						E2	0.162E-00
				670	62.8	M1	0.576E-02
						E2	0.156E-00
				961	120.0	M1	0.123E-01
						E2	0.359E-00
				1411	42.2	M1	0.517E-02
						E2	0.169E-00
				1547	53.8	M1	0.697E-02
						E2	0.238E-00

Table 20 (Continued)

Ep (MeV)	J	Γ_p (eV)	$\Gamma_{p'}$ (eV)	E_f (keV)	Γ_γ (meV)	Multi-polarity	Γ_γ (W.u.)
2.6664	(3/2-)	5	0.195	0	11.3	M1	0.819E-03
						E2	0.189E-01
				670	10.6	M1	0.973E-03
						E2	0.263E-01
				961	17.8	M1	0.182E-02
						E2	0.531E-01
2.6675	3/2-	20	0.164	0	13.3	M1	0.961E-03
						E2	0.222E-01
				670	21.2	M1	0.195E-02
						E2	0.528E-01
				961	51.3	M1	0.525E-02
						E2	0.153E-00
2.6704	(3/2-)	5	0.228	0	77.2	M1	0.557E-02
						E2	0.128E-00
				670	9.3	M1	0.848E-03
						E2	0.229E-01
				961	7.9	M1	0.811E-03
						E2	0.236E-01
				1547	19.7	M1	0.254E-02
						E2	0.864E-01

The new chamber was designed with a separate pumping station. A four inch oil diffusion pump with a maximum pumping speed of 1200 liters/sec was selected. A multicoolant baffle was selected to fit between the pump and the target chamber. This baffle is cooled by freon refrigeration which maintains the temperature of the baffle at less than 0° F. With this arrangement the pumping speed at the mouth of the baffle is about 500 liters/sec and backstreaming is almost eliminated.

The chamber and collimator assembly were built by the Duke Instrument Shop. Figure 38 shows a cross sectional view of the chamber and collimator. The inner walls of the chamber are gold plated. The cold finger surrounding the target rod is also gold plated, while the collimator is nickel plated. The interior of the collimator housing is lined with 5 mil molybdenum foil and the collimation apertures are made of molybdenum.

In the new chamber the vacuum obtained is less that 5×10^{-7} torr. The former problems associated with poorer vacuum are much reduced. This new chamber provides much greater flexibility. A surface barrier detector is mounted at 135° to monitor the proton cross section while measuring capture excitation functions. As many as four NaI crystals can be used simultaneously to measure angular distributions. Alternatively, a Ge(Li) detector can be rotated from 25° to 125° at a target-detector distance as close as 3.17 cm.

Monte Carlo Techniques

The statistical significance of a given correlation was determined using Monte Carlo techniques. These procedures are discussed in this

Figure 38 Side view of the new target chamber and collimator

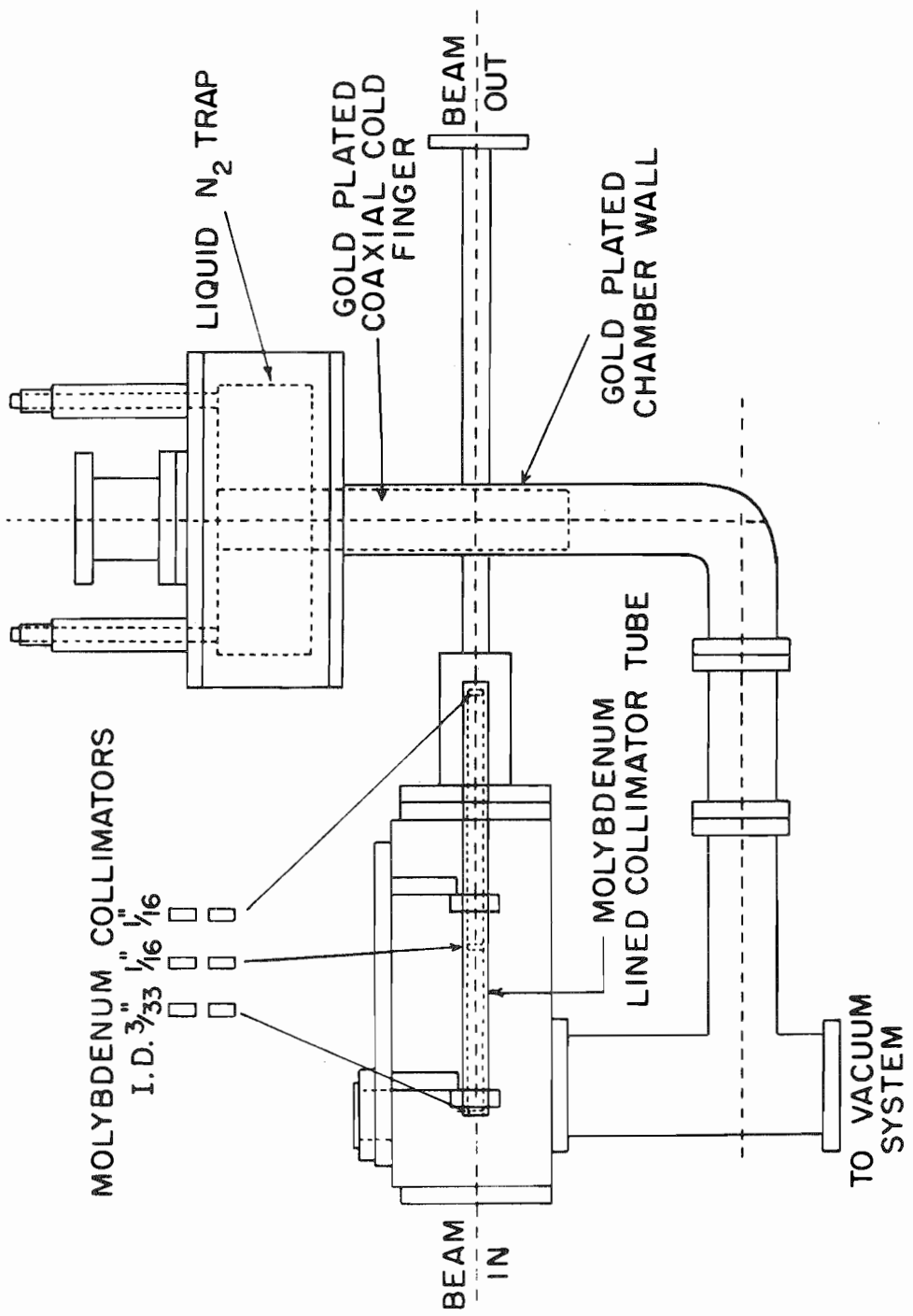
LIQUID N_2 TRAP
GOLD PLATED COAXIAL COLD FINGER
BEAM OUT
GOLD PLATED CHAMBER WALL
MOLYBDENUM COLLIMATORS
I.D. 3/33" 1/16" 1/16
MOLYBDENUM LINED COLLIMATOR TUBE
TO VACUUM SYSTEM
BEAM IN

appendix. Conceptually the problem is very simple. For example, given N widths, one can determine the frequency distribution of the linear correlation coefficient r by choosing a large number of sets of N widths from a given distribution, correlate the sets of widths with the given set and then make a frequency distribution of the linear correlation coefficient r.

The method used to generate random numbers from any non-uniform distribution P(x) (such as the chi-squared distributions) is the acceptance-rejection method (Zelen and Severo, 1964). The procedure for this method is as follows:

1) Assume a finite domain (a,b) for the distribution P(x). If the domain is infinite, a finite subset must be chosen for computational purposes.
2) Let M be the maximum value of P(x) on (a,b).
3) Generate a pair of random numbers, r and s, from a uniform distribution.
4) Choose Xo = a + (b - a)*s .
5) If r < P(Xo)/M , then choose Xo as the random number. Otherwise, generate another pair of random numbers and try again.

The acceptance ratio for random numbers generated by this method is $((b-a)M)^{-1}$.

For a Porter-Thomas distribution, M is infinite on any interval including zero so this method cannot be used directly. However, random numbers from a Porter-Thomas distribution can be obtained by

generating random numbers from a Gaussian distribution (since the square of Gaussian random numbers are distributed according to the Porter-Thomas distribution).

To generate a pair of random numbers on a uniform distribution the Power Residue Method (IBM, 1969) was used. For binary computers whose word size is $m=2^b$, the procedure is as follows: choose an odd integer Io for a starting value and choose an integer J such that J = 3(mod 8). Calculate I_{n+1} = In*J (mod 2^b) using fixed point arithmetic but interpret the result as a binary fraction. This fraction is the desired random number. For best results J should be approximately the square root of the computer word size. As with all algorithms for generating random numbers with a machine, after some point the machine will begin repeating. An important feature of the Power Residue Method is that is will generate 2^{b-2} terms before repeating. For the DDP-224 computer, this limitation is about 2.1 million numbers.

The above procedures were incorporated into a computer code to determine the statistical significance of the measured correlations. As used in this dissertation, the significance level for a linear correlation coefficient r between two sets of widths is the probability of obtaining a smaller linear correlation coefficient for r (or, if r is less than the most probable value, the probability of obtaining a linear correlation coefficient greater than r) if the sets contain only random numbers. Shown in Figures 39 and 40 are the frequency distributions of r for several different cases. These distributions were obtained from generation of 10,000 correlation.

Figure 39 Frequency distributions for the cases where 10, 14, 18, and 38 widths are correlated with widths taken at random off a Porter-Thomas distribution; on the right is the significance level curve for a given L_{CC} ; if the LCC is less than the most probable value (if the L_{CC} is greater than the most probable value, then the significance level is 100% minus the value read from the curve)

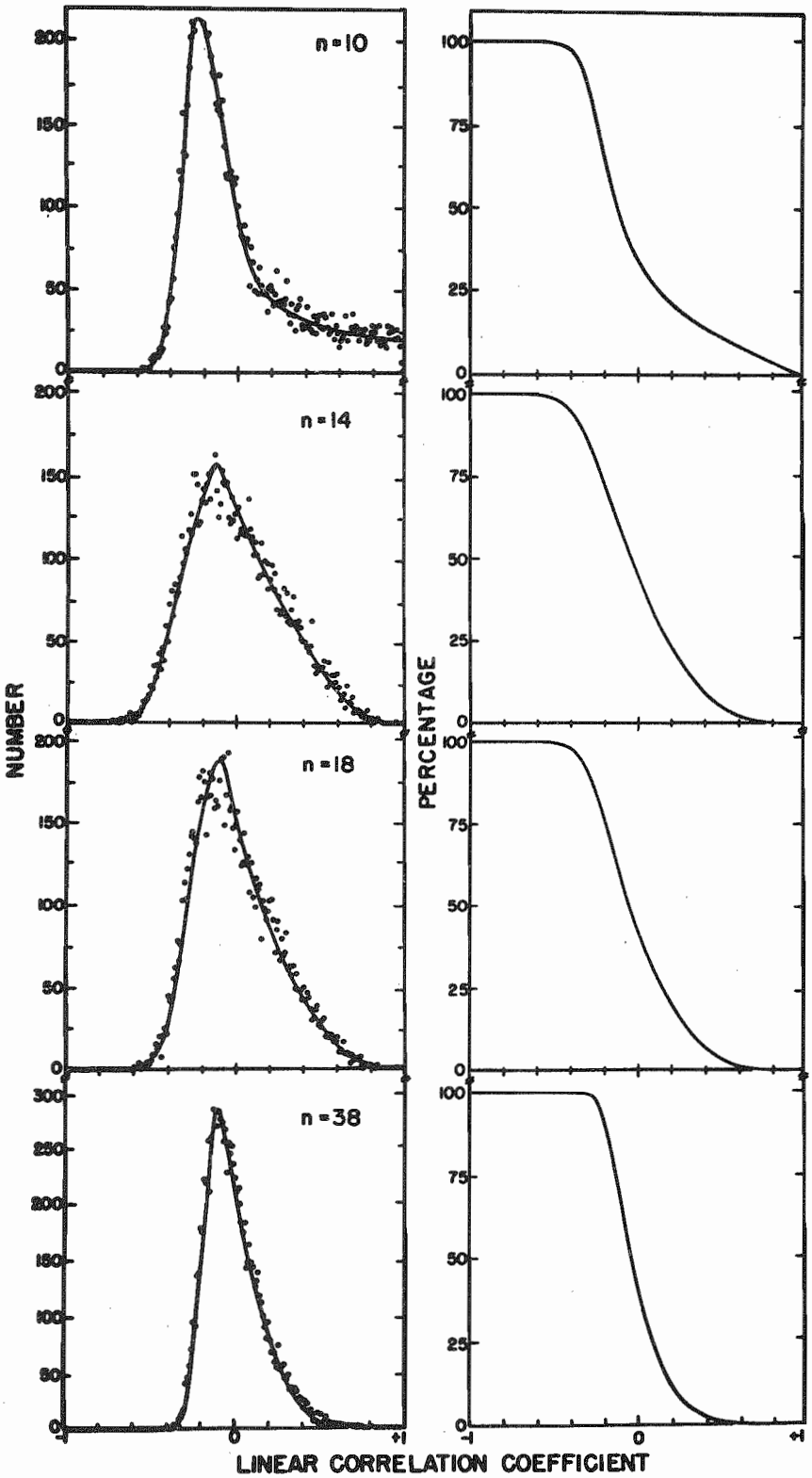
n=10
n=14
n=18
n=38
NUMBER
PERCENTAGE
LINEAR CORRELATION COEFFICIENT
-1
0
+1

Figure 40 Frequency distributions for the cases where 14 and 21 widths are correlated with widths taken at random off a Porter-Thomas distribution; on the right is the significance level curve for a given LCC if the LCC is less than the most probable value (if the LCC is greater than the most probable value, then the significance level is 100% minus the value read from the curve)

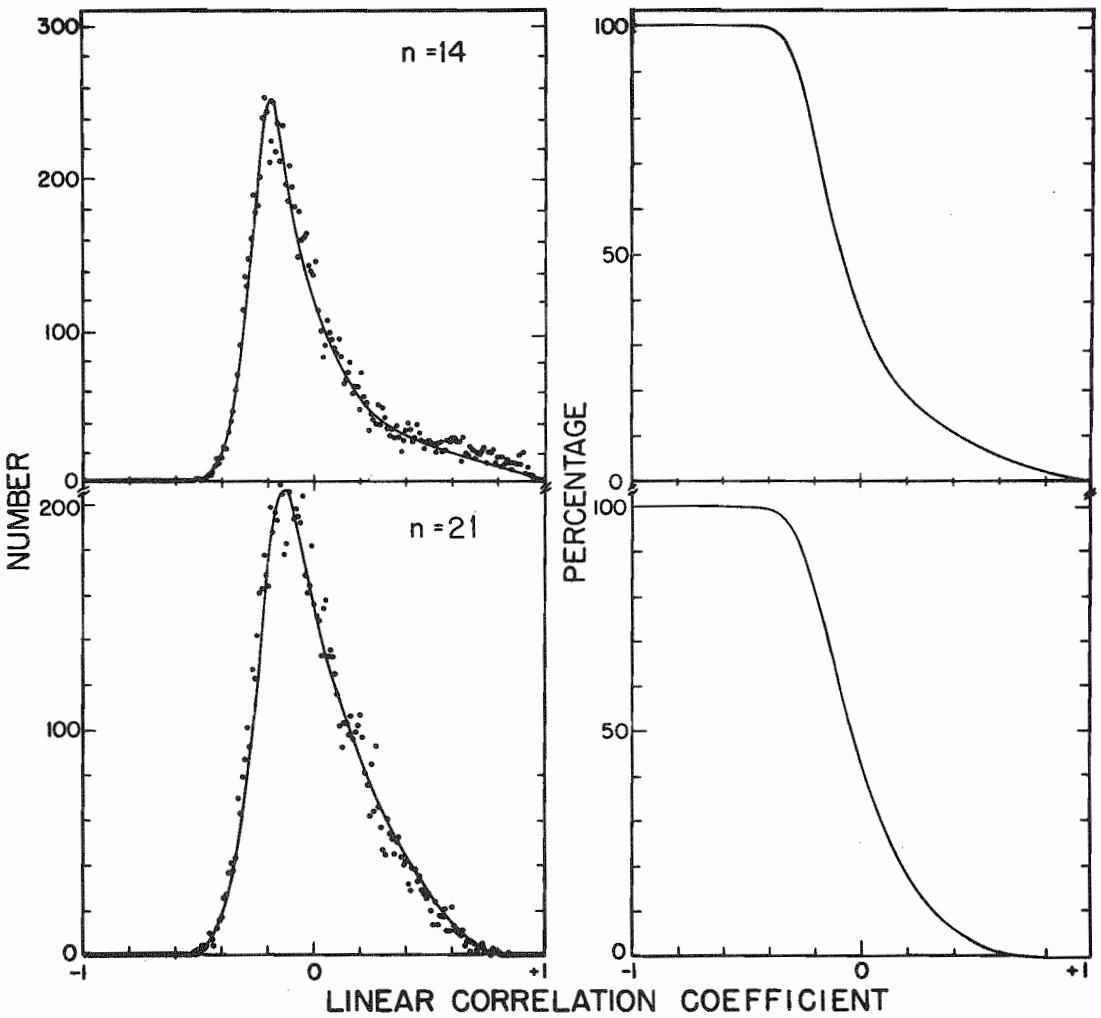
n =14
n =21
NUMBER
PERCENTAGE
300
200
100
0
200
100
0
100
50
0
100
50
0
-1
0
+1
-1
0
+1
LINEAR CORRELATION COEFFICIENT